Summer 2011

Fundamentals and applications of co-crystal methodologies: reactivity, structure determination, and mechanochemistry

Manza Battle Joshua Atkinson
University of Iowa

FUNDAMENTALS AND APPLICATIONS OF CO-CRYSTAL METHODOLOGIES: REACTIVITY, STRUCTURE DETERMINATION, AND MECHANOCHEMISTRY

by

Manza Battle Joshua Atkinson

An Abstract

Of a thesis submitted in partial fulfillment
of the requirements for the Doctor of
Philosophy degree in Chemistry
in the Graduate College of
The University of Iowa

July 2011

Thesis Supervisor: Professor Leonard R. MacGillivray

This thesis describes applications in co-crystal reactivity, structure determination, and mechanochemical preparation. We also investigate the solution-phase reactivities of products derived from a template-directed synthesis. Specifically, we described the acid treatment of an achiral molecular ladder of C_{2h} symmetry composed of five edge-sharing cyclobutane rings, or a [5]-ladderane, that results in *cis*- to *trans*- isomerization and/or oxidation of end pyridyl groups. Solution NMR spectroscopy and quantum chemical calculations support the isomerization to generate two diastereomers; namely, an achiral and a unique chiral ladderane. The NMR data, however, could not lead to unambiguous configurational assignments of the two isomers. Single-crystal X-ray diffraction was employed to determine each configuration. One isomer readily crystallized as a pure form and X-ray diffraction revealed the molecule as being achiral based on C_i symmetry. The second isomer resisted crystallization under a variety of conditions. Consequently, a strategy based on a co-crystallization was developed to generate single crystals of the second isomer. Co-crystallization of the isomer with a carboxylic acid readily afforded single crystals that confirmed a chiral ladderane based on C_2 symmetry. We also demonstrate how the stereochemistry can be retained upon treatment with acid. It will be shown how a monocyclobutane can be used as a model system when investigating the reactivity of the [5]-ladderane.

While investigating the reactivity of a diene diacid we determined that a bicyclobutyl that bears six carboxylic acid groups results from a trimerization of the solid in pure form in the solid state. Powder X-ray diffraction and a co-crystallization are used to solve the structure of the diene and elucidate the stereochemistry of the bicyclobutyl, respectively. Having established the reactivity of the diene diacid we used hydrogen-bond-acceptor (HBA) templates to assemble the diacid in the solid state in a photoactive solid for an intermolecular [2 + 2] photocycloaddition as well as a photostable solid.

To enhance strategies to generate stereocontrolled products derived from reactive co-crystals mechanochemical methods were applied to eliminate or reduce the solvent used to prepare the co-crystal solids. In particular, we show how supermolecules with olefins organized by hydrogen-bond donor and acceptor templates that react in the solid state rapidly form co-crystals *via* solvent-free and liquid-assisted grinding.

Abstract Approved: _____

Thesis Supervisor

_____

Title and Department

_____

Date

FUNDAMENTALS AND APPLICATIONS OF CO-CRYSTAL METHODOLOGIES: REACTIVITY, STRUCTURE DETERMINATION, AND MECHANOCHEMISTRY

by

Manza Battle Joshua Atkinson

A thesis submitted in partial fulfillment
of the requirements for the Doctor of
Philosophy degree in Chemistry
in the Graduate College of
The University of Iowa

July 2011

Thesis Supervisor: Professor Leonard R. MacGillivray

Graduate College
The University of Iowa
Iowa City, Iowa

CERTIFICATE OF APPROVAL

_____

PH.D. THESIS

_____

This is to certify that the Ph.D. thesis of

Manza Battle Joshua Atkinson

has been approved by the Examining Committee
for the thesis requirement for the Doctor of Philosophy
degree in Chemistry at the July 2011 graduation.

Thesis Committee: _____
Leonard R. MacGillivray, Thesis Supervisor

_____
Claudio Margulis

_____
Chris Pigge

_____
Daniel Quinn

_____
Kevin Rice

To those who made this possible.

Most people have the will to win, few have the will to prepare to win.

Bobby Knight

ACKNOWLEDGMENTS

I would like to begin by thanking my Mother and Father. Thanks for encouraging me to learn and also for believing in me at times when I didn't believe in myself. I would also like to thank my family for their love and support: My wife Karina, my son Kimathi, Bitsy, Junior, Kambarage, April Brooks, April Atkinson, Malarie, Aunt Carrie, Aunt Valarie, Aunt Sandy, Uncle Perry (rest in peace, don't know if I be in this position without you), Zandra and LaShonda Stancil, Uncle Tommy (Bishop Manuel P. Stancil), Chris Payne, Mike and Mario, Charmaine, Greg, Cousin Henrietta, Maria, Adrian Silva. Much appreciation is given to my high school chemistry teacher who introduced me to chemistry, Ms. Heiman, as well as my undergraduate family at NC A&T SU who prepared me for graduate school through the MARC U STAR program and excellent mentoring, Dr. Claude Lamb, Dr. James Williams, and Mr. David Pollard.

Professionally, I would first like to thank my advisor. Len, I want to thank you for being a great mentor and advisor since 2002. I now have two Father's, my biological and my academic. Thank you for setting the standards high and never accepting anything less from me. You have inspired me with your patience, wisdom, and hard work and I will always be appreciative. I also want to thank all the members of the MacGillivray group who have become some of my dearest friends, past and present: Kreso, Ivan, Tony, Tamara, Tomislav, Chu, David, Guo, Jelena, John, Beth, Poonam, and Joe. Thank you to all the undergraduate researchers who assisted my research projects, Naif, Mahmood, Chancity, Asher, Brittany, and Mick. I would like to thank Diana Bryant and Joseph Henry of the SROP program, which provided the opportunity and funded my internship in 2002 to come to the UI.

I would like to thank the following people for their friendship and camaraderie: Martin, Paul, Jose, Josh, Jim Gloer, Arun, Vanja, Reginald, Ken, Kathy, Dean Keller,

Andy Jenkins, Santhana V., Zadok, Adrian Taylor, Charisse L., Brandon, Dede, Alex, James H., Brian Berry, Donna W., Shelly Serin, Joseph Lang.

A big thank you is also necessary for the UI chemistry department staff members: Shonda Monette, Sharon Robertson, Janet Kugley, Vic Parcell, Peter Hatch, Tim Koon, Andy Lynch, Brian Morrison, and Earlene Erbe.

I would like to thank those individuals for their scientific contributions to the work presented in this thesis: Dr. Santhana Velupillai, for performing solid state NMR experiments; Dr. Dale Swenson who performed the data collection on all the single crystals; Jonas Baltrusaitis for providing the computational data; Vic Parcell and Lynn Teesch for assistance in collect mass spectrometry data; Dr. Ivan Halasz and Dr. Robert E. Dinnebier for providing the PXRD structure solution data.

I would like to thank the members of my committee: Claudio Margulis, Chris Pigge, Daniel Quinn, Kevin Rice.

Lastly, thank you to the UI Graduate College for financial support through the Dean’s Fellowship.

ABSTRACT

This thesis describes applications in co-crystal reactivity, structure determination, and mechanochemical preparation. We also investigate the solution-phase reactivities of products derived from a template-directed synthesis. Specifically, we described the acid treatment of an achiral molecular ladder of C_{2h} symmetry composed of five edge-sharing cyclobutane rings, or a [5]-ladderane, that results in *cis*- to *trans*- isomerization and/or oxidation of end pyridyl groups. Solution NMR spectroscopy and quantum chemical calculations support the isomerization to generate two diastereomers; namely, an achiral and a unique chiral ladderane. The NMR data, however, could not lead to unambiguous configurational assignments of the two isomers. Single-crystal X-ray diffraction was employed to determine each configuration. One isomer readily crystallized as a pure form and X-ray diffraction revealed the molecule as being achiral based on C_i symmetry. The second isomer resisted crystallization under a variety of conditions. Consequently, a strategy based on a co-crystallization was developed to generate single crystals of the second isomer. Co-crystallization of the isomer with a carboxylic acid readily afforded single crystals that confirmed a chiral ladderane based on C_2 symmetry. We also demonstrate how the stereochemistry can be retained upon treatment with acid. It will be shown how a monocyclobutane can be used as a model system when investigating the reactivity of the [5]-ladderane.

While investigating the reactivity of a diene diacid we determined that a bicyclobutyl that bears six carboxylic acid groups results from a trimerization of the solid in pure form in the solid state. Powder X-ray diffraction and a co-crystallization are used to solve the structure of the diene and elucidate the stereochemistry of the bicyclobutyl, respectively. Having established the reactivity of the diene diacid we used hydrogen-bond-acceptor (HBA) templates to assemble the diacid in the solid state in a photoactive solid for an intermolecular [2 + 2] photocycloaddition as well as a photostable solid.

To enhance strategies to generate stereocontrolled products derived from reactive co-crystals mechanochemical methods were applied to eliminate or reduce the solvent used to prepare the co-crystal solids. In particular, we show how supermolecules with olefins organized by hydrogen-bond donor and acceptor templates that react in the solid state rapidly form co-crystals *via* solvent-free and liquid-assisted grinding.

TABLE OF CONTENTS

LIST OF TABLES

Table

LIST OF FIGURES

Figure

CHAPTER 1. INTRODUCTION

1.1. The Organic Solid State

Within an organic solid, molecules are held together by intermolecular forces (*e.g.* hydrogen bonds) that limit or restrict mobility.[1-4] The aggregation of molecules in solids creates a single entity termed *supermolecule*.[1-4] The structural arrangement or packing within the crystal is influenced by the sizes,[5,6] shapes,[7,8] and functionalities of organic molecules.[1,9] Indeed, strategies based on principles of *crystal engineering*, which involves the understanding and investigation of fundamental properties that dictate molecular arrangement, is essential for the rational design, control, and useful applications of organic solids.[2,10-12]

A means to design a target supermolecule is with the use of a *supramolecular synthon*.[1,13] Supramolecular synthons provide adhesive forces in the form of non-covalent bonds that establish specific connectivity between molecules in organic solids. These relatively robust interactions commonly impose directionality on molecular assemblies.[14] There are two types of synthons: the *homosynthon* and the *heterosynthon*.[1] The former is comprised of self-complementary functional groups (Figure 1a) and the latter is composed of complementary groups that differ in functionality (Figure 1b).[15,16]

a) homosynthon **b) heterosynthon**

Figure 1. Schematic representation of complementary hydrogen-bonded supramolecular homo- and heterosynthons: a) carboxyl-carboxyl synthon; b) carboxyl-pyridyl synthon.

In the solid state the supramolecular synthons allow crystal engineers to predict the structural outcome within a solid to a reasonable degree. In the case of the benzene carboxylic acids such as benzoic, terephthalic, and trimesic acid, the molecules self-assemble to form multidimensional assemblies based on the positions of the carboxylic acid groups (Figure 2).[3] Benzoic acid

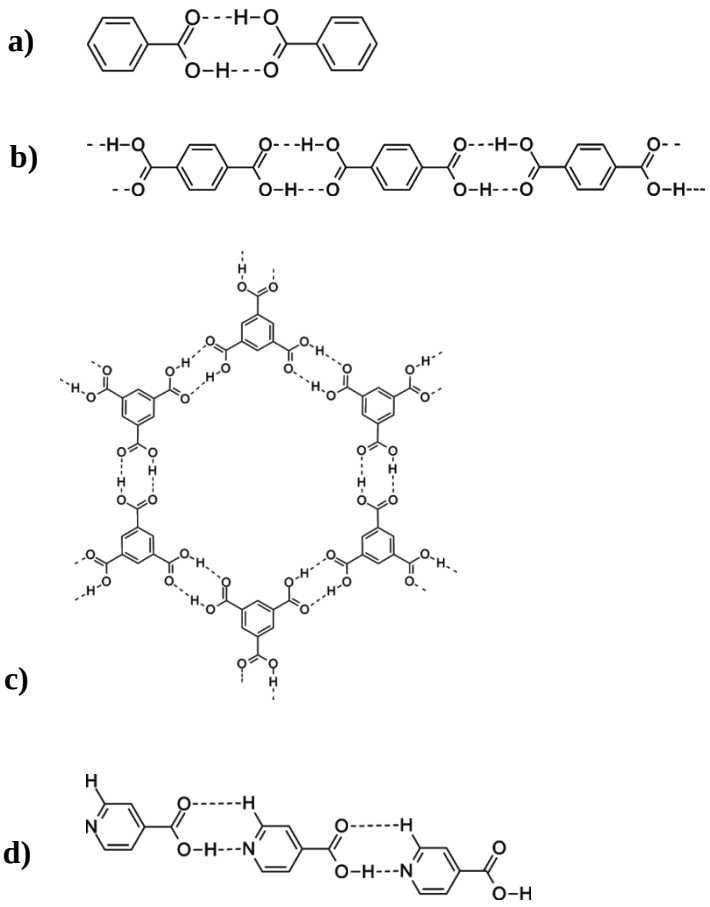

Figure 2. Schematic representation of solid state arrangement of supramolecular architectures: a) benzoic acid; b) isophthalic acid; c) trimesic acid; d) isonicotinic acid.

containing one carboxyl group forms a discrete assembly while terephthalic acid functionalized with carboxyl groups at the para positions forms a linear one-

dimensional (1D) assembly. Similarly, trimesic acid with carboxyl groups at the 1, 3, 5-positions forms a three-connected honeycomb-like architecture (Figure 2c). Similarly, a linear hydrogen-bonded 1D chain of isonicotinic acid is sustained by pyridyl-carboxylic acid interactions (Figure 2d).[17] The examples above provide a few examples of supramolecular assemblies that can be constructed by design.

1.2. Emergence of Co-crystals: Definitions, Applications, and Preparation

Having established that functional groups form homo- and heterosynthons, chemists have started to rationally design multiple-component assemblies in the form of *co-crystals*. A co-crystal can be defined as a crystalline solid composed of two or more molecules that are solids at ambient temperatures that interact via charge neutral non-covalent bonds.[18,19] Another interpretation of a co-crystal is a case wherein a target molecule is co-crystallized with a crystallizing agent called a co-crystal former (CCF). The intermolecular interactions within a co-crystal govern the molecular arrangement of the components in the solid.

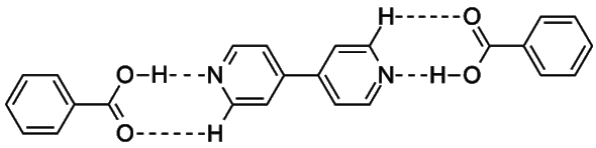

Figure 3. Schematic representation of the co-crystal of 4,4'-dipyridine and benzoic acid. In the solid, the pyridyl-carboxylic acid synthon facilitates the zero-dimensional assembly.

A co-crystal exhibits modularity. A CCF, depending on the nature of the interactions with the target molecule, can be exchanged without compromising the covalent linkage and/or arrangement of the target molecule. Consequently,

this alters the composition and, thereby, can change the bulk properties of the solid (*i.e.* melting point, solubility).[20] The modularity has inspired applications of co-crystals in solid-state organic synthesis,[21] organic semiconductors,[22] structural determination of small organic molecules,[23-25] and materials science particularly in the area of pharmaceutics.[26] An example of how co-crystals are currently being applied is in the area of pharmaceutics.[27-30]

A common approach of modifying or altering the physiochemical properties of an active pharmaceutical ingredient (API) is to create a salt. Salt formation, however is limited to an API with an acid or base ionizable site.[31] Co-crystals represent a viable alternative to salt formation in pharmaceutics. For instance, Itraconazole is a highly water-insoluble antifungal drug (Figure 4).[32] Currently, the drug is formulated in an

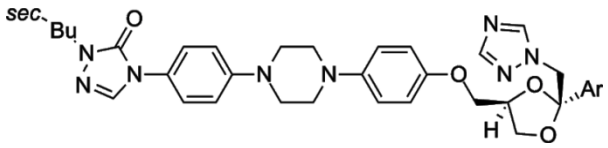

Ar = 2,4-dichlorophenyl

Figure 4. Schematic representation of *cis*-Itraconazole

amorphous form (Sporanox capsule) that has to be ingested with acidic beverages in order to obtain the maximum absorption through dissolution. The patent literature reveals that attempts to modify the properties of the drug via salt formation proved unsuccessful. Moreover, Almarsson *et al.* were able to alter the solid-state properties of the drug with the use of co-crystals. Figure 5 shows intraconazole co-crystallized with succinic acid. Two molecules of intraconazole are located *anti* and bridged by a succinic acid *via* triazole-carboxyl hydrogen

bonds. Dissolution profiles of the intraconazole co-crystals revealed higher concentrations than that of the commercial Sporanox

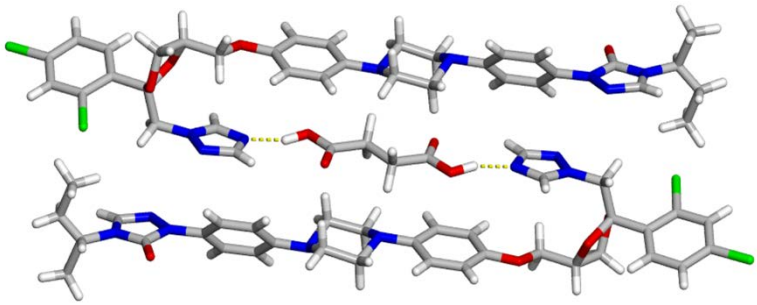

Figure 5. Wireframe representation of 3-component assembly of succinic acid and itraconazole co-crystal from the single crystal X-ray structure.

capsule. The finding demonstrates an excellent application of the use of co-crystals.

The emergence of applications of co-crystal solids have motivated solid state chemists to develop alternative or efficient means of preparation.[33,34] Traditionally, a co-crystal has been prepared by dissolving the solid components in a solution and allowing co-crystallization *via* slow evaporation or sublimation.[35] It is well established that solution-based crystallization provides well-defined and highly-ordered crystals with excellent opportunity for purification; however, there are disadvantages associated with the conventional routes. Solution crystallizations may sometimes require toxic solvents, which can have a harmful impact on the environment as well as generate costly expenses from the use and waste disposal. Moreover, the solvent can also form solvates with the individual components rather than form the pure co-crystal or lead to undesired metastable polymorphs.[27,36]

To circumvent the disadvantages of solution-based crystallizations, mechanochemical methods have been employed to generate co-crystals with little or no use of solvent.[33,34] *Mechanochemistry* is the act of grinding or milling solids to induce the formation or breaking of a chemical bond.[37] Typically, the grinding is carried out using a mortar and pestle or an automated ball and mill.[37] Substantial increases in heat and pressure are exerted on the solids. For a co-crystal formation, non-covalent interactions are, thus, formed and broken. Moreover, given the significance of co-crystals, obtaining these highly useful materials with little or no use of solvent makes the materials appealing from numerous perspectives.[34] However, the application of mechanochemistry, in the context of co-crystal synthesis, remains in its infancy.

1.3. Organic Solid-State Reactivity: *trans*-Cinnamic Acid

The solid state is a useful medium for the synthesis of organic molecules. The ability to align molecules in positions suitable for a chemical reaction in solids offers a useful medium for highly regio- and stereospecific synthetic transformations.[21] Reactions in organic solids have been studied since the late 1800's.[38] Early solid-state photochemical investigations demonstrated that two different crystalline forms of *trans*-cinnamic acid (t-ca) react to form two different stereoisomers; namely, α-truxillic acid (α-ta), and β-truxinic acid (β-ta) when the solids were exposed to UV-irradiation (Figure 6).[38,39] The observation

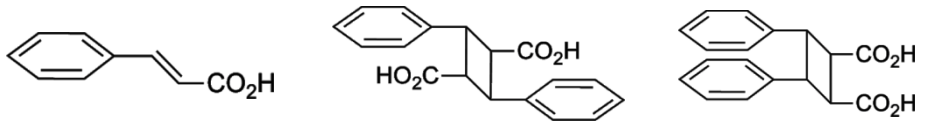

a) *trans*-cinnamic acid **b) α-truxillic acid** **c) β-truxinic acid**

Figure 6. Schematic depiction of a) *trans*-cinnamic acid b) photoproduct isomers α-truxillic acid, and c) β-truxinic acid.

suggested the existence of *polymorphic* crystals, which means that the acid exhibited different structural orientations in different crystalline forms.

Later, Schmidt determined from crystallization experiments that t-ca exists in three crystal polymorphs; namely, α-, β-, and γ-forms.[38] The α-form is prepared in ether or benzene by slow evaporation and the β-form is prepared by hot supersaturated solutions of ether, followed by washes of light petroleum at 0°C. While the γ-form is photostable, photoirradiation of the α- and β-form produces α-truxillic acid (α-ta) and β-truxinic acid (β-ta), respectively, in 100% yield. It also important to note that β-form is metastable at different temperatures. Irradiation of the β-form at temperatures above 45°C affords mixtures of α-ta and β-ta, while temperatures below 45°C affords only β-ta.

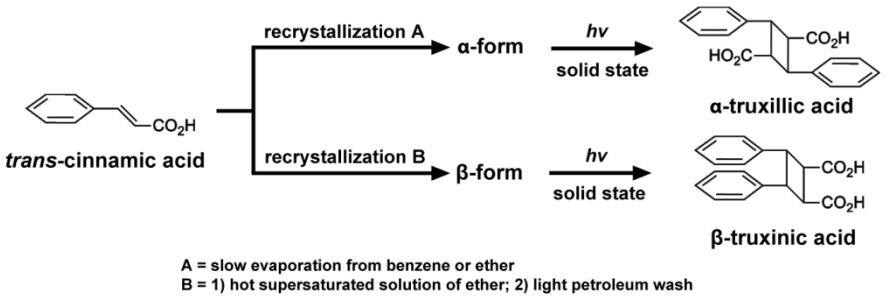

Figure 7. Schematic of reactions showing the recrystallizations of *trans*-cinnamic acid to obtain of α- and β-polymorphs. Photoirradiation of the solids provides α-truxillic acid (α-ta) and β-truxinic acid (β-ta), respectively.

Schmidt then examined the crystal structures of the α-, β-, and γ-forms of t-ca.[39] It was determined that in α-t-ca, the molecules arrange in alternating stair-like stacks, consisting of hydrogen-bonded acid pairs. The stacks orient the t-ca molecules in a head-to-tail fashion placing the two nearest double bonds parallel

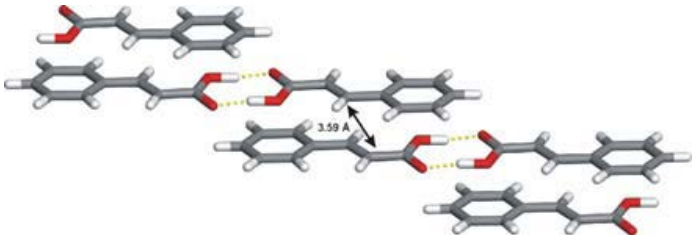

Figure 8. A wireframe representation of the arrangement of molecules in a crystal of α-cinnamic acid.

and separated by 3.59Å (Figure 8). The β-form also consists of hydrogen-bonded acid pairs yet possess stacks in the same orientation that places the molecules in a head-to-head fashion, with nearest neighboring double bonds parallel and separated by 3.9Å. The photostable γ-form placed the nearest neighbor double bonds between 4.7 to 5.1Å.

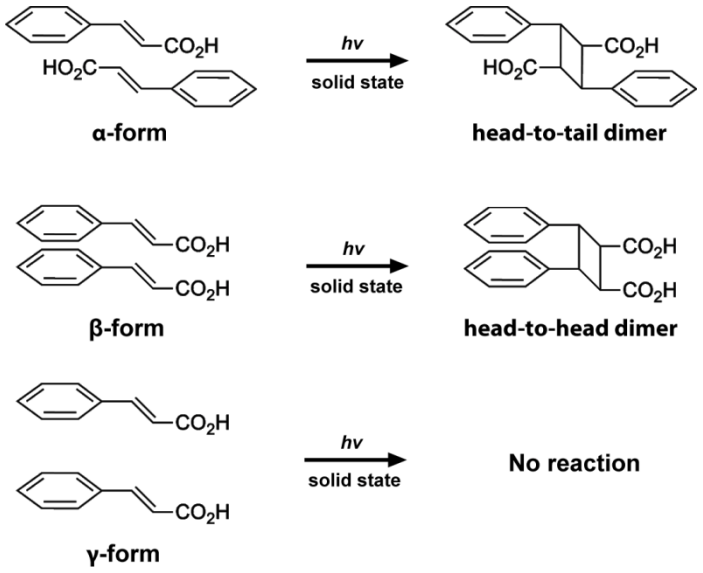

Figure 9. Schematic of solid-state reactions showing the result of exposing the α-, β-, and γ-forms to UV-irradiation.

Having gained an understanding between structural orientation and reactivity, Schmidt explored the molecular criteria for [2 + 2] photodimerizations of halogenated, ortho-substituted, and hydroxyl substituted derivatives of cinnamic acids.[39-42] Schmidt also studied the solid-state reactivity of polyenes.[43-50] The studies were highly significant, since the studies would provide the foundation for understanding and conducting organic reactions in solid media, whilst providing opportunities to obtain regio- and stereocontrolled products.

1.3.1. The Topochemical Postulate

Extensive studies by Schmidt *et al*. provided underlying principles for [2+2]-photodimerizations to occur in solids.[40] From these observations Schmidt determined criteria for a photoreaction of two olefins, which are termed the '*topochemical postulate*'. The postulate states geometric requirements for two carbon-carbon double bonds to react in the solid state. Thus, the olefins must be generally parallel and separated less than 4.2Å. The principles provided a foundation for numerous studies of photochemical transformations in organic solids.[21,51]

1.3.2. The 'Gold Rush' of Solid-State Reactivity

The systematic work of Schmidt demonstrated the utility of the solid state as a medium for reactivity and also X-ray crystallography as a valuable tool to correlate pre-organized structure in a crystalline lattice with the photochemical products derived from solids. Establishing topochemical criteria associated with the formation of a [2 + 2] photodimerization of olefins highlighted the ability to conduct stereo- and regiocontrolled organic reactions, a unique facet of solid phase synthesis that is difficult to achieve in solution. This, in turn, prompted chemists to attempt to understand and exploit means to dictate and optimize solid-state reactions.[52-54] Moreover, given the recent advancements in crystal structure

analysis via single-crystal (*i.e.* rapid data collection using CCDs) and powder X-ray diffraction (PXRD), it is now apparent that the extent to which reactions that occur in solids can impact organic synthetic chemistry is yet to be fully realized and developed.

1.4. Engineering Molecular Arrangement in Organic Co-crystals: Towards Control of a [2 + 2] Photodimerization

Solid state chemists have set to apply principles of supramolecular chemistry to engineer co-crystals for the purpose of dictating topochemical reactions of olefins in solids.[21] With this in mind, co-crystals based on electron donor/acceptor,[55] chloro-,[56] fluoro-,[53] alkoxyaryl groups,[54] as well as hydrogen bonding interactions, have been used to align olefins in solids for [2+2] photodimerizations.

1.4.1. Donor/Acceptor Interactions

Desiraju *et al*. demonstrated the utility of positioning olefins in co-crystals based on donor/acceptor groups.[55] Co-crystallization of 2,5-dimethoxy- and 3,5-dinitro-substituted cinnamic acid derivatives provided photoactive co-crystals sustained by carboxy synthons and alkoxy-nitro charge transfer intermolecular interactions (Figure 10). The solid upon exposure to UV-irradiation yielded the formation of an unsymmetrical cyclobutane in 60% yield.

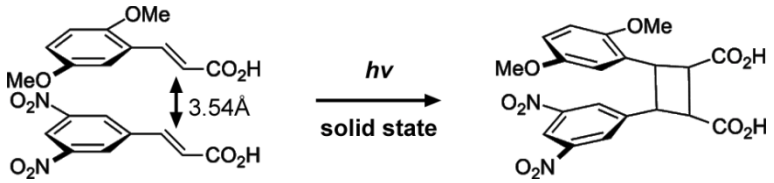

Figure 10. Schematic representation of olefins aligned by donor/acceptor groups in the form of nitro/methoxy interactions.

Extending studies involving the use of alkoxy-nitro interactions to control the organization of olefins, Codding forced the diene (*E*,*E*)-1-(2-methoxyphenyl)-4-(4-nitrophenyl)-1,3-butadiene, in a position for a photoreaction with the use of an alkoxy and nitro groups on aromatic subsituents at opposite ends of the molecules.[54]

Desiraju used chloro-chloro (Cl···Cl) interactions to manipulate the assembly of two chlorosubstitued acids into a 2:1 co-crystal 2-(6-chloro-3,4-(methy1enedioxy)-cinnamic acid)·(2,4-dichlorocinnamic acid) to form an unsymmetrical cyclobutane in the solid state after UV-irradiation of the solid (Figure 11).[56] Moreover, the stereochemistry of the photoproduct correlated well with the molecular arrangement before photoreaction. Figure 11 shows the Cl···Cl interaction between overlapping Cl atoms, that helps facilitate the assembly of the molecules.

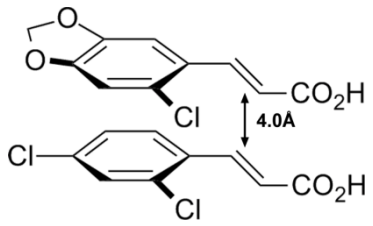

Figure 11. Schematic representation of the Cl···Cl interaction used to facilitate alignment in complex 2-(6-chloro-3,4-(methy1enedioxy)-cinnamic acid)·(2,4-dichlorocinnamic acid) which leads to the formation an unsymmetrical cyclobutane.

Grubbs *et al.* employed phenyl-perflourophenyl interactions to induce the face-to-face stacking of mono- and diolefins in a cofacial position for an intermolecular photoreaction.[53] Figure 12 shows the X-ray crystal structure of *trans*-pentafluorostilbene. The molecules are stacked in position for a [2 + 2] photodimerization directed by the phenyl-perflourophenyl interaction. UV-

irradiation of both the co-crystal and the single molecule leads to the stereocontrolled formation of the cyclobutane photoproducts in up to 98% yield.

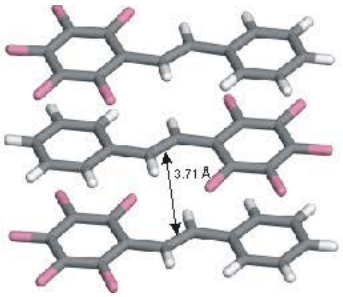

Figure 12. Wireframe representations of photoactive molecular stacks in 1,2,3,4,5-pentafluorostilbene.

In a similar experiment, Vishnumurthy *et al*. applied phenyl-perflourophenyl interactions to align diolefins in the form of 1,3-butadienes in position for a [2 + 2] photodimerization to obtain [3]-ladderanes.[57]

1.5. Auxiliary Components to Achieve a [2 + 2] Photodimerization

The predictability and control of arranging olefins in position for [2 + 2] photodimerization with the use of synthons is, ultimately, the objective of the crystal engineer whose interest involve the solid state organic synthesis of cyclobutanes. In the mid 90's, chemist began to use auxiliary components to organize reactants in the solid state in position for photochemical reaction.[21] An auxiliary assists the formation of the supermolecule, but is not covalently linked to the final product. The utilization of auxiliaries provided an alternative to two-component structural modifications of olefinic molecules.

1.5.1. Double Salt Formation of Cinnamic Acid Using Amines

In 1995, Ito showed that di, tri, and tetraamine auxiliaries could align cinnamate ions in the form of salts for reaction.[58] The premise behind the experimental design was to control the stereoisomer formation of the cyclobutane products by obtaining a coiled conformation of an amine and two molar equivalents of cinnamic acid (Figure 13). It was determined that the cinnamic acid salts formed with ethyl di-, penta-, and hexylamine adopted an anti, partial, and fully extended conformation, respectively.

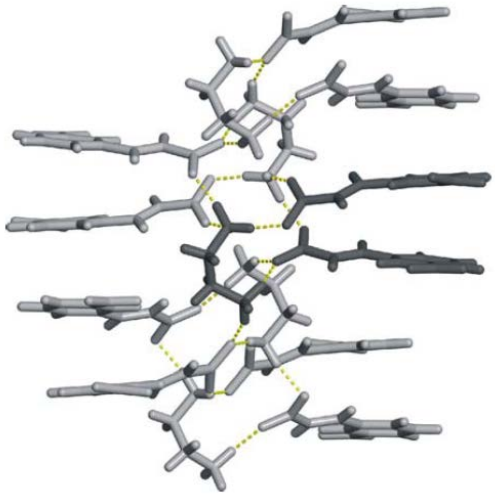

Figure 13. Wireframe representation of ethylenediammonium 2-nitrocinnamate depicting a discrete photoactive assembly. A single photoactive assembly is depicted dark.

Notably, crystals of *trans*- and *cis*-1,2-cyclohexanediamine gave mixtures of photoproducts ε-truxillic acid:δ-truxinic acid (43:5) β-truxinic acid:δ-truxinic acid (64:3), respectively. X-ray analysis, however, could not be conducted owing to poor diffraction quality, but the photoproducts suggested the possibility a photoactive overlapped configuration of the acids. Ito had shown a unique

approach to directing reactivity with the use of an auxiliary, however, the system was not efficient.

1.5.2. Template-Directed Solid-State Synthesis

In 2000, MacGillivray *et al*. developed a strategy to control the reactivity of olefins in the solid state with the use of ditopic molecules in the form of templates.[21] The templates serve to facilitate the arrangement of reactant molecules in positions for a [2 + 2] photodimerization via complementary non-covalent interactions, particularly, in the form of discrete hydrogen bonded molecular assemblies (Figure 14). After the photoreaction, the templates can be removed and reused.

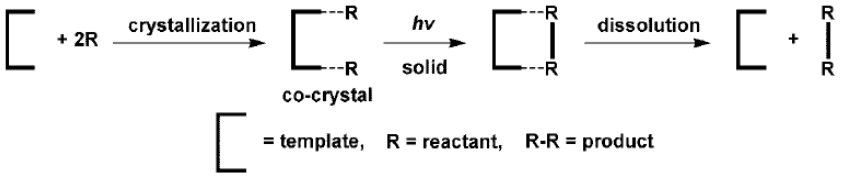

Figure 14. Schematic representation of template-directed solid-state synthesis.

1.5.2.1. Resorcinol and *trans*-1,2-bis-(4-pyridyl)ethylene

MacGillivray *et al*. first reported the use of a template in the form of resorcinol (res) to align 1,2-bis-(4-pyridyl)ethene (4,4,'-bpe) in position for a photoreaction.[59] The reactant molecule, 4,4'-bpe in its pure form is photostable. As shown in Figure 15a, the crystal structure of 4,4'-bpe places the double bonds in position that lie 5.7 Å apart, outside of the criteria proposed by Schmidt. When combined with res in a 1:1 ratio a co-crystal of composition 2(res)·2(4,4'-bpe) is obtained. As shown in Figure 15b, the res molecules force a discrete 4-

component assembly that places the bpe molecules in parallel positions and 4.2 Å apart.

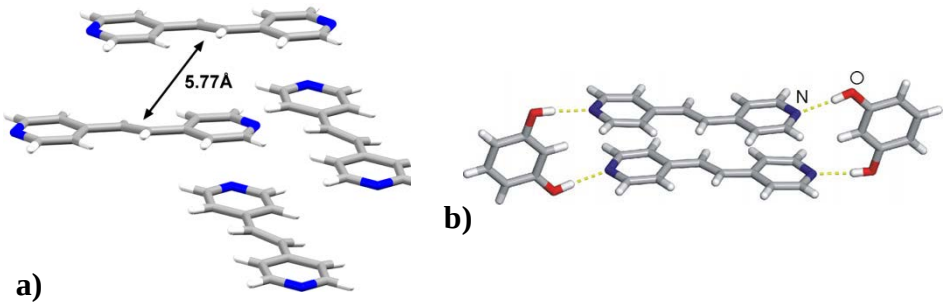

Figure 15. Wireframe models of 4,4’-bpe pure solid and 2(res)·2(4,4,’-bpe): a) neighboring 4,4’-bpe molecules in photostable solid and b) discrete co-facial alignment of co-crystal assembly.

UV-irradiation of 2(res)·2(4,4,’-bpe) affords *rctt*-tetra(4-pyridyl)cyclobutane (tpcb-1a) stereospecifically in 100% yield (Figure 16).

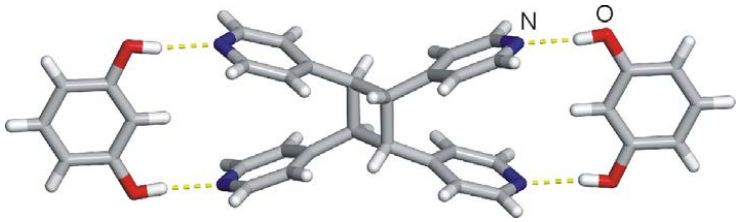

Figure 16. Wireframe representation of the assembly involving 4,4'-tpcb and res, obtained after recrystallization of photoreacted 2(res)·2(4,4'-bpe).

1.5.2.2. Exploring Generality and Modularity in Template-Directed Synthesis

Having established the supramolecular behavior of 4,4’-bpe and res, MacGillivray *et al*. set to explore the generality of this approach by systematically

substituting reactants and/or templates[60] based on the predictable nature of the directional complementary functionality.[21,59,61] Such a design, in theory, would provide access to a variety of regio- and stereocontrolled synthesis of organic products virtually inaccessible in solution.[21,62] It was, thus, that a co-crystal of 2,2'-bpe, could be obtained with res of composition 2(res)·2(2,2'-bpe) (Figure 17). UV-irradiation of the solid produced the *rctt*-cyclobutane isomer in 100% yield.[63]

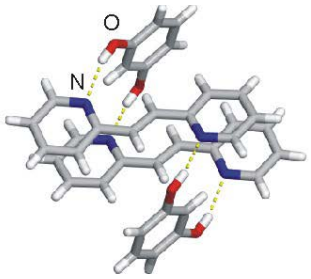

Figure 17. Wireframe representation of the discrete solid-state assembly of 2(res)·2(2,2'-bpe).

1.5.2.3. Reversing the Code: Hydrogen-Acceptor Templates

Having established topochemical control of hydrogen-bond acceptor reactant molecules and the modularity of hydrogen-donating ditopic templates, it was suggested that the functionality of both the template and reactant could be reversed.[64] In 2005, it was demonstrated by MacGillivray *et al*. the co-crystallization of fumaric acid (fum), a ditopic hydrogen-bond donor (HBD), with a hydrogen-bond acceptor (HBA) 2,3-bis(4-methylenethiopyridyl)naphthalene (2,3-nap). The co-crystal 2(2,3-nap)·2(fum) forms a four-component discrete assembly (Figure 18). The HBA serves to align the fumaric acid molecules

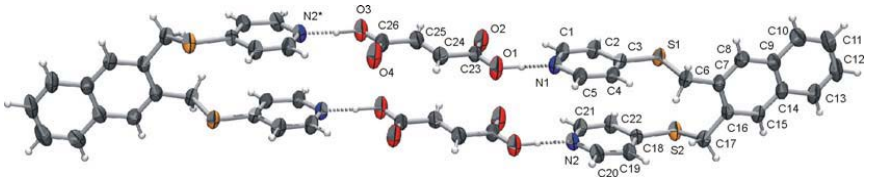

Figure 18. ORTEP model four-component molecular assembly in the co-crystal of 2(fum)·2(2,3-nap). Non-hydrogen atoms are shown as ellipsoids at 30% probability level.

3.86Å apart in position for a [2 + 2] photodimerization. UV-irradiation affords *rctt*-isomer of 1,2,3,4-cyclobutanetetracarboxylic acid (*rctt*-cbta) in 70% yield (Figure 19).

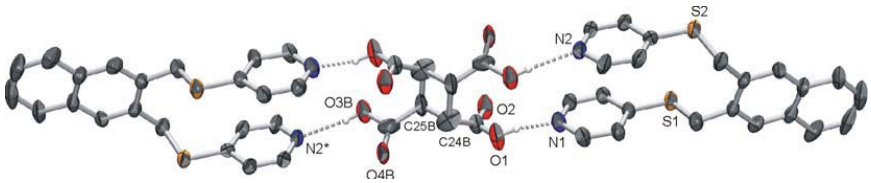

Figure 19. ORTEP representation of photoreacted co-crystal of 2(fum)·2(2,3-nap). Non-hydrogen atoms are shown as ellipsoids at 30% probability level.

1.5.2.4. Expanding Complexity of Reactants Leads to Complex Products

MacGillivray *et al*. set to explore the reactivity of pyridyl-functionalized polyenes for use with molecular templates.[65] It was discovered that the templates arranged the polyenes 'in-phase' for a photoreaction. For the double bonds to be in an 'in-phase' configuration means that the reactant molecules are superimposed, while an 'out-of-phase' arrangement places reactant molecules

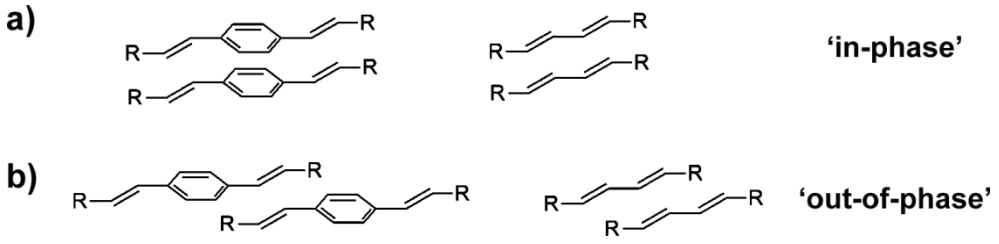

Figure 20. Solid-state depiction of an'in-phase' and 'out-of-phase' arrangement of diolefin reactants.

offset (Figure 20).[66] As shown in Figure 21, 5-methoxyresocinol (5-OMe-Res) arranges the diolefin 1,4-bis[2-(4-pyridyl)ethenyl]benzene (1,4-bpeb) 'in-phase' for a [2 + 2] photodimerization in 60% yield.[59] A later report involved a

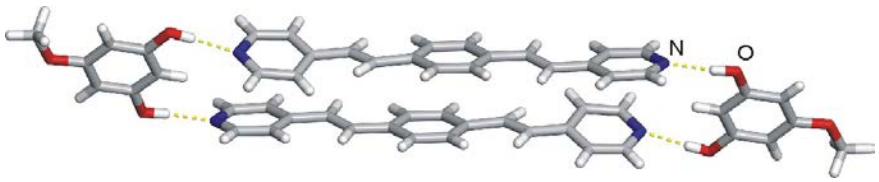

Figure 21. Wireframe model of the discrete solid-state assembly of: 2(5-OMe-res)·2(4,4'-bpe); b) 2(5-OMe-res)·2(1,4-bpeb).

'template-switching' approach to achieve 100% yield of the corresponding [2.2]paracyclophane with the use of 5-benzylresorcinol as a template with 1,4-bpeb.[63] In 2004, it was reported that 5-methoxyresorcinol (5-OMe-res) co-crystallized with *E,E*-bis(4-pyridyl)poly-*m*-ene [(4-pyr-poly-*m*-ene); (where m = 2 or 3)] afforded co-crystals of composition 2(5-OMe-res)·2(4-pyr-poly-2-ene) and/or 2(5-OMe-res)·2(4-pyr-poly-3-ene) (Figure 22). UV-irradiation of the

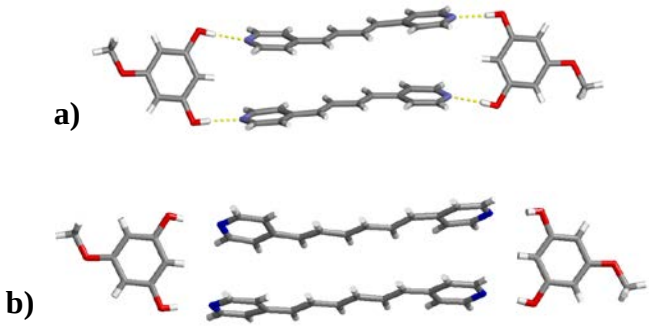

Figure 22. Wireframe representation of ladderane supramolecular precursors: a) 2(5-OMe-res)·2(4-pyr-poly-2-ene); b) 2(5-OMe-res)·2(4-pyr-poly-3-ene).

solids afforded the stereospecific, quantitative formation of 4-pyridyl-functionalized [3]- and [5]-ladderanes, respectively (Figure 23). With the exception of Hopf,[67,68] who produced ladderanes from intramolecular [2 + 2] photodimerizations using a paracyclophane scaffold, synthetic ladderanes were often achieved in low yields in solution and the solid state.[69] It is important to note, that naturally occurring

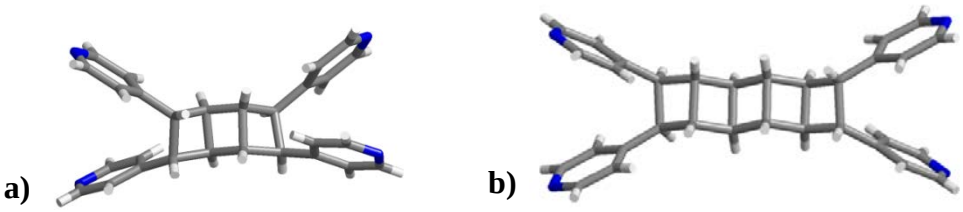

Figure 23. Wireframe model of: a) *rctt*-tetrakis(4-pyridyl)-[3]-ladderane; b) *rctt*-tetrakis(4-pyridyl)-[5]-ladderane (lad-1a).

ladderanes were discovered as lipids in the biomembranes of the anaerobic oxidizing bacteria that serve to mediate the permeability of toxic intermediates involved in nitrogen fixation, the relevance of which will be discussed in the next chapter.[70,71]

1.5.3. Opening Pandora's Box: Other Auxiliaries

In the context of both supramolecular and covalent synthesis, MacGillivray *et al*. pioneered and demonstrated the advantages of solid-state reactivity with the use of an auxiliary.[21,51] Shortly after the report of a template-directed solid-state synthesis,[59] chemists set to exploit organic solid-state reactivity with the use of an auxiliary, as well as apply and understand properties that govern the intermolecular [2 + 2] photodimerization of double bonds.[21,51]Although examples of utilizing auxiliaries to align double bonds in position for a photoreaction have been achieved in solution,[72-74] this section will focus on the use of organic auxiliaries to exploit the reactivity of olefins for a [2 + 2] photodimerization in the solid-state.

1.5.3.1. Macrocyclic Auxiliaries

Garcia-Garibay and Stoddart have showed that 4,4'-bis(benzylammonium)stilbene (4,4'-bbs) could be placed in position for a solid-state intermolecular photoreaction with the use of crown ether bis-*p*-phenylene[34]-crown[10] (BPP34C10) (Figure 24).[75] As shown in Figure 25, the

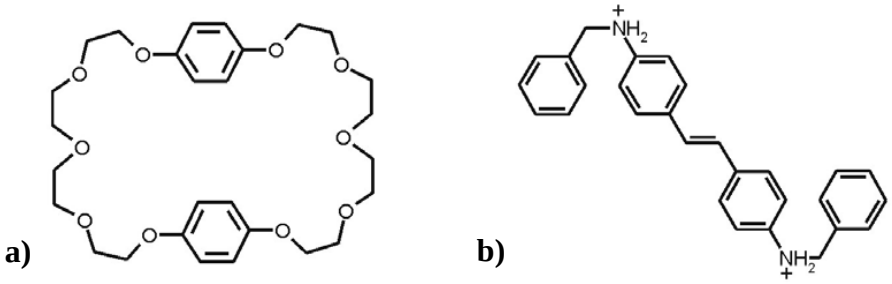

Figure 24. Schematic representations of:) bis-*p*-phenylene[34]-crown[10] molecule; b) 4,4'-bis(benzylammonium)stilbene cation.

components form a cationic assembly of composition [2(4,4'-bbs)·2(BPP34C10)]$^{4+}$ sustained *via* N^+-H···O hydrogen bonds and N^+-H···π interactions. UV-irradiation of the solid affords 1,2,3,4-tetrakis(4-benzylammoniumphenyl)cyclobutane in 80 % yield.

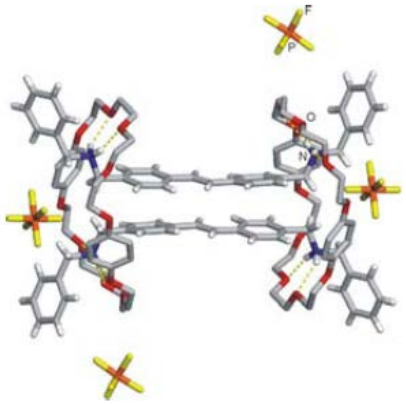

Figure 25. Wireframe representation of the three-component assembly.

1.5.3.2. Infinite Hydrogen-Bonded Assemblies

Jones has demonstrated a [2 + 2] photodimerization of 4,4'-bpe using auxiliaries that give rise to photoactive 1D assemblies.[76,77] As shown in Figure 26, molecules in the co-crystal of 4,4'-bpe and 1,2,4,5-benzenetetracarboxylic acid (bta) arrange in a 1D assembly that allows for the topochemical alignment of the neighboring olefins. A trifunctional clip, tricarballylic acid (tca) positions 4,4'-bpe molecules in a 1D stacked 'sandwhich' formation to achieve a supramolecular tape. Three molecules of 4,4-bpe are arranged vertically within the tape (Figure 26). The intratape distances between the double bonds of the 4,4'-bpe are 3.82 and 3.80 Å, respectively, while neighboring intertape stacks place the double bonds 3.59 Å apart, but out of position for a [2 + 2] photodimerization. UV-irradiation of the solid affords the tpcb-1a in 90% yield.

Although two-thirds of the olefinic molecules meet the topochemical criteria, a movement of the neighboring tapes during photoreaction may alter the position of the intertape alignment thus placing the unreacted 4,4'-bpe molecules in position for a [2 + 2] photodimerization.

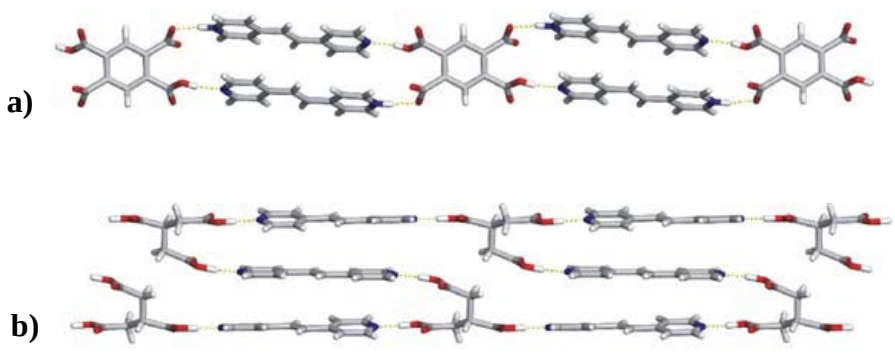

Figure 26. Wireframe representation of hydrogen-bonded tapes in crystals of: a) bta·2(4,4'-bpe); b) tca·1.5(4,4'-bpe).

Recently, Ramamurthy has shown that the solid-state photoreactivity of 4,4'-bpe can be achieved by the use of thiourea (tu) as a template.[78] The basis for using thiourea was to find a universal template that could circumvent 'template switching' by adapting to the movement of neighboring atoms or molecules during a solid-state photochemical reaction, as well as the physical restrictions of the crystal packing. As shown in Figure 27, the co-crystal of (tu)·(4,4'-bpe) reveals that tu serves as an infinite 1D tape sustained *via* nitrogen/sulfur (N-H···S) hydrogen-bonds, that locks the 4,4'-bpe in a suitable position for a [2 + 2] photodimerization. The solid (tu)·(4,4'-bpe) upon exposure to UV-irradiation produces yields up to 90% of tpcb-1a. Though the tu served as an excellent template for the photodimerization of a variety of bpe and stilbazole molecules,

the template lacked the ability to control the orientation of reactant molecules that would otherwise form head-to-head or head-to-tail photoproducts.

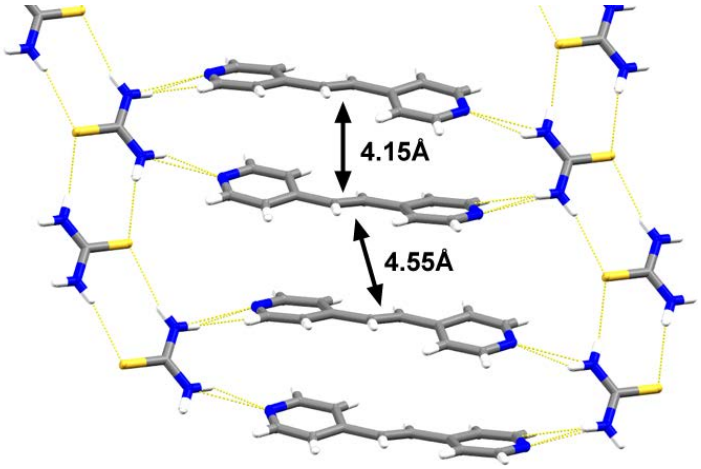

Figure 27. Wireframe representation of packing arrangement of (tu)·(4,4'-bpe).

1.5.3.3. Halogen-Bond Assisted Photoreactions

Despite being weaker than hydrogen bonds, halogen bonds have successfully been employed to direct the arrangement of olefins in the solid state for a [2 + 2] photodimerization.[79] Exploiting the directionality of primarily the intermolecular halogen bond, specifically the nitrogen-iodo (N···I) bond, as well as π···π intramolecular interactions, Resnati *et al.* provided the first well-designed example of directing the formation of 4,4'-bpe using a tetratropic halogen-bonding donor pentaerythritol ether (pete) in the form of a co-crystal of composition (pete)·2(4,4'-bpe).[79] The co-crystal consists of 1D halogen-bonded ribbons with 4'4'-bpe pairs within the assembly in a co-facial alignment with parallel double bonds that meet topochemical distances for a [2 + 2] photodimerization (Figure 28). Exposure of the co-crystalline solid for three hours produces tpcb-1a in 100% yield.

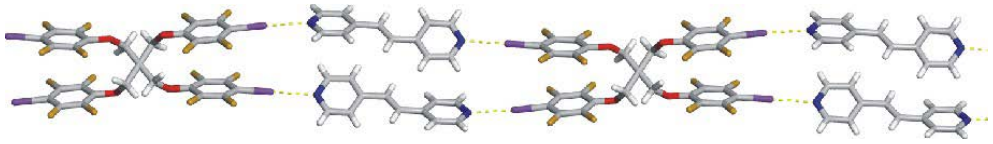

Figure 28. Wireframe model of 1D halogen-bonded polymer chain of co-crystal (pete)·2(4,4'-bpe).

1.5.3.4. Organic Salt Auxiliaries

An infinite arrangement of protonated π-stacked 4,4'-bpe molecules sustained *via* nitrate anions was accomplished by Schröder *et al*. in the form of a salt of composition (4,4'-bpe-H_2)$(NO_3)_2$. The distances between the bpe molecules lie 3.69Å apart (Figure 29).[80] The solid, upon exposure to UV-irradiation after 12 hours, yields 100% of *rctt*-4,4'-tpcb as discovered by Vittal *et al*.[51]

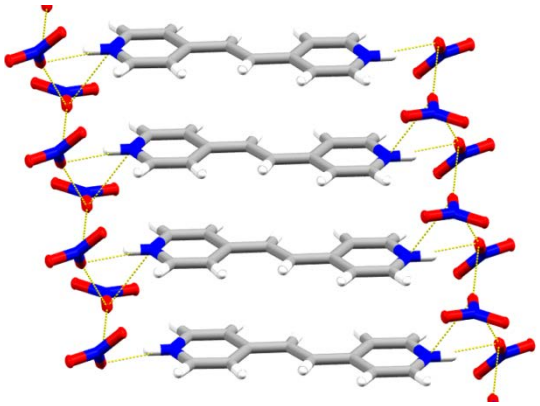

Figure 29. Wireframe perspective of 1D-stack of (4,4'-bpe-H_2)$(NO_3)_2$.

A photostable solid, *trans*-3-(4-pyridyl) acrylic acid (4-PA) is made photoactive by protonation of the pyridyl group with trifluoroacetic acid (CF_3CO_2H) and/or nitric acid (HNO_3) in the form $(C_{10}H_8F_3)(NO_3)$ and $(C_8H_8NO_2)_3(SO_4)(H_2SO_4)(H_2O)$, respectively.[81] The anions served to facilitate

the arrangement of the molecules in a topochemical position suitable for a [2 + 2] photodimerization. Solid $(C_{10}H_8F_3)(NO_3)$ arranges in a head-to-tail fashion, while $(C_8H_8NO_2)_3(SO_4)(HSO_4)(H_2O)$ arranges in a head-to-head orientation (Figure 30). UV-irradiation of the single-crystals of the former results in 100%

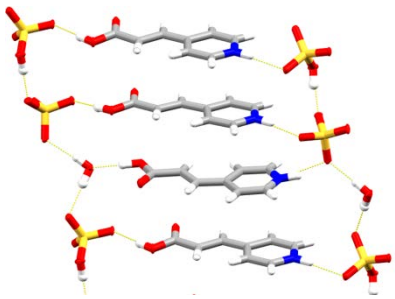

Figure 30. Wireframe infinite head-to-head arrangement of (4-PAH^+).

yields and irradiation of latter provides 66% yield. It was determined that $(C_8H_8NO_2)_3(SO_4)(HSO_4)(H_2O)$, once ground into finely powdered crystalline material, undergoes a cycloaddition in 100% yield. The observation was likely a structural transformation in the crystal lattice as a result of desolvation.[82]

Vittal recently reported the 100% yield of tpcb-1a-H_2^+ from the UV-irradiation of a solid containing protonated 4,4'-bpe molecules sustained by trifluoroacetate in the form $2(4,4'\text{-bpeH}_2)_3 \cdot 2(CF_3CO_2)$ (Figure 31).[83] It was determined that the photoreacted solid dissolved in DMSO-d_6 and heated to 100°C afforded the acid-catalyzed photoproduct *rtct*-4,4'-tpcb (tpcb-1b) (Figure 31).

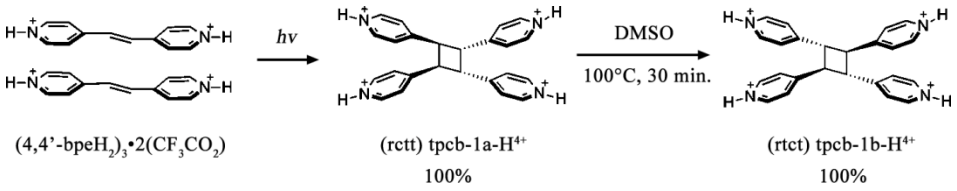

Figure 31. Schematic representation of solid-state photoreaction of salt $2(4,4'\text{-bpeH}_2)_3 \cdot 2(CF_3CO_2)$ that affords tpcb-1a and acid-catalyzed tpcb-1b.

1.5.3.5. Solid-State Reactivity in Perspective

Chemists have demonstrated creative approaches towards the synthesis of organic molecules based on [2 + 2] photodimerizations in the solid-state. The many approaches listed in this chapter demonstrate the versatility of using the solid-state as a medium for reactivity. The use of auxiliaries has been the primary means to overcome the effects of the crystal lattice. Despite the emergence of many routes to obtain photodimerized products, the use of ditopic templates has remained the most modular, efficient, and versatile system to counter the effects of crystal packing. This is also demonstrated by the fact that all of the auxiliaries available, only the resorcinol-based ditopic templates have successfully been employed for the synthesis of ladderanes.

1.6. Applications of Products Derived from Template-Directed Synthesis

It has been demonstrated that template-directed synthesis can provide access to photoproducts in stereo- and regioselective quantitative yields. In addition, a highly appealing feature of the photoproducts is that 1) they are lined with functional groups in the form of mainly pyridyl groups and carboxylic acids of which are hydrogen bond acceptor and/or donor sites, 2) they contain rigid cyclobutanes that in combination with the functional group substituent provide a high degree of directionality. With this in mind, the products are promising as

precursors to complex molecules, molecular building blocks for the construction of metal organic frameworks (MOFs), and metal organic polyhedra (MOP) which have become increasingly important (*i.e.* gas storage) and/or hydrogen-bond based self-assembled structures.[84-89] In fact, we have demonstrated that our pyridyl-functionalized products from a template-directed synthesis can effectively be incorporated into MOFs or MOPs and a recent application involves the formation of a hydrogel.[86,90-96]

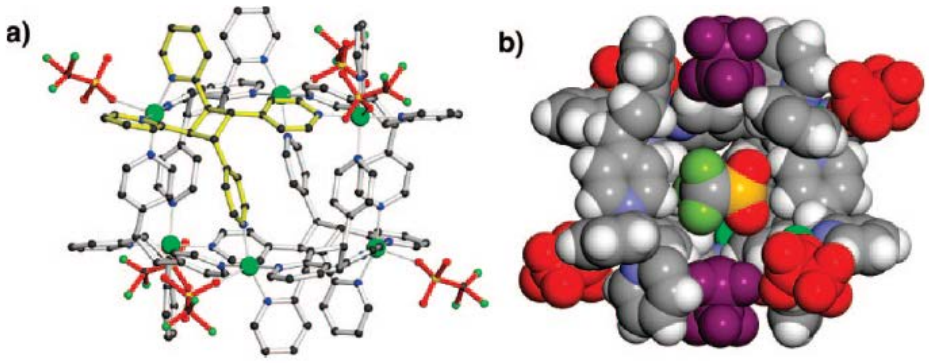

Figure 32. X-ray structure of MOP $[Cu_6(2,4'\text{-tpcb})_6(CF_3SO_3)_6](CF_3SO_3)_6 \cdot 18H_2O$: a) Ball and stick model depicting 2,4'-tpcb in yellow and $CF_3SO_3^-$ in red and b) cut-away showing capping $CF_3SO_3^-$ anions (purple) and $CF_3SO_3^-$ guest (green = Cu, yellow = S, yellow-green = F, red = O, blue = N, gray = C, white = H).[94]

1.7. The Scope of the Dissertation

This thesis aims to bridge organic synthesis and supramolecular chemistry. In this context, the objective of this research has been to determine the reactivity of pyridyl-functionalized ladderanes derived from a template-directed synthesis, to apply mechanochemistry to generate reactive co-crystals, to use co-crystallization as a means to authenticate a chiral ladderane that resists crystallization, and to explore the reactivity of hydrogen-bond donor diolefin reactants using hydrogen-bond acceptor templates.

Chapter 2 focuses on reactivity of a [5]-ladderane and a model monocyclobutane system, in the presence of *meta*-chloroperoxybenzoic acid (*m*-CPBA), glacial acetic acid (AcOH), and hydrogen peroxide (H_2O_2). In the presence of *m*-CPBA the pyridyl substituents of the ladderane become oxidized to afford pyridyl-*N*-oxides with retention of stereochemistry, while treatment with AcOH to the ladderane, induces isomerization to afford two structurally ambiguous stereoisomers, an achiral and a chiral. The achiral ladderane crystallizes as a benzene solvate, however the chiral ladderane resists crystallization. Treatment with H_2O_2 in an AcOH medium produces both isomerized and oxidized products.

Chapter 3 deals with the growth of single crystals for the structural determination of a chiral ladderane that resists crystallization *via* co-crystallization. A co-crystal strategy is designed based on a co-crystal former (CCF) that provides access to carboxylic acid-pyridine synthon interactions and an ordered lattice that facilitates the growth of single crystals.

Chapter 4 describes the organic solid-state reactivity of a carboxyl-functionalized 1,3-butadiene with and without the use of HBA templates. In continuation of work previously explored to determine the solid-state reactivity of the diacid monoolefin fum, we set to use HBA templates to arrange a diacid diolefin in a position that permits a [2 + 2] photodimerization. We discovered that the diacid in pure form produces an unusual bicyclobutyl photoproduct. We used a co-crystal to confirm the structure of the bicyclobutyl hexaacid. Co-crystallization of the diacid with the HBA templates achieved the formation of a reactive solid as well as photostable solids.

Chapter 5 explores the generality of the application of mechanochemistry to a solid-state template-directed synthesis. Given that the template-directed solid-state synthesis is recognized as an efficient, modular, and solvent-free

process for generating stereospecific photoproducts in quantitative yields, we set to apply mechanochemical methods to further reduce the amount of solvent necessary to obtain photoproducts. We will show how the application of mechanochemistry eliminates or reduces the amount of solvent needed to generate photoactive co-crystals from a template-directed synthesis.

CHAPTER 2: ACID-INDUCED ISOMERIZATION OF RCTT-4-PYRIDYL-[5]-LADDERANE

2.1. Introduction

n-Ladderanes (*i.e.*, where *n* = 3, 4, 5, ...) are strained molecules composed of *n* edge-fused cyclobutane rings (Figure 33).[67] Ladderanes have been identified as building blocks of optoelectronic materials and, very recently, discovered in natural products, being integral components of marine bacteria.[70,71,97] The ladderanes in the bacteria are present as lipids, serving a structural role of providing extraordinary rigidity to internal membrane components.[98]

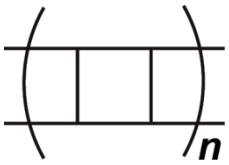

Figure 33. Schematic representation of *n*-ladderane (where n ≥ 3).

Computational studies have also demonstrated that ladderanes can exhibit novel forms of fluxional behavior.[99] The unusual structures of ladderanes have made these molecules appealing from a variety of perspectives.[97] Whereas the properties and potential applications of ladderanes are of growing interest, efficient synthetic routes have remained elusive.[100-102] Difficulties to synthesize ladderanes generally arise from controlling the oligomerization of alkene and/or alkyne precursors into the prerequisite polycyclobutane skeleton.[67,69]

In this context, Gao *et al*. reported in 2004 the syntheses of ladderanes in the organic solid state.[103] They showed that small molecule templates based on resorcinol can assemble functionalized polyenes *via* hydrogen bonds into

supramolecular architectures suitable for intermolecular [2+2] photodimerizations that generate [3]- and [5]-ladderanes (Figure 34). Co-crystallization of 5-methoxyresorcinol (5-OMe-res) with either an all-*trans* terminal 4-pyridyl-substituted 1,4-butadiene or 1,6-hexatriene yielded four-component hydrogen-bonded molecular assemblies of general composition 2(template)·2(polyene). UV-irradiation of the crystalline assemblies produced the corresponding end-functionalized C_{2h}-symmetric ladderanes stereospecifically, in quantitative yield, and in gram amounts. This method takes advantage of the principles of crystal

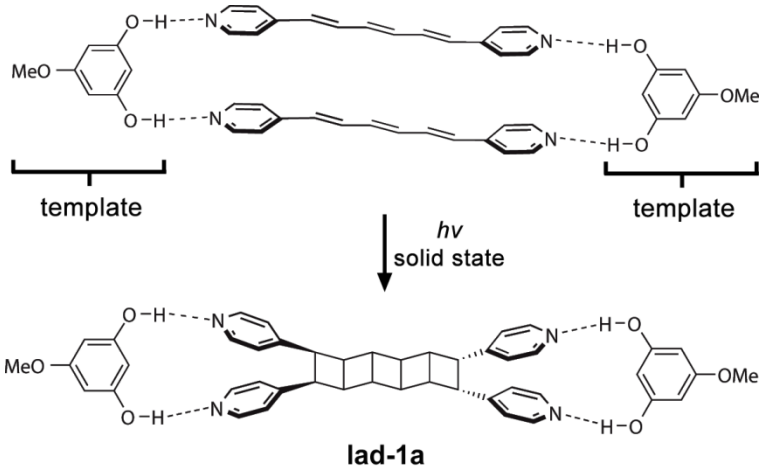

Figure 34. Schematic involving template-directed solid-state synthesis of lad-1a from a triene precursor.

engineering, specifically, the directionality of hydrogen bonds and the constrained, yet flexible, environment of the solid state to produce ladderanes with high efficiency. The ladderanes that are generated in the solid state are cumbersome to make using conventional methods of organic synthesis.[67] Difficulties are evidenced by the fact that ladderanes lacking internal functional groups,[104] such as those in the natural products, are rare, with exceptions being

ladderanes derived from intramolecular reactions of cyclophanes.[69] Recent reports by Corey on the first total and enantioselective syntheses of the most abundant of the ladderane lipids, as well as attempted syntheses from polyenes in solution and the solid state, highlight these difficulties.[100,101]

In this chapter, solution-phase reactivity studies of ladderanes, as well as related studies on a model monocyclobutane, will be demonstrated. A general goal is to apply post synthetic modifications to ladderanes so as to provide efficient synthetic access to ladderane derivatives derived from our solid-state preparation. Moreover, that we can generate the ladderanes stereospecifically and in large amounts means that our method is attractive to produce more complex ladderane structures. We expect the synthesis of these unique molecules to provide applications such as precursors to the natural products and serve as ligands for metal-organic framework (MOF) materials.

2.1.2. Approaches to Synthesize Ladderanes

Early synthetic approaches to the formation of ladderanes involved the use of cyclobutene or cyclobutadiene precursors as building blocks.[67] In 1964, Nenitzescu *et al.* reported that the treatment of sodium or lithium amalgam to cyclobutene dichloride affords a *syn* or *anti* diene, respectively (Figure 34).[105] Subsequent hydrogenation of the dimers afforded the *syn*- and *anti*-[3]-ladderanes isomers. It is important to note ladderane nomenclature prior to the work of Hopf,[67] included cyclobutene rings in the total number of ladderane rings.[106]

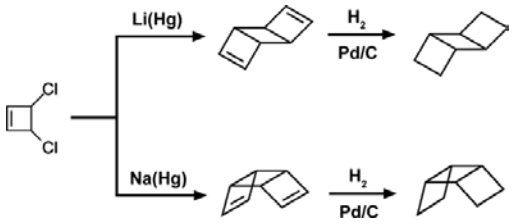

Figure 35. Schematic representation of the synthesis of [3]-ladderane isomers from cyclobutene dichloride precursor.

In 1965, it was determined by Fitzpatrick *et al*. that the cyclobutadiene-iron complex in the presence of cesium(IV) and a substituted alkyne react to produce the 4-fused ring pterodactyladiene. Hydrogenation of the dienes affords a [4]-ladderane (Figure 36).[107]

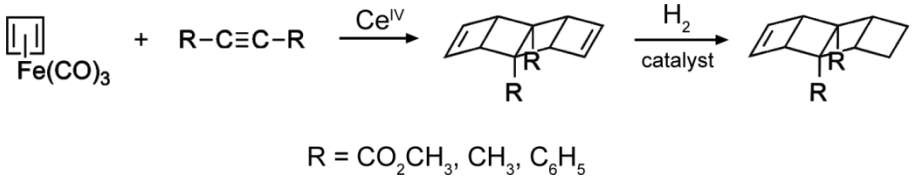

Figure 36. Schematic representation of ladderane formation *via* cyclobutadiene-iron complex.

Eight years later, in order to study the thermolytic behavior of pterodactyladienes, Martin *et al*. determined that pterodactyladiene could be produced from a reaction of dewar benzene with cyclobutadiene,[108] as well as expanding the reactivity of cyclobutadiene-iron complexes involving *s*-tetrazines.[109] An alternative route was introduced to produce the synthesis of pterodactyladienes beginning with a photochemical step involving acetylene and maleic anhydride precursors to produce the two-ring fused dianhydride (Figure 37).[110] A series of steps involving a conversion of the dianhydride to the

dithioester, followed by treatment with *N*-chlorosuccinimide, and Ramburg–Bäcklund ring contraction provided the four-ring fused pterodactyladiene.

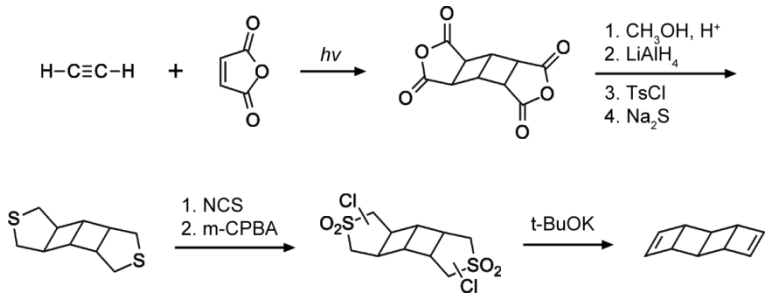

Figure 37. Schematic representation of synthetic route to pterodactyladiene.

In 1990, Warrener synthesized several ladderane motifs with the incorporation of norbornane.[111-113] When the norbornane-fused cyclobutene 3,4-diester was treated with cyclobutadiene, the major product was treated with dimethyl acetylenedicarboxylate (DMAD) in the presence of a Ru^0 catalyst (Figure 38).[113] The sequence is repeated to afford a stereocontrolled synthesis of a [9]-ladderane. In a later report aza[3]- and [5]-ladderanes were synthesized using a similar procedure.[114]

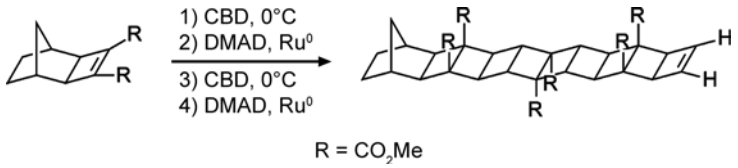

Figure 38. Reaction schematic depicting tandem synthetic route to norbornane-fused ladderane (CBD = cyclobutadiene).

Mehta *et al.* introduced a controlled oligomerization for the purpose of achieving longer ladderanes with the use of a iron-tricarbonyl cyclobutadiene.[104]

When the iron was released from the complex, dimethyl 1,2-cyclobutadienedicarboxylate oligomerization of the cyclobutadiene in the presence of cerium(IV) ammonium nitrate (CAN) afforded odd numbered [3]-, [5]-, and [7]-ladderanes in 55% yield (3:2:1 ratio), respectively (Figure 39). Metha later discovered that by varying the concentration and lowering the temperature oligomers could be obtained, specifically six odd-membered [3]-, [5]-, [7]-, [9]-, [11]-, [13]-ladderanes in 2, 4, 19, 22, 11, and 2% yield, respectively (Figure 39), also [6]- and [8]-ladderanes were obtained from an 'end-correction' sequence.[115] In another report, [3]-, [5]-, and [7]- ladderanes were found to undergo thermal-induced reorganization upon thermolysis.[116] Fox *et al*. further investigated the chromophoric behavior of naphthalene derivatives of the [3]-, [5]-, [7]- and [9]-ladderanes.[117]

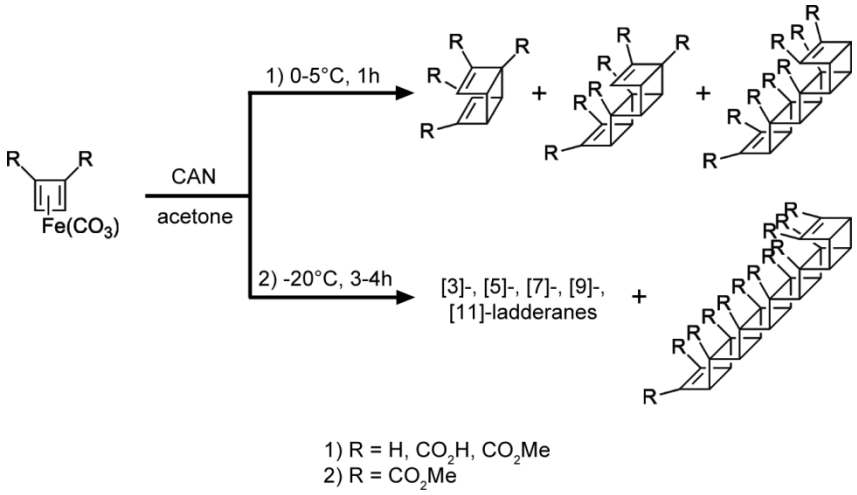

Figure 39. Schematic of cyclobutadiene reaction pathway to various ladderanes.

The syntheses of fluoro-functionalized [3]-ladderanes was reported by Weigert[118] and Antipin.[119] Treatment of perfluoro-1,3-butadiene with 1,3-butadiene affords a *syn*- and *anti* -isomers of the tricyclooctane, as intermediate

fractions, and heating of hexafluoro-1,3-butadiene to 150°C for 120 hours, produces the dodecafluorotricyclooctane as a mixture of products in 4% yield (Figure 40).

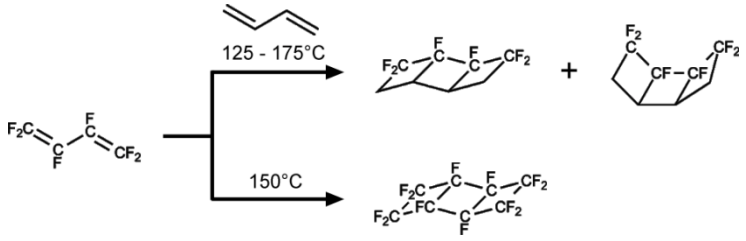

Figure 40. Schematic involving perfluoro-1,3-butadiene to obtain [3]-ladderanes.

2.1.3. Naturally Occurring Ladderanes

In 2002, based on findings in a wastewater treatment plant, Damasté *et al.* reported the discovery of naturally occurring ladderane lipids in the ANAMMOX (anaerobic ammonium oxidizing) bacteria, that served to mediate the permeability of toxic intermediates hydroxylamine and hydrazine during the catabolism of inorganic nitrogen to nitrogen gas.[70,71,120] Located in the intracellular compartment of the bacteria called the anammoxasome, the ladderanes were postulated to efficiently pack such as to provide an exceptionally dense membrane (Figure 41).[98] The slow metabolism of the bacteria make the high density of the biomembrane critical for the survival of the cell. The ladderanes contain *cis* fused junctions ranging from three to five fused cyclobutane rings.

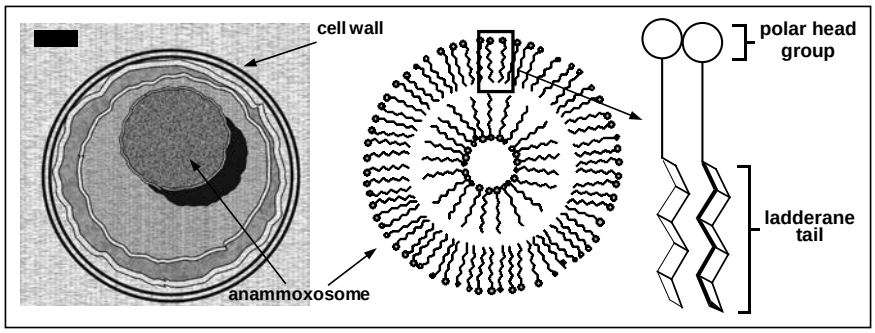

Figure 41. Model of the anammox cell (left) (scale bar, 100 nm), anammoxosome membrane (center), and two ladderane lipids (right).

2.1.3.1. Total Synthesis of Pentacycloanammoxic Methyl Ester

The most abundant of the ladderane lipids in two strains of *Candidatus* 'B. anammoxidans' is the pentacycloanammoxic methyl ester (Figure 42).[70] Due to the lack of sufficient material available for study, the absolute configuration has not been experimentally determined.[100,101,120] The biosynthetic pathway of these unique molecules is also unknown.

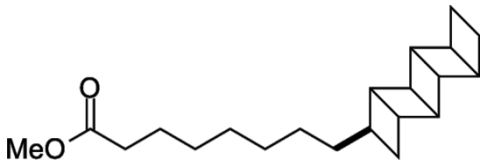

pentacycloanammoxic methyl ester

Figure 42. Schematic representation of one of the naturally occurring ladderanes.

In 2004, for the purpose of providing sufficient material for biochemical and biophysical investigations, Corey developed the first total synthesis of the (±)-pentacycloanammoxic ester, involving 15 steps in 2.2 % yield.[100] The most

challenging portion of the synthesis was the formation of the ladderane scaffold. The limiting step was the photochemical initiated reaction involving a nitrogen extrusion reaction to afford the ladderane in 6 % yield (Figure 43). Later, Corey achieved the enantioselective synthesis of the ester involving 16 steps in total yield of 2.24 %.[101] The development of the enantioselective route was an improvement; however, the yield remained relatively low.

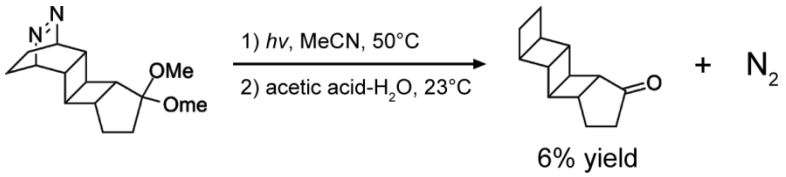

Figure 43. Schematic representation of nitrogen extrusion step in the first total synthesis of pentacycloanammoxic ester.

2.1.4. Topochemical Reactions

In 1995, Hopf *et al*. achieved the synthesis of [3]- and [5]-ladderanes by covalently linking two polyenes to a [2.2]cyclophane scaffold for an intramolecular [2 +2] photodimerization.[69] Inspired by the work of Schmidt, Hopf investigated topochemical reactions in solution. It was determined that by covalently linking mono- and polyolefins *via* a pseudo-geminal [2.2]paracyclophane or cinnamophanes, the double bonds are placed in position for a topochemical [2+2] photodimerization (Figure 44). The paracyclophane serves to reduce movement of the double bonds in solution. The influence, however, of the cyclophane is reduced as the number of olefins increase. Full spectroscopic details of the pseudo-*geminal* cinnamophanes,[121] as well as additional reactivity studies involving pseudo *ortho-*, *meta-*, and *para-* cinnamophanes[68] synthesis were published in later work.

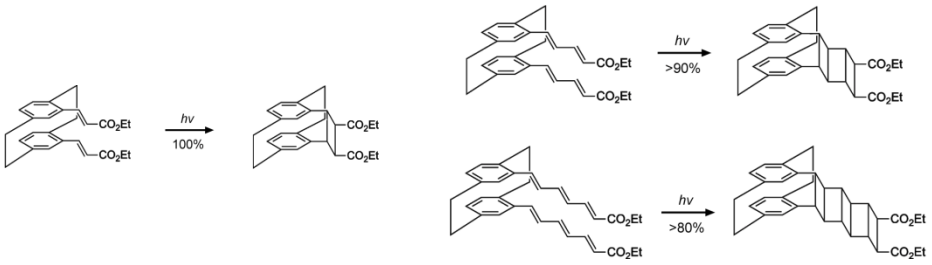

Figure 44. Schematic reactions of paracyclophane directed [2 + 2] photodimerizations of mono- and polylenes.

In 2002, Vishnumurthy *et. al.* induced the [2 + 2] photodimerization of all *trans* 1,3-butadiene derivatives (1*E*,3*E*)-1-pentafluorophenyl-4-(4-methoxyphenyl)buta-1,3-diene, (1*E*,3*E*)-1-pentafluorophenyl-4-(4-methylphenyl)buta-1,3-diene, and (1*E*,3*E*)-1-pentafluorophenyl-4-phenylbuta-1,3-diene by use of fluorine substitution.[57] The phenyl-perflourophenyl arrangement dictates head-to-tail orientations in each case (Figure 45). Exposure to UV-irradiation of the solids provided the photoproducts that resemble molecular ladders (23-25% yields).

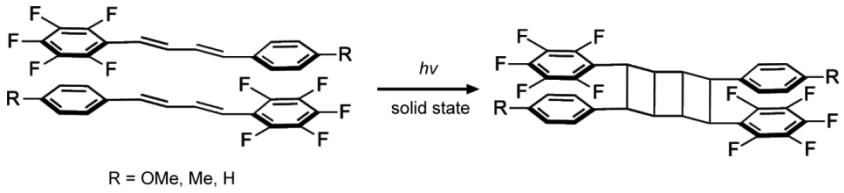

Figure 45. Schematic involving intermolecular construction of [3]-ladderane *via* phenyl-perfluorophenyl interactions.

In 2006, Erker *et al*. attached butadienyl substituents on cyclopentyl (Cp) metallacene rings to position the dienes for a [2 + 2] photodimerization in solution.[122] As confirmed by NMR spectroscopy, irradiation of

bis(butadienylcyclo-pentadienyl) dichlorozirconium in dichloromethane at -80°C afforded the [3]-ladderane, a cyclooctadiene, and a tricyclooctandiyl moiety in 36, 25, and 20% yields, respectively (Figure 46).

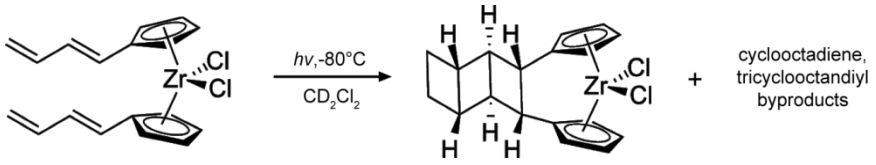

Figure 46. Schematic representation of topochemical [3]-ladderane reaction in solution *via* organometallic cyclopentyl-zirconium complex.

In relation to the natural product synthesis of pentacycloanammoxic acid, to circumvent difficulties associated with the formation of the ladderane scaffold from solution, Corey explored topochemical routes *via* solid state photochemistry.[102] The first attempt was to dimerize the diene (2*E*,4*E*)-methyl-5-(3-methoxyphenyl)penta-2,4-dienoate (mpd) to form the photoproduct (Figure 47). It was determined the reaction affords a head-to-tail monocyclized product in 63% yield.

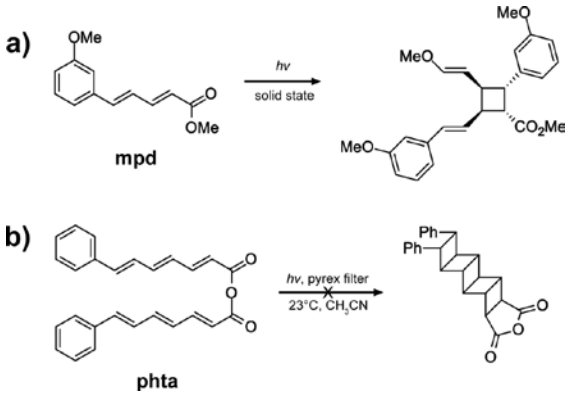

Figure 47. Schematic depiction of solid-state reaction involving a) the formation of a monocyclized product from a dienoate precursor; b) photostable trienoate.

Corey next attempted to dimerize the trienoate (2*E*,4*E*,6*E*)-7-phenylhepta-2,4,6-trienoic anhydride (phta) shown in Figure 47. UV-irradiation of phta yielded polymeric materials. X-ray analysis of the trienoate before photoreaction revealed the molecules arranged in a head-to-head fashion, however, with the exception of one olefin, the distance between the double bonds did not meet the topochemical criteria for photoreaction. It was reasoned that connecting the polyolefins with an anhydride linker at one end would position the double bonds in close proximity for an intramolecular [2+2]photocycloaddition. A cyclobutane was not obtained, as confirmed *via* X-ray crystallography. To attempt to achieve further control over the position of the triene, an anhydride was added to both termini to generate the macrocycle all *trans*-3,16-di-tert-butyl-1,5,14,18-tetraoxacyclohexacosa-7,9,11,20,22,24-hexaene-6,13,19,26-tetraone (*t*-b-tetraone) for an intramolecular photochemical reaction. X-ray crystallography revealed distances of 5.17, 5.21, and 5.26 between the double bonds (Figure 48). The distances showed that the double bonds were well outside the criteria for a photoreaction.

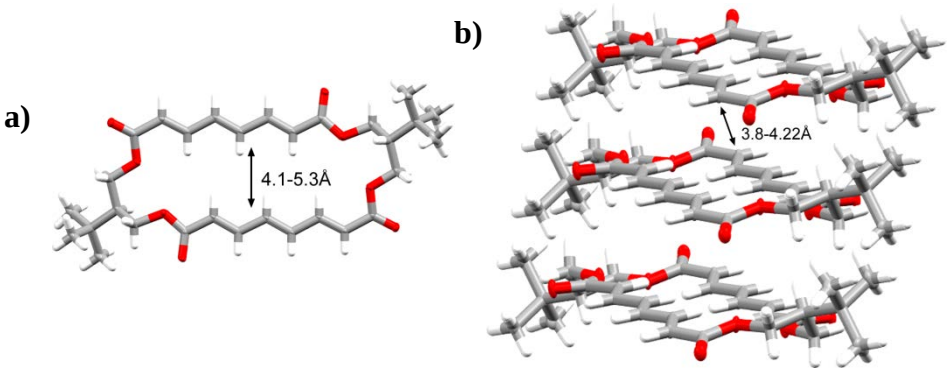

Figure 48. Wireframe model of ester-functionalized macrocycle: a) intramolecular distance between double bonds; b) intermolecular distance between vertically stacked macrocycles along the *c*-axis.

2.1.5. Developments and Applications of Our Ladderanes

Having established that the ladderanes derived from a template-directed synthesis are formed in quantitative yields and can be easily removed from the template, these molecules provide an excellent opportunity for the construction and design of complex molecular targets (e.g. MOFs, natural products). To realize this goal, it will be important to determine reactivities of the ladderanes. In this context, Vittal *et al*. had shown that treatment of the related monocyclic tpcb-1a with trifluoroacetic acid results in an acid-catalyzed isomerization of tpcb-1a to a give a mixture of two stereoisomers; namely, the tpcb-1b and *rcct*-4,4'-tpcb (tpcb-1c) products in 10% yield (Figure 49).[123] In later experiments, a salt in the form of trifluoroacetic acid and 4,4'-bpe was irradiated to afford the monocyclized product $[\text{tpcb-1a-H}_4]^{4+}$.[83] Heating a solution of this photoproduct in DMSO-d_6 for 30 minutes yielded 100% of the isomerized product tpcb-1b. With this mind, using the structurally similar

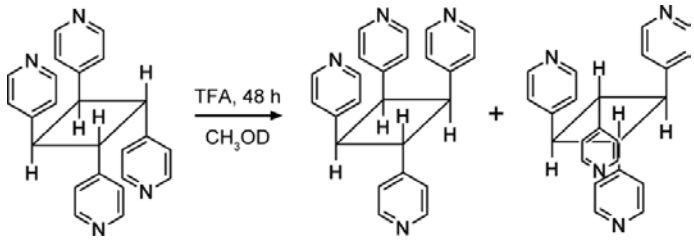

tpcb-1a ***(rctt)*** **tpcb-1c** ***(rcct)*** **tpcb-1b** ***(rtct)***

Figure 49. Schematic depicting acid-catalyzed isomerization of tpcb-1a.

monocyclobutane analog as a model system, we sought to determine whether treatment of lad-1a with acid results in an isomerization of the cyclobutane rings of the ladderane that, in turn, could eventually be used as an entry to more complex products.

2.1.6. Chapter Overview

In this chapter, we describe the synthesis of [5]-ladderane and monocyclobutane derivatives derived from a series of reactivity experiments involving the treatment of various acids to lad-1a and tpcb-1a obtained from the solid state (Figure 50). Solution NMR spectroscopy and density-functional theory (DFT) calculations support the isomerization to generate two diastereomers, an achiral lad-1b and chiral lad-1c ladderane from the C_{2h}-symmetric lad-1a. The NMR data, however, could not lead to unambiguous configurational assignments of the two isomers. Single-crystal X-ray diffraction was employed to determine each configuration. One isomer readily crystallized as a pure form and X-ray diffraction revealed lad-1b as being achiral based on C_i symmetry. The second isomer chiral lad-1c expected to have C_2 symmetry resisted crystallization under a variety of conditions as a pure form. ^{1}H NMR spectroscopy suggest that treatment of lad-1a with peroxyacid (H_2O_2) in an AcOH medium produced both oxidized and isomerized ladderanes achiral lad-2a and chiral lad-2b pyridyl-*N*-oxides, while treatment of lad-1a with *meta*-peroxybenzoic acid (m-CPBA) produced oxidized ladderane lad-2c with retention of stereochemistry as confirmed by X-ray crystallography. We show how a model monocyclobutane system, specifically, tpcb-1a, can be used to guide the synthesis of the [5]-ladderane derivatives.

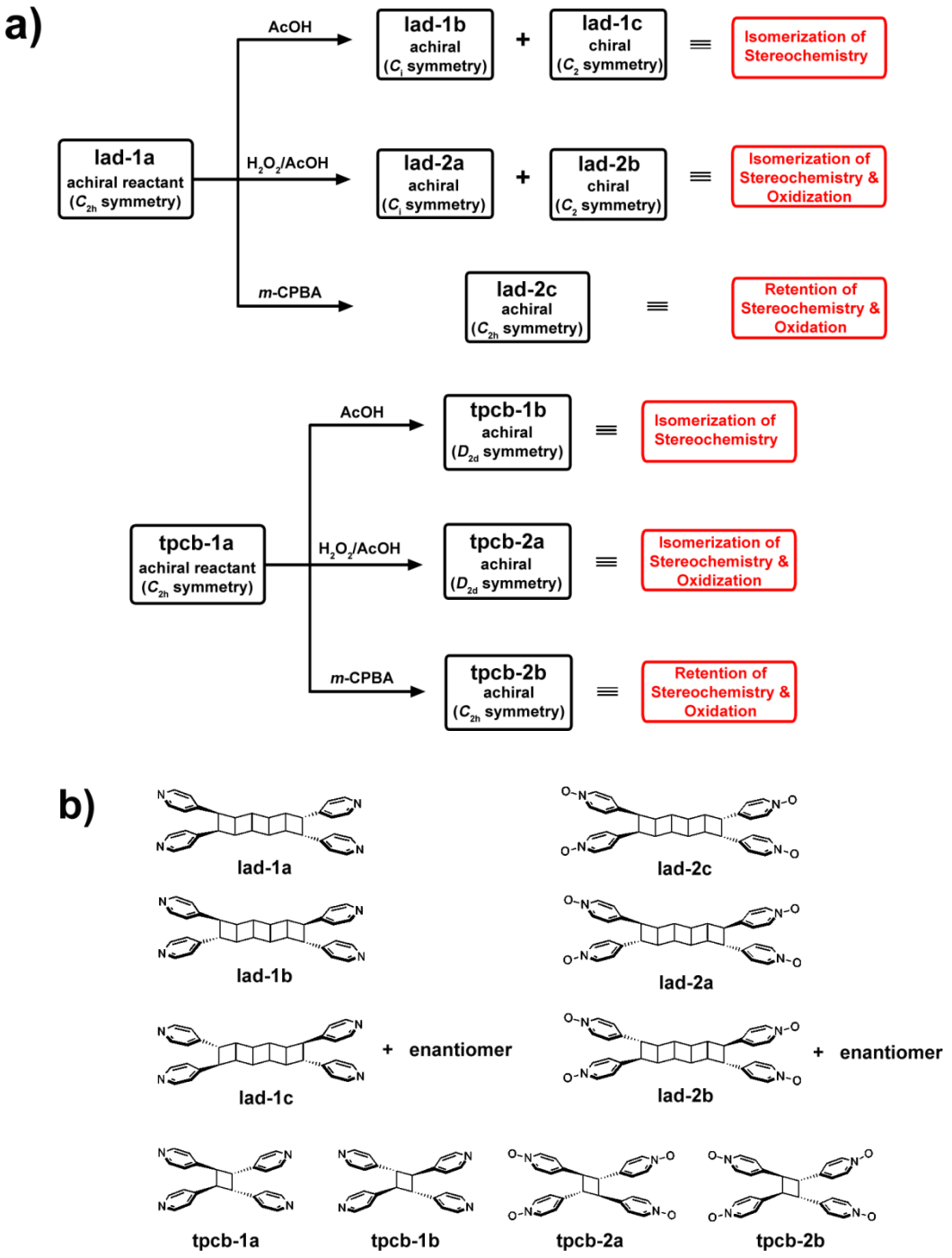

Figure 50. Schematic of a) reactivities of a lad-1a and tpcb-1a b) structures of lad-1a and tpcb-1a derivatives

2.2. Experimental

2.2.1. General Procedure

Reagents glacial acetic acid (ACS reagent, ≥ 99.7%, Sigma-Aldrich), hydrogen peroxide (30 wt. % in H_2O, ACS reagent, Sigma-Aldrich) , Sigma-Aldrich), *meta*-chloroperoxybenzoic acid (≥ 99%, Aldrich Chemical Co.), acetonitrile (ACS reagent, ≥ 99.5%, Sigma-Aldrich), benzene (anhydrous, 99.8%, Sigma-Aldrich). All products were characterized using Avance-400 and Avance-600 Bruker NMR spectrometers (Billerica, MA) operating at 400 and 600 MHz, respectively. ^{1}H and ^{13}C chemical shifts were referenced with the residual proton and carbon chemical shifts of the solvents (DMSO-d_6, ^{1}H, 2.50 ppm; ^{13}C, 39.5 pm). Fractions with milligram quantities of the product were characterized by a battery of 1D and 2D homonuclear and ^{1}H-^{13}C heteronuclear experiments [^{1}H, 1D correlated spectroscopy (COSY), nuclear Overhauser effect spectroscopy (NOESY), ^{13}C, ^{13}C-distortionless enhancement by polarization transfer (DEPT), heteronuclear multiple quantum coherence (HMQC), and heteronuclear multiple bond correlation (HMBC)]. Gradient-assisted versions of the pulse sequences and inverse detection were used for these 2D experiments. Typical parameters for the NMR experiments were as follows: ^{1}H (TD, 64k; NS, 4k), ^{13}C (TD, 128k; NS, 10000), ^{13}C-DEPT (TD, 128k; NS, 5000), 1D COSY (TD, 64k; NS, 512), NOESY (TD, 2k; TD1, 256; NS, 32; DS, 32; mixing times, 1.0, 1.5, and 2.0s), ^{13}C-^{1}H HMQC (TD, 2k; TD1, 128; NS, 32; DS, 128); and 13C-1H HMBC (TD, 2k; TD1, 128; NS, 32; DS, 128). TD, NS, and DS refer to time domain data points, number of scans, and dummy scans, respectively. All of NMR data were processed with TOPSPIN 1.3 suite of software programs. 1D ^{1}H data were processed with zero-filling to 64k data points and 0.2 Hz exponential line broadening, whereas ^{13}C spectra were processed with zero-filling to 128k data

points and 1.0 Hz of exponential line broadening. The 2D NMR data were processed with the zero-filling to 2048 points and 1024 points in acquisition and second dimension, respectively. Relative numbers of proton signals multiplied by the integral areas were used for the quantification.

2.2.2. Synthesis of *r(eq)ttc*-tetrakis(4-pyridyl)[5]-ladderane (lad-1b)

In a closed reaction vessel, lad-1a (100 mg, 0.21 mmol) was dissolved in 1 mL of glacial acetic acid (AcOH). The reaction solution was stirred in a closed vessel for 12 hours at 50°C. The reaction solution was quenched by the addition of excess 1 molar potassium hydroxide solution (30 mL) to achieve an off white precipitate lad-1b and lad-1c. The off white precipitate was filtered, washed with 30 mL of distilled water, and dried to yield 97 mg. The dried precipitate was dissolved in 10 mL of acetonitrile and allowed to slowly evaporate overnight to afford lad-1b in 35% yield (35 mg, 0.07 mmol). ^{1}H NMR (DMSO-d_6, 600 MHz) δ 8.52 (d, J = 5.6 Hz, 1H), 8.48 (d, J = 5.4 Hz, 1H), 7.34 (d, J = 5.4 Hz, 1H), 7.24 (d, J = 5.6 Hz, 1H), 4.20 (dd, J = 8.7 Hz, 8.7 Hz 1H) two peaks are overlapped, 3.97 (dd, J = 8.9 Hz, 3.1 Hz 1H), 3.20 (dd, J = 8.4 Hz, 3.8 Hz 1H), 2.91 (s, 1H), 2.77 (s, 1H), 2.61 (s, 1H); ^{13}C NMR (DMSO-d_6, 600 MHz) δ 153.3, 149.5, 149.4, 149.2, 122.0, 121.6, 48.3, 46.9, 46.1, 43.1, 41.8, 41.4.

2.2.3. Synthesis of *r(eq)tct*-tetrakis(4-pyridyl)[5]-ladderane (lad-1c**)**

The remaining filtrate from the reaction above was evaporated to dryness to afford an off white crude amorphous solid (35 mg, 0.07 mmol, 35 %). ^{1}H NMR (DMSO-d_6, 600 MHz) δ 8.51 (d, J = 6.0 Hz, 1H), 8.48 (d, J = 5.4 Hz, 1H), 7.37 (d, J = 5.4 Hz, 1H), 7.22 (d, J = 6.0 Hz, 1H), 4.18 (dd, J = 8.7 Hz, 8.6 Hz 1H) two peaks are overlapped, 4.00 (dd, J = 8.7 Hz, 3.2 Hz 1H), 3.17 (dd, J = 8.6

Hz, 3.6 Hz 1H), 2.90 (s, 1H), 2.87 (s, 1H), 2.48 (s, 1H); ^{13}C NMR (DMSO-d_6, 600 MHz) δ 153.3, 149.8, 149.7, 149.6, 122.4, 122.1, 48.1, 47.2, 46.1, 43.8, 42.4, 42.1.

2.2.4. Synthesis of *r(eq)ttc/rtct*-tetrakis(4-pyridyl)[5]-ladderane-*N*-oxide mixture (lad-2a, lad-2b).

In a closed reaction vessel, lad-1a (150 mg, 0.320 mmol) and H_2O_2 (0.235 mg, 1.6 mmol) were dissolved in 2 mL of glacial AcOH.[124,125] The reaction was stirred and allowed to heat for approximately 12 hours at 50°C. The solution was evaporated to dryness to afford a mixture of lad-2a and lad-2b. (167 mg, 0.31 mmol, 98 %). ^{1}H NMR (DMSO-d_6, 400 MHz): δ 8.5 (m, 1H), 8.15 (m, 1H), 7.72 (m, 1H), 7.42 (m, 1H), 7.30 (m, 1H), 4.16 (m, 1H), 3.93 (m, 1H), 3.21 (m, 1H), 2.80 (m, 1H), 2.75 (m, 1H).

2.2.5. Synthesis of *r(eq)ctt*-tetrakis(4-pyridyl)[5]-ladderane-*N*-oxide (lad-2c)

In a closed reaction vessel, lad-1a (100 mg, 0.213 mmol) and m-CPBA (185 mg, 1.067 mmol) were dissolved in 2 mL of dichloromethane.[125,126] The reaction was allowed to stir at 25°C for approximately 12 hours. The solution was evaporated to dryness and washed three times with hot acetone. The crude yellow solid was filtered and dried. Recrystallization in DMF afforded clean lad-2c (63 mg, 0.11 mmol, 55%). Single crystals were grown from a mixture of water:ethanol (1:10) (32.5 mg, 0.06 mmol, 28%). ^{1}H NMR (D_2O, 400 MHz): δ 8.11 (d, 6.2 Hz, 1H), 7.36 (d, 6.4 Hz, 1H), 4.54 (s, 1H), 3.40 (s, 1H), 3.22 (s, 1H).

2.2.6. Synthesis of *rtct*-4,4'-tetrakis(4-pyridyl)cyclobutane

Compound tpcb-1a (100 mg, 0.27 mmol) was prepared according to the literature.[59] In a closed reaction vessel, tpcb-1a was dissolved in 2 mL of glacial

AcOH. The reaction solution was heated for 12 hours at 50°C. The reaction solution was neutralized with an excess of 1M potassium hydroxide solution, filtered, and dried. Recrystallization from benzene afforded rtct-4,4'-tpcb (89 mg, 0.24 mmol, 89 %) as colorless crystals. 1H NMR (DMSO-d6, 400 MHz): δ 8.51 (d, 5.3 Hz, 1H), 7.41 (d, 5.4 Hz, 1H), 3.85 (s, 1H); 13C NMR (DMSO-d6, 400 MHz): δ 149.8, 149.0, 122.5, 48.75.

2.2.7. Synthesis of *rtct*-4,4-tetrakis(4-pyridyl)cyclobutane-*N*-oxide (tpcb-2a).

In a closed reaction vessel, tpcb-1a (1 g, 2.7 mmol) and 30% H_2O_2 (v:v) (2 mL, 13.5 mmol) were dissolved in 2 mL of glacial AcOH.[124] The reaction was stirred and allowed to heat for approximately 12 hours at 50°C. The solution was evaporated to dryness and washed three times with hot acetone. The solid was filtered and dried. Recrystallization from a mixture of water:isopropanol (1:12) afforded tpcb-2a (0.85 g, 1.98 mmol, 72 %). ^{1}H NMR (D_2O, 400 MHz): δ 8.33 (d, 7.2 Hz, 1H), 7.63 (d, 8 Hz, 1H), 4.16 (s, 1H).

2.2.8. Synthesis of *rctt*-tetrakis(4-pyridyl)cyclobutane-*N*-oxide (tpcb-2b).

In a closed reaction vessel, tpcb-1a (50 mg, 0.14 mmol) and m-CPBA (118 mg, 0.137 mmol) were dissolved in 2 mL of dichloromethane. The reaction was allowed to stir at 25°C for approximately 12 hours. The solution was evaporated to dryness and washed three times with hot acetone. The solid was filtered and dried. Recrystallization from a mixture of methanol:toluene (1:1) provided tpcb-2b (25 mg, 0.05 mmol, 43%). ^{1}H NMR (D_2O, 400 MHz): δ 8.21 (d, 7.6 Hz, 1H), 7.51 (d, 7.2 Hz, 1H), 4.91 (s, 1H).

2.2.9. X-ray Crystallography

All crystal data were collected on a Nonius KappaCCD single-crystal X-ray diffractometer using MoK_α radiation (λ = 0.7107 Å). Data collection, cell refinement and data reduction were performed using *Collect*[127] and *HKL Scalepack*/*Denzo*[128] respectively. Structure solution was accomplished with the aid of SHELXS-97, while refinement by full-matrix least-squares based on F^2 was conducted using SHELXL-97.[129] All non-hydrogen atoms were refined anisotropically.

Table 1. Relevant general and crystallographic parameters for lad-1b·1.5(benzene) and lad-2c.

Compound reference	lad-2c	lad-1b·1.5(benzene)
Chemical formula	($C_{32}H_{28}N_4O_4$)	($C_{24}H_{20}N_4$)·1.5(C_6H_6)
Formula Mass	606.29	481.6
Crystal system	Monoclinic	Monoclinic
a/Å	24.922(5)	8.9631(9)
b/Å	9.3957(19)	28.749(3)
c/Å	13.015(3)	10.5823(11)
α/°	90	90
β/°	96.81(3)	93.320(5)
γ/°	90	90
Unit cell volume/Å^3	3026.1(11)	2722.3(5)
Temperature/K	150(1)	190(2)
Space group	*C*2/*c*	*P*21/*c*
No. of formula units per unit cell, *Z*	4	4
Radiation type	MoKα	Mo*K*α
Absorption coefficient, μ/mm^{-1}	0.091	0.07
No. of reflections measured	9389	14582
No. of independent reflections	2659	4721
R_{int}	0.0271	0.0412
Final R_1 values ($I > 2\sigma(I)$)	0.0539	0.0521
Final $wR(F^2)$ values ($I > 2\sigma(I)$)	0.1551	0.129
Final R_1 values (all data)	0.0644	0.09
Final $wR(F^2)$ values (all data)	0.1638	0.1426
Goodness of fit on F^2	1.056	1.087

Table 2. Relevant general and crystallographic parameters for tpcb-1b, tpcb-2a, tpcb-2b.

Compound reference	tpcb-2b	tpcb-1b	tpcb-2a
Chemical formula	$C_{24}H_{30}N_4O_9$	$(C_{24}H_{20}N_4)\cdot 1.5(C_6H_6)$	$(C_{24}H_{20}N_4O_4)\cdot 2(H_2O_2)$
Formula Mass	518.52	481.6	496.47
Crystal system	Monoclinic	Monoclinic	Monoclinic
a/Å	17.4863(17)	8.9631(9)	17.4340(17)
b/Å	9.3196(9)	28.749(3)	7.5204(8)
c/Å	18.2229(18)	10.5823(11)	17.5936(18)
α/°	90	90	90
β/°	107.454(5)	93.320(5)	94.373(5)
γ/°	90	90	90
Unit cell volume/Å^3	2833.0(5)	2722.3(5)	2300.0(4)
Temperature/K	293(2)	190(2)	463(2)
Space group	*P*21/*c*	*P*21/*c*	I 2/a
No. of formula units per unit cell, *Z*	4	4	4
Radiation type	MoKα	Mo*K*α	MoKα
Absorption coefficient, μ/mm^{-1}	0.094	0.07	0.109
No. of reflections measured	18029	14582	9038
No. of independent reflections	4931	4721	2541
R_{int}	0.0444	0.0412	0.0417
Final R_1 values ($I > 2\sigma(I)$)	0.1192	0.0521	0.058
Final $wR(F^2)$ values ($I > 2\sigma(I)$)	0.3654	0.129	0.1326
Final R_1 values (all data)	0.1455	0.09	0.0817
Final $wR(F^2)$ values (all data)	0.3997	0.1426	0.1394
Goodness of fit on F^2	1.092	1.087	1.086

2.2.10. Computational Data

The following computational data were provided in collaboration with Dr. Jonas Baltrusaitis of the CMRF at the University of Iowa. Ground state geometry optimizations were performed in the gas phase using spin restricted resolution of identity (RI) B-P functional combined with TZVP basis set.[130,131] Symmetry constraints were used during the geometry optimization. Geometry optimization convergence was signaled when energy change between two consecutive optimization iterations was less than 10^{-6} and change in gradient was less than 10^{-3} atomic units. All geometry optimizations were performed using TURBOMOLE.[132] Accurate single point energies were calculated in the gas phase using spin restricted resolution of identity (RI) approximation combined with MP2 level of theory and TZVP basis set using RI-BP/TZVP obtained geometries.[131]

2.3. Results and Discussion

2.3.1. Ladderane Studies

Our studies begin with the C_{2h}-symmetric lad-1a, which is obtained in the solid state using 5-OMe-res as a template.[133] Our goal was to treat this molecule with the following acids: 1) AcOH 2) H_2O_2/AcOH and 3) m-CPBA.

2.3.1.1. Treatment of lad-1a with Glacial AcOH

When lad-1a was reacted with glacial AcOH for a period of 12 hours at temperatures 25^{o}C and 50^{o}C, a ^{1}H NMR spectrum of the reaction mixture suggested that the ladderane underwent an isomerization in near quantitative yield (Figures 51). An isomerization was evidenced by a multiplication of the ^{1}H resonances in the spectrum in the pyridyl (7.00-8.50 ppm) and cyclobutane (polycyclobutyl, 2.40-4.50 ppm) regions and the disappearance of peaks

associated with lad-1a. The α- and β- protons of the 4-pyridyl groups shifted downfield by as much as 0.35 ppm (8.25 to 8.45-8.55 ppm, α; 7.02 to 7.2-7.4 ppm, β) indicating changes to aromatic rings. An examination of the ^{13}C NMR spectrum of the mixture also revealed that the resonance associated with the γ-carbon atoms of the pyridyl groups downfield shifted by 3.9 ppm (Appendix A), which suggested a change to the outer cyclobutane rings. Any vinylic resonances expected from possible opening of the cyclobutane rings were not present in the 5.80-6.60 ppm range.

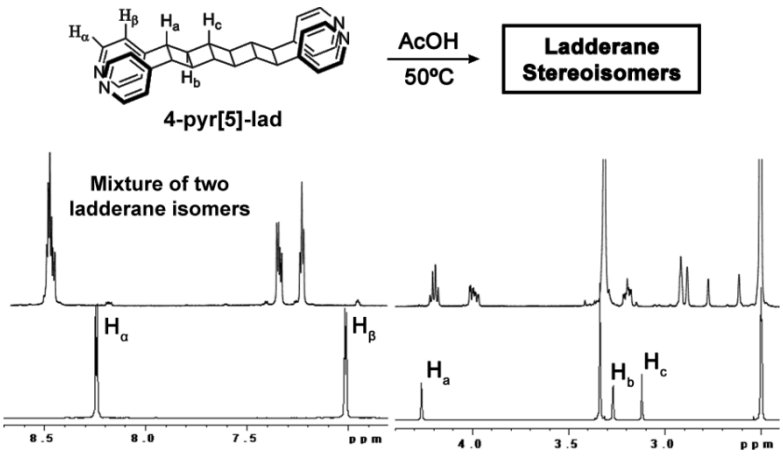

Figure 51. NMR spectra of reaction of lad-1a with AcOH (unreacted lad-1a below, reaction mixture above).

2.3.1.1.1. Possible Ladderane Stereoisomers

In principle, an acid-catalyzed isomerization of lad-1a that involves a perturbation of the outer cyclobutane rings can afford six stereoisomers (Figure 52). The seven total stereoisomers include four achiral ($2 \times C_{2h}$, C_i, C_s symmetry) and three chiral (C_2, $2 \times C_1$) molecules. The achiral isomer lad-1b and two closely-related isomers lad-1d and lad-1e (C_{2h} and C_s) are bisected by a mirror plane. Both C_{2h} isomers are symmetrical along the length of the ladderane and

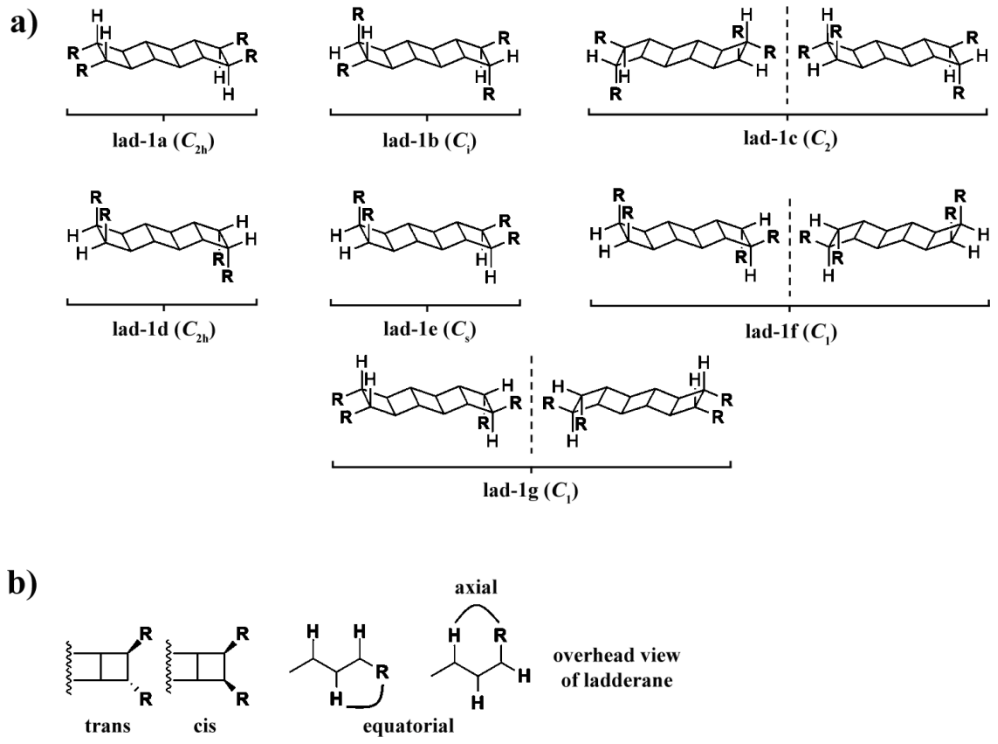

Figure 52. Schematic a) of all possible ladderane stereoisomers from an isomerization, (where R = 4-pyridyl); b) *Trans* and *cis*-, as well as axial (*ax*) and equatorial (*eq*), stereochemistries.

bear either all *axial (ax)* or all *equatorial (eq)* substituents, while the C_s isomer is asymmetrical and bears one end with all *ax* and the other end with all *eq* substituents (Figure 52). Each achiral isomer (C_{2h}, C_s) possesses 4-pyridyl groups that adopt a *cis*-geometry at each end of the molecule. In contrast, the 4-pyridyl groups of the C_i isomer point in opposite directions along the top and bottom of the molecule. Each end of the molecule thus possesses both an *ax* and *eq* pyridyl group, with the substituents adopting *trans*-geometries. The chiral isomers are either dissymmetric in the form lad-1c C_2 or asymmetric in the forms of lad-1f and lad-1g ($2 \times C_1$) with respect to the long axis of the ladderane. The 4-pyridyl groups of the C_2 symmetric ladderane lad-1c effectively point to the corners of an elongated tetrahedron and, thus, similar to the C_i isomer, possess pyridyl groups

that adopt *trans*-geometries involving *ax* and *eq* substituents. The chirality is, thus, a manifestation of the rigid all-*trans*-configuration of the edge-sharing cyclobutane rings, which essentially prohibit an improper rotation axis in the molecule. The C_1 chiral ladderanes involve terminal pyridyl groups that adopt a combination of *eq* or *ax* based on *cis*- and *trans*-geometries.

To our knowledge, notwithstanding the recently-discovered chiral ladderanes present in anammox bacteria,[134] the isomers of lad-1a described here detail the first cases of how chirality can be incorporated into a ladderane framework. In contrast to the natural products, the chirality results from a change in the relative disposition of the terminal pyridyl groups of lad-1a.

2.3.1.1.2. NMR Studies of Reaction Mixture

Given that a total of six stereoisomers of lad-1a can form from an acid-catalyzed isomerization involving the cyclobutane rings, a further inspection of the NMR data suggested that the reaction likely resulted in one of three possible outcomes. More specifically, an examination of a ^{1}H-^{1}H COSY spectrum revealed 12 groups of resonances in the polycyclobutane region with two sets of six groups correlating as separate J-coupling networks (Figure 53). The presence of the two coupling networks suggested that the reaction resulted in two isomers; more specifically, a mixture of either C_i and C_s isomers, C_s and C_2 isomers, or C_i and C_2 isomers. Only these combinations of isomers can result in two sets of six groups of ^{1}H resonances since each isomer contains either a mirror plane or 2-fold rotation axis as a principle element of symmetry. When the reaction was conducted at 25^{o}C for a period of 12 hours, the ^{1}H NMR spectrum was more complex, with additional resonances in the pyridyl and polycyclobutane region. (Appendix A). The additional peaks can be attributed to the formation of isomers

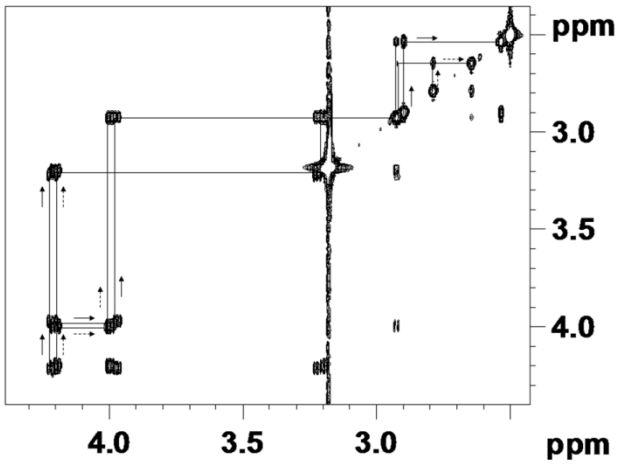

Figure 53. ^{1}H-^{1}H COSY cross section of reaction mixture showing two separate coupling networks (dashed and non-dashed arrows correspond to a group).

of lower symmetries. Collectively, our observations are consistent with an isomerization that is thermodynamically-controlled with the reaction initially proceeding to generate partially-isomerized ladderanes in the form of asymmetrical products. Given that the isomerization of a cyclobutane ring tends to result in the substituents adopting a *trans*-geometry, the reaction when conducted at more elevated temperatures would likely proceed to generate those isomers in which the pyridyl groups adopt exclusively the *trans*-configuration at each end of the molecule; namely, the C_i and C_2 isomers.

2.3.1.1.3. Density-functional Theory (DFT) Calculations

We employed DFT calculations to determine relative energies of the seven stereoisomers of the [5]-ladderane (Table 3). Ground state geometry optimizations on each of the isomers were performed in the gas phase with symmetry constraints used during optimization. From our calculations, we

Table 3. Relative energies of [5]-ladderane stereoisomers.

Stereoisomer	Relative E (kcal/mol)
lad-1c (C_i)	0
lad-1b (C_2)	0.27
lad-1g (C_1)	1.33
lad-1f (C_1)	1.69
lad-1a (C_{2h})	5.22
lad-1e (C_s)	12.18
lad-1d (C_{2h})	18.91

determined the highest energy isomers to bear pyridyl groups in a *cis* geometry; specifically, the two C_{2h} and C_s isomers. In particular, the *eq*- and ax-C_{2h} isomers exhibited energies of 5.22 kcal mol^{-1} and 18.9 kcal mol^{-1}, respectively. The relative higher energy of the axial conformer can be attributed to the presence of a more sterically-congested environment that lies in close proximity to the polycyclobutane framework (Figure 54). The asymmetric C_s isomer exhibited an energy of 12.18 kcal mol^{-1}, which lies between *ax*- and *eq*-*C*. The presence of *trans* substitutents at each end of the ladderane framework was determined to result in isomers of lower energies. In particular, both the *ax*- and *eq*-C_1 isomers, which also possess *cis*-substituents in *ax* and *eq* configurations, exhibited energies of 1.69 kcal mol^{-1} and 1.33 kcal mol^{-1}, respectively. C_i and C_2 are determined to be nearly equal in energy (~ 0.27 kcal/mol) and lower than the parent lad-1a (~ 5 kcal/mol). The relatively low energies can be attributed to the more sterically-favorable *trans* configuration of the end pyridyl groups. Isomers C_i and C_2 are, thus, closely-related diastereomers based on constitutionally-identical centers of chirality (C), with the senses of the chirality being opposite ($C_RC_RC_SC_S$) and identical ($C_RC_RC_RC_R$ or $C_SC_SC_SC_S$) at the corners of the ladderanes, respectively.

Notwithstanding the ladderanes derived from the marine bacteria, C_2 details the first case of how terminal substituents generate a chiral ladderane.

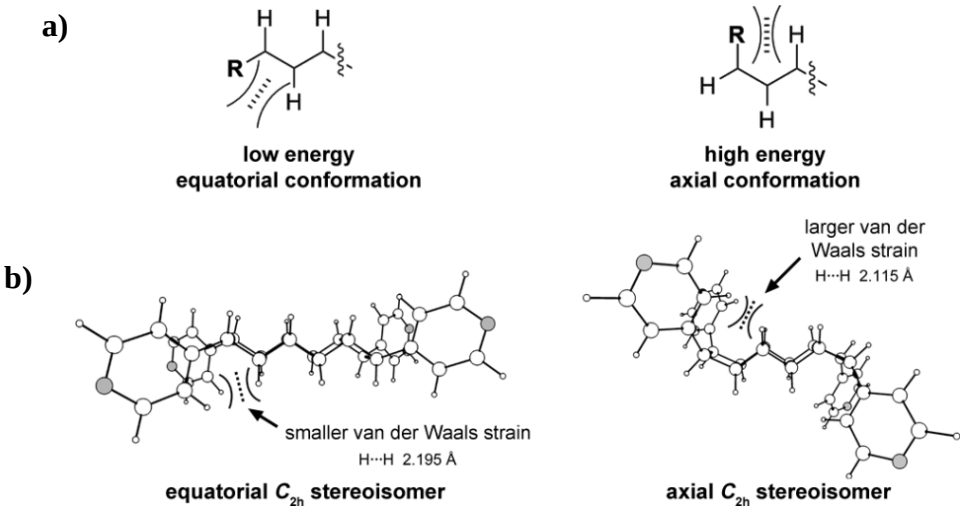

Figure 54. a) Structural orientation of equatorial (*eq*) and axial (*ax*) substituents (R = pyridyl groups). b) DFT-structures depicting equatorial and axial C_{2h} ladderane isomers.

2.3.1.1.4. Isolation and Characterization of Products

Whereas ^{1}H NMR data and DFT calculations supported the reaction of lad-1a to result in an isomerization that affords a mixture that consists of the C_2 and C_i isomers, and/or possibly the C_s isomer, attempts to isolate the products were difficult. Thin-layer (TLC) and column chromatography analyses using solvents of different polarities (*e.g.* ethylacetate, methanol, hexanes) resulted in yellow streaks that were unresolvable using various solvent combinations. To determine the stereochemistry of the products, we turned to solubility experiments. More specifically, we hypothesized that subjecting the solid obtained directly from the reaction to different crystallization conditions could afford an environment from which a single product selectively crystallizes. A

selective crystallization would be possible particularly given that no more than two products likely formed in the isomerization reaction.

2.3.1.1.5. Solubility Experiments

When the solid from the reaction mixture was dissolved in acetonitrile, a white precipitate formed. A ^{1}H NMR spectrum revealed well-defined peaks in the pyridyl and polycyclobutane regions (Figure 55a). The spectrum showed two pairs of doublets in the pyridyl region centered at 8.50 and 7.35 ppm and three pairs of signals in the polycyclobutane region at 4.15, 3.10, and 2.15 ppm. Each of the peaks was also present in the product mixture. A ^{1}H-^{1}H COSY experiment revealed the signals in the spectrum to correlate as a single J-coupling network, which indicated that a single product had precipitated from solution (Appendix A). That the peaks were present as well-resolved pairs was an additional measure of support for lad-1a having isomerized to give either C_2 or C_i or closely related C_s as a product.

A ^{1}H NMR spectrum of the solid obtained from the supernatant, similar to the precipitate, revealed a simplified spectrum that consisted of well-defined peaks (Figure 55b). The spectrum showed a pair of doublets centered at 7.15 ppm, as well as six clearly distinguishable peaks in the polycyclobutane

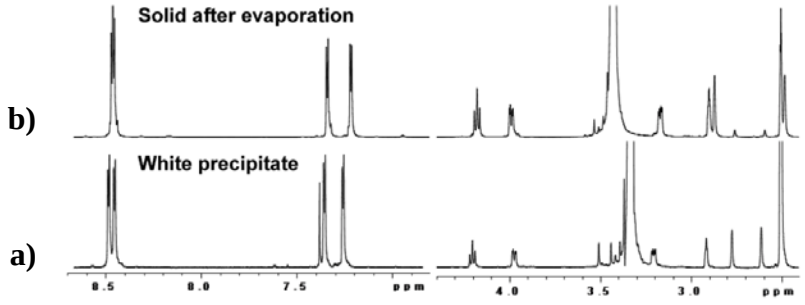

Figure 55. ^{1}H NMR spectra of products from treatment of lad-1a with AcOH: a) precipitate and b) remaining reaction mixture dissolved in DMSO-d_6.

region. Each of the peaks in the spectrum was present in the ^{1}H NMR spectrum of the reaction mixture while a ^{1}H-^{1}H COSY spectrum confirmed the presence of a single product (Appendix A). A homodecoupling experiment performed on the signal at 8.52 ppm revealed the peak to consist of two overlapping doublets. That the peaks in the ^{1}H NMR spectrum of the supernatant were well-defined and different than the precipitate was consistent with the isomerization having afforded only two products, with the product present in the supernatant being either the C_i, C_2, or C_s isomer. We note that the peaks in the region between 3.0 – 2.4 ppm have distinguishing differences.

A ^{1}H NMR spectral feature that distinguishes C_i and C_2 from C_s is the J-splitting pattern for Ha' and Ha that result from the neighboring vicinal protons and relative orientations (Figure 56a). The *anti*-like orientations (torsion angle, 0 - 38°, 123 - 180°) generally show a J-coupling in the range of 8-10 Hz, whereas *syn*-like orientations (torsion angle, 42 - 122°) show a coupling constant in the range of 3-4 Hz. Adjacent to Ha' and Ha on both C_i and C_2 are two coupling partners, specifically, two inequivalent vicinal protons that are both locked in an *anti/anti* and *anti/syn* conformation, respectively, that are likely to involve to two separate coupling constants. Terminal protons Ha' and Ha of C_s have only single *syn* and *anti* coupling partners, respectively, owing to a horizontal mirror plane. This means that both end protons of C_s will each give a single coupling constant. ^{1}H NMR spectroscopy revealed that the splitting patterns of the resonances at ~ 4.2 and ~ 4.0 ppm that correspond to protons for both the precipitate and supernatant exhibited two different coupling constants on the order of 3 - 4 and 8 – 9 Hz, respectively (Figure 56b). This observation ruled out the C_s isomer being a product of the reaction. Given that complete relative configuration of C_i and C_2 could not be assigned with certainty on the basis of conventional methods of

NMR spectroscopy, we aimed to grow single-crystals suitable for X-ray diffraction analysis to allow unambiguous assignment of the configurations.

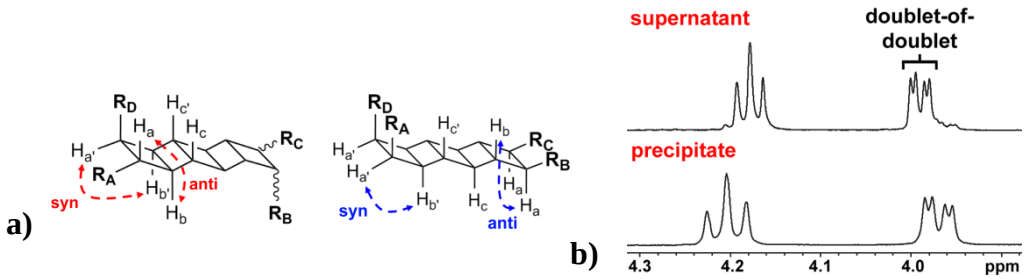

Figure 56. Relationships of a) Ha and Ha' highlighting *anti* and *syn* orientations of terminal cyclobutane protons (*anti/anti* shown) and b) ^{1}H NMR spectra showing splitting patterns of Ha and Ha'.

Although we managed to separate the two ladderanes *via* a selective crystallization, the NMR data could not be used to unambiguously confirm the relative configuration of each isomer. NOESY data were inadequate to identify stereochemical differences while Ha and Ha', which reflect relative orientations of the cyclobutyl protons adjacent to the pyridyls, exhibited indistinguishable J-coupling and splitting patterns. As a result, we next attempted to grow single crystals of each isomer to employ X-ray diffraction to determine each configuration.

2.3.1.1.6. Crystallization Experiments

From extensive crystallization studies, single crystals of the initial white precipitate were obtained by slow evaporation of a benzene solution over a period of *ca.* 2 days. Moreover, a single-crystal X-ray diffraction study confirmed the stereochemistry as achiral C_i in the form of the solvate (C_i-lad)·2(benzene). An

X-ray diffraction study of the single crystals confirmed the structure of the achiral ladderane. As expected, the isomer C_i-lad, which sits around a crystallographic center of inversion, is of C_i symmetry with four pyridyl groups that point in opposite directions along the top and bottom of the molecule (Figure 57). The ladderanes interact *via* C-H···N and C-H···π forces in the solid to form bilayers separated by disordered benzene molecules.

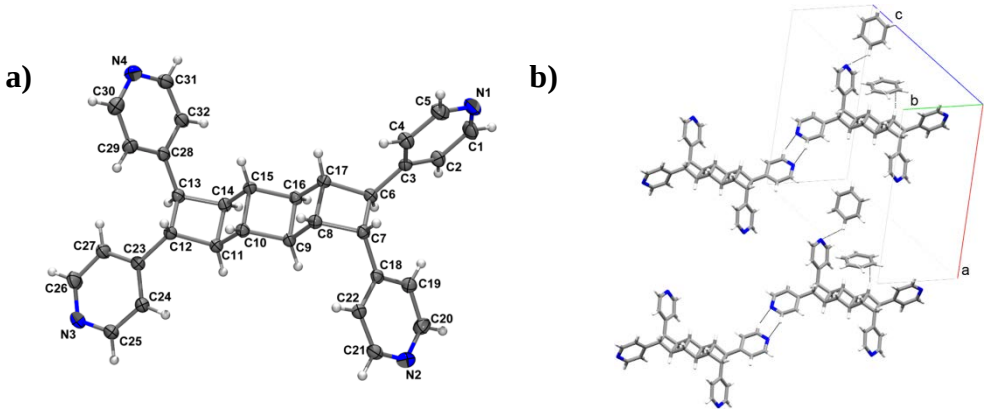

Figure 57. X-ray structure of the C_i ladderane: a) Ortep representation, b) bilayer packing involving benzene molecules. Selected C–C distances (Å): C6–C7 1.563(2), C8–C17 1.569(2), C9–C16 1.586(2), C10–C15 1.587(2), C11-C14 1.577(2), C12–C13 1.553(2).

Whereas we confirmed the structure of the C_i diastereomer by recrystallizing the filtrate from benzene, the solid obtained from the supernatant was determined to strongly resist crystallization from common organic solvents. Attempts to recrystallize the solid typically afforded amorphous solids. That the solid, in contrast to C_i, resisted crystallization, however, provided a measure of support for the product being the chiral C_2 isomer given that chiral molecules tend to pack less favorably in a 3D lattice.[9,135] To facilitate a crystallization of the solid from the supernatant, we turned to a co-crystallization. In particular, we

hypothesized that co-crystallization of the ladderane with a molecule capable of interacting with the pyridyl groups *via* hydrogen bonds would offer a means to form crystals that effectively embed the ladderane as a neutral form in a crystal lattice different compared to that provided by the pure molecule. A co-crystallization was applied to obtain single-crystals for X-ray analysis that confirmed the stereochemistry of the C_2 isomer. The relevance and structural details of our investigations will be discussed in the next chapter.

2.3.1.2. Treatment of lad-1a with Glacial AcOH/H_2O_2

Having established that lad-1a isomerizes in AcOH to produce two unexpected stereoisomers, we set to oxidize the ladderanes with the use of an oxidizing agent, H_2O_2. We anticipated that isomerization and oxidization was a likely outcome based the reactivity of lad-1a in the presence of AcOH.[83,123] When lad-1a was treated with H_2O_2 in glacial AcOH for a period of 12 hours at temperatures of 25^{o}C and 50^{o}C, the reaction displayed virtually identical behavior as evidence from NMR spectroscopy. An isomerization was evidenced by a multiplication of the ^{1}H resonances in the spectrum in the pyridyl (7.22-8.54 ppm) and cyclobutane (polycyclobutyl, 2.74-4.19 ppm) regions and the disappearance of peaks associated with lad-1a, while the oxidation was evidenced by differences in the chemical shifts of lad-1b and lad-1c. NMR spectroscopy and studies involving the reactivity of lad-1a in AcOH suggest the formation of lad-2a and lad-2b in the reaction mixture.

2.3.1.2.1. Crystallization Studies

Solubility studies of the reaction mixture in excess 1M potassium hydroxide solution have resulted in the precipitation of the achiral ladderane isomer lad-2a as verified by X-ray crystallography (Figure 58). X-ray analysis of the single crystals revealed that the pyridyl groups of lad-1a had been oxidized

and the terminal-end substituents had isomerized to the thermodynamic all *trans* product lad-2a that crystallized out of the solution. The molecule lad-2a crystallizes in the $P\bar{1}$ space group. As expected, the C_i-isomer, which sits around a crystallographic center of inversion, is of C_i symmetry with four pyridyl-*N*-oxide groups that point in opposite directions along the top and bottom of the molecule. The ladderanes interact *via* O-H(water)···$^{-}$O-N^{+}, C-H(cyclobutane)···N, and (pyridyl···pyridyl) π···π forces. The ladderanes form a 2D assembly in which water molecules form a tetramer that bounds the ladderanes *via* an oxygen of the *N*-oxide and a nearby water molecule. Future studies will focus on the complete spectroscopic and characterization of lad-2a as well as any remaining compound in the supernatant.

.

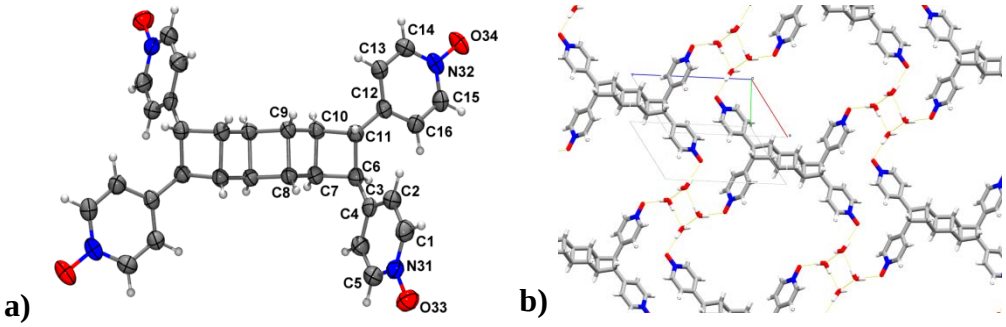

Figure 58. Single-crystal X-ray structure of lad-2a. a) Ortep representation, b) 2D assembly sustained via hydrogen-bonded water tetramer.

2.3.1.3. Treatment of lad-1a with m-CPBA

Having established that oxidation of the isomerized products could be obtained with H_2O_2 in an AcOH medium, we next oxidized lad-1a with an oxidizing agent of different pKa to perform oxidation without isomerization of stereochemistry. We, thus, chose to treat lad-1a with m-CPBA. The acid (pKa =

7.57)[136] is weaker in strength than that of AcOH acid (pKa = 4.78).[136] Upon treatment of lad-1a with m-CPBA a ^{1}H NMR spectrum revealed the similar chemical shifts splitting pattern to that of lad-1a, specifically, two doublets in the pyridyl region and three singlets in the cyclobutane region. These results suggested that the C_{2h}-symmetry of lad-1a was retained, resulting in an oxidation to afford lad-2c.

2.3.1.3.1. Crystallization Studies

Single-crystals were obtained by slow evaporation of water:isopropanol (1:7) for a period of three days. The C_{2h}-symmetry of lad-2c was confirmed *via* single-crystal X-ray diffraction. The X-ray study revealed the stereoisomer to crystallize in the monoclinic space group *C*2/c. The solid-state structure of lad-2c reveals oxidized pyridyl groups and the retention of the stereochemistry (Figure 59). The ladderane is sustained *via* C-H···$^{-}$O-$^{+}$N, C-H···π, and π···π intermolecular forces.

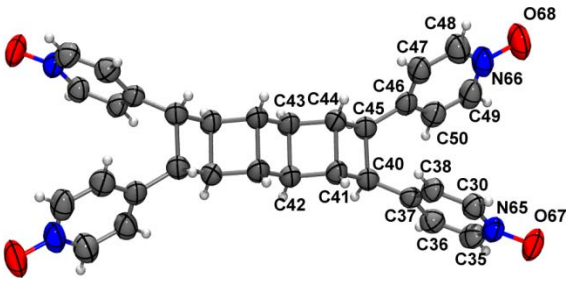

Figure 59. Single X-ray crystal structure of lad-2c. Ortep representation (displacement ellipsoids 50% probability).

2.3.2. Model System: Reactivity Studies of a Monocyclobutane

Having achieved reactivity of the acids with the tetra-pyridyl [5]-ladderane, we set to investigate whether tpcb-1a could afford similar reactivity by

treatment with acids under the same conditions: 1) AcOH 2) H_2O_2/AcOH and 3) m-CPBA.

2.3.2.1. Treatment of tpcb-1a with AcOH

When tpcb-1a was reacted with glacial AcOH for a period of 12 hours at temperatures 25°C and 50°C, a ^{1}H NMR spectrum of the reaction mixture suggested that the tpcb-1a underwent an isomerization in near quantitative yield. Chemical shift values were consistent with the literature of Vittal *et al*. having afforded a mixture of stereoisomers at 25°C and only tpcb-1b at 50°C.[83]

The D_{2d}-symmetry of the *rtct*-stereoisomer tpcb-1b was confirmed *via* single-crystal X-ray diffraction (Figure 60). Single crystals of the *rtct*-isomer were readily achieved from a benzene solution that was allowed to slowly evaporate. The X-ray study revealed the *rtct*-isomer to crystallize in the monoclinic space group $P2_1/c$ in the form of (tpcb-1b)·1.5(benzene). The monocyclobutane self-assembles in the solid *via* C-H···N and C-H···π forces to give cavities that accommodate ordered and disordered benzene solvent molecules.

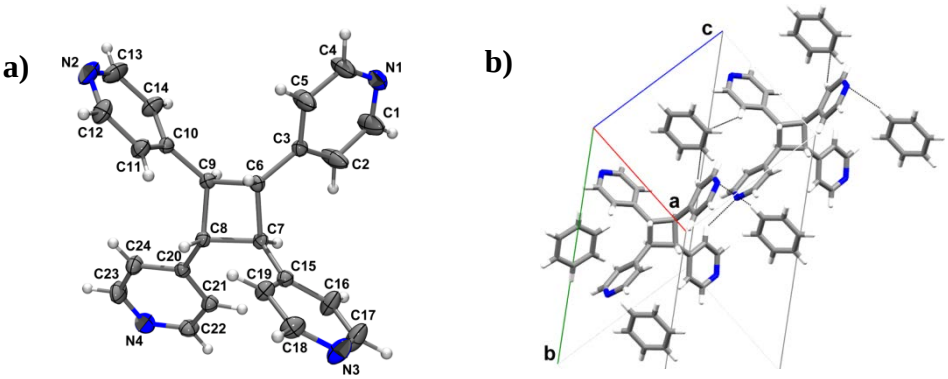

Figure 60. Single-crystal X-ray structure of (*rtct*-4,4'-tpcb)(benzene): a) Ortep representation depicting *trans*-isomeric D_{2d} symmetry (displacement ellipsoids 50% probability); b) Wireframe representation of packing involving benzene.

2.3.2.2. Treatment of tpcb-1a with Glacial AcOH/H_2O_2

When tpcb-1a was reacted with glacial AcOH and H_2O_2 in a 1:5 molar ratio for a period of 12 hours at 50°C, a ^{1}H NMR spectrum of the reaction mixture suggested that the ladderane underwent an isomerization and oxidation in near quantitative yield to the more thermodynamically stable D_{2d}-symmetric *rtct*-stereoisomer tpcb-2a.[83,123] The oxidations were evidenced by up- and downfield shifts of the α- and β-protons of the pyridyl rings, while the cyclobutane peak exhibited a large upfield shift from 4.65 to 3.88 ppm in the ^{1}H NMR spectrum.

Single crystals of the tpcb-2a were readily achieved from a water:isopropanol (1:12) solution that was allowed to slowly evaporate over a period of two days. The structure of tpcb-2a was confirmed *via* single-crystal X-ray diffraction. The X-ray study revealed the *rtct*-isomer to crystallize in the monoclinic space group *I*2/a in the form of (tpcb-2a)·2(H_2O_2) (Figure 61). The monocyclobutane interacts *via* O-H···$^-$O-N$^+$ and C-H···$^-$O-N$^+$ H-bonding to give a 2D square-shaped assembly with each oxygen of the *N*-oxide forming a hydrogen-bond with the peroxy acid. The square shaped cavities are 16.3Å x 16.3Å in dimension and are occupied by interpenetrating assemblies.

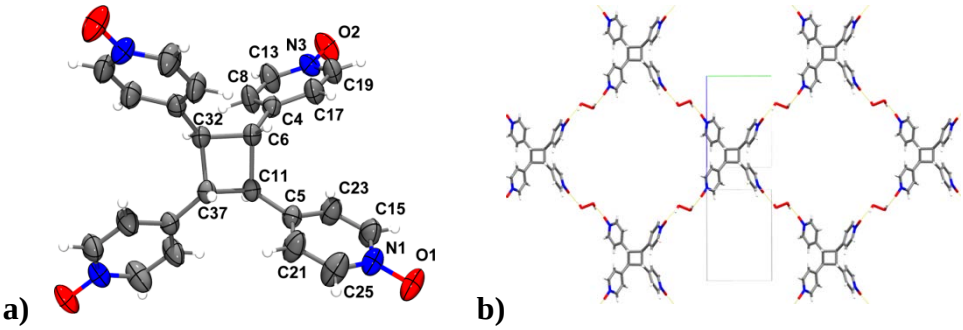

Figure 61. Single-crystal X-ray structure of (tpcb-2a)·2(H_2O_2): a) Ortep representation depicting *trans*-isomerized and oxidized D_{2d} symmetry (displacement ellipsoids 50% probability); b) Wireframe representation of packing involving peroxy acid.

2.3.2.3. Treatment of tpcb-1a with m-CPBA

Similar to lad-1a, we set to treat tpcb-1a with m-CPBA to oxidize and retain the stereochemistry. Upon treatment of tpcb-1a with m-CPBA, a ^{1}H NMR spectrum revealed a small upfield shift of the singlet in the cyclobutane region from 4.65 ppm to 4.55 ppm. The chemical shift suggested a chemical transformation consistent with the oxidation of a pyridyl group.[137]

Single-crystals of the product were readily grown as prisms from water:ethanol (1:6) and for a period of three days. The X-ray study revealed the *rctt*-isomer tpcb-2b to crystallize in the monoclinic space group $P2_1/c$ (Figure 62). The monocyclobutane is sustained *via* C-H···$^{-}$O-N^{+}, C-H···π, and π···π intermolecular forces.

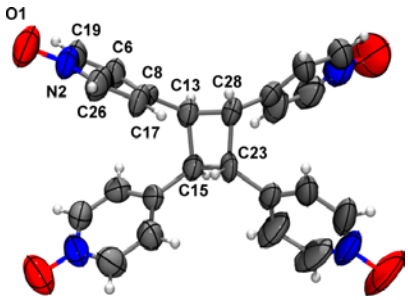

Figure 62. Single-crystal X-ray structure of tpcb-2c: Ortep representation depicting the retention of stereochemistry and the oxidized pyridyl groups (displacement ellipsoids 50% probability).

2.4. Conclusion

Our ability to generate the stereoisomers and *N*-oxide derivatives of both the lad-1a and tpcb-1a quantitatively provided ready access to gram quantities of each cyclobutane product. We have determined that lad-1a and tpcb-1a isomerize in the presence of AcOH, while treatment of lad-1a and tpcb-1a with *m*-CPBA produces *N*-oxides with retention of stereochemistry. Having induced an acid-

catalyzed isomerizaton and/or retaining the stereochemistry in the presence of an acid makes reactivity studies of lad-1a in the presence of acids of varying strengths of interest. Although the mechanism is not known, the change of stereochemistry of lad-1a and tpcb-1a from treatment of acid supports the assertion that the protonation and/or generation of a cation on the pyridyl substituents of a cyclobutane facilitates an isomerization.[123] Having gram quantities of each product afforded a ready means to prepare single crystals for structure determination. The monocyclic tpcb-1a undergoes similar reactivities as lad-1a when treated with acid, which may in the future serve as a useful model system. We expect the isomerization reported here to be useful for studies that focus upon the properties of ladderanes, where applications of ladderanes as building blocks in materials science, synthetic chemistry, and biology are being actively pursued.

CHAPTER 3. STRUCTURE DETERMINATION OF A CHIRAL LADDERANE THAT RESISTS CRYSTALLIZATION VIA CO-CRYSTALS

3.1. Introduction

To determine the stereochemical constitution of a small organic molecule, X-ray crystallography provides critical structural information. Crystals of well defined shapes and sizes are essential to obtain high-resolution data to confirm structure. Despite the fact that a variety of methods are now available, the growth of single crystals suitable for X-ray analysis can be difficult. One widespread method to obtain single crystals suitable for structure determination involves the addition of an auxiliary component during crystallization.[25,138-144] Salt formation is the most popular use of an auxiliary component, particularly in the case of natural products, since crystal stability can be achieved owing to the presence of ionic components (*e.g.* H^+, Br^-) and the ability of the components to participate in hydrogen bonds (*e.g.* $H\cdots Cl^-$).[138,143,145] However, salt formation requires transfer of a proton and, thus, can be limited to molecular components that act as moderately strong acids and bases.[146,147] The generation of a salt can also, in principle, disrupt the chemical structure of a target molecule.[25]

In this chapter, we demonstrate the use of a co-crystallization for structural authentication of the ladderane generated from the acid-catalyzed reaction of lad-1a in the previous chapter. Given the developments in the past few decades of crystal engineering, we hope to provide insight to key aspects of a co-crystal strategy that can be used to facilitate structure determination.

3.1.1. Why Use Crystallization for Characterization?

If ‘seeing is believing’, then intuitively speaking a 3D crystal structure of a molecule clearly stands out among other means of characterization. An early

example of the practical use of X-ray crystallography involved the structural clarification of several steroid compounds.[143] Wieland and Windaus had provided extensive groundwork for studies involving the structures of biological molecules. In particular, their proposed work led to the widely accepted 4-component ring structure. Bernal provided crystal structures of five steroid compounds that revealed the correct ring framework.[143,148,149] Whereas obtaining data from X-ray diffraction and data processing had previously taken up to months; now several crystal structures can be determined and prepared for publication in a day using CCD technology.[150] Despite technological advances, however, the limiting factor of obtaining a crystal structure can be the growth of single crystals suitable for X-ray diffraction.

3.1.2. Routine Methods to Prepare Single Crystals of Organic Compounds

There are currently four common methods of crystal growth: 1) slow evaporation generally at room temperature, 2) cooling a hot supersaturaed solution, 3) sublimation and 4) derivatization.[151] Slow evaporation is the most convenient means of obtaining crystals. The target compound is dissolved in a chosen solvent and the solvent slowly evaporates from the vessel. The solvent of choice will depend on the solubility of the solute. Although mixtures of solvents can produce changes in the polarity of the solvents, solubility can remain problematic and limit the range of solvents available. The second method which involves the target molecule in a partially soluble solvent can produce single-crystals at a faster rate, however, solubility is the limiting factor in this case as the compound may be too soluble in a variety of solvents. Sublimation can provide single crystals, however, the method has many limitations. The compound has to be thermally stable, crystals may be fragile and thin, as a result depending on the

apparatus design, the crystals may crack upon removal from a sublimation apparatus. These methods are generally the first lines of defense towards the growth of single crystals. In the cases where the standard methods do not provide access to single crystals, an alternative is to synthesize a derivative of the molecule. Modification through covalent derivatization or salt formation is a useful and often used approach to achieve single crystals. The target molecule is generally derivatized with a component that increases symmetry and/or order in the crystal by the directivity of intermolecular contacts.

3.1.3. Co-crystallization for the Structure Determination of Small Molecules

The field of crystal engineering involves the rational design of solids with predictable and/or tunable properties. Although co-crystals can be used to achieve single-crystals of a target molecule, co-crystals have rarely been applied to engineer single-crystals for the purpose of small molecule structure determination. Indeed, the structure determination of biological macromolecules is invariably determined using a co-crystallization approach;[152] however, for structure determination becoming a bottleneck approach, small molecule structure elucidation *via* co-crystallization is a promising but underdeveloped approach with only a few notable examples.

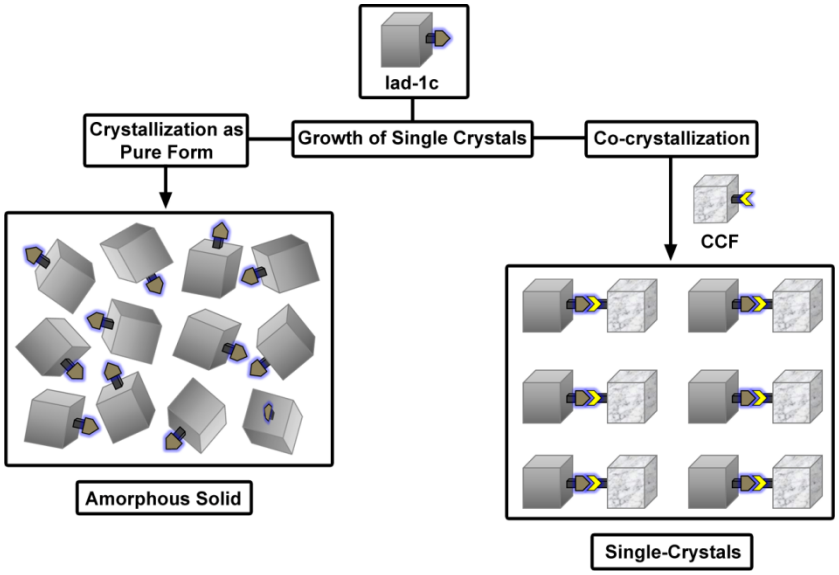

Figure 63. Schematic representation of routes to the growth of single crystals.

3.1.3.1. Pioneering Studies Involving Co-crystals

In 1965, Norton demonstrated the utility of co-crystals for structural determination.[23] Early approaches towards the growth of single crystals involved the covalent linkage of heavy atoms. In some cases, however, the steroids were shown to exhibit distortion which could be misleading when interpreting the molecular structure. To circumvent distortion, it was anticipated that neutral complexation with a heavy atom could afford diffraction quality crystals without compromising the molecular structure. To test this hypothesis, Norton used known androgenic steroids (*e.g*. testosterone) and *p*-bromophenol as a complexation agent. Given that many androgenic steroids are decorated with ketones, it was anticipated the generation of a stable neutral complex between the ketone, acting as a proton acceptor, and a hydroxyl group on a phenol acting as the proton donor (Figure 64). As determined by X-ray crystallography and

infrared absorption spectroscopy, a variety of co-crystals were obtained in varying stoichiometric ratios.

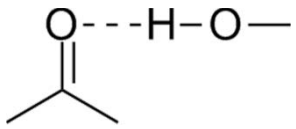

Figure 64. Schematic representation of hydroxyl-ketone hydrogen bonding interaction.

3.1.3.2. Determination of Conformation

The complexation strategy of Norton was later applied in work of Duax,[153] to determine the A-ring conformation of 2*β*,17*β*-diacetoxy-4-androsten-3-one (2*β*-hydroxytestosterone diacetate = htd), a natural metabolite of testosterone (Figure 65). The conformation of the A-ring is important due the relation of the conjugation of the *α*, *β*-unsaturated ketone. Optical rotary dispersion (ORD),

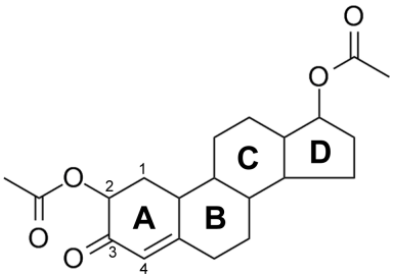

Figure 65. Schematic representation of testosterone derivative htd.

circular dichroism (CD), and NMR analysis suggested that the conformation of the A-ring containing a 4-en-3-one *α*, *β*-unsaturated ketone was predicted to be in a half-boat or "non-steroidal" half-chair or twist conformation. To determine the A-ring conformation of the testosterone derivative, the authors set out to obtain a

crystal structure from X-ray diffraction analysis; however the growth of single-crystals was unsuccessful. Single-crystals suitable for X-ray diffraction were obtained by a complexation with *p*-bromophenol (*p*-bp). An inverted 'half-chair' conformation of htd was revealed. It was determined that *p*-bp and htd interacted *via* a hydrogen bond in the form of the hydroxyl group of the phenol and oxygen of the ketone (O-H···O=C) hydrogen bond as well as bromine-oxygen contacts (Br-O).

3.1.3.3. Confirmation of Structure

Whereas it was in the mid 1960's and early 70's that co-crystallization was used to confirm structure, it was not until approximately three decades later that a co-crystal was used to determine the structure of an organic molecule difficult to crystallize.[154] Goroff introduced a CCF into the growth of single crystals to confirm the synthesis of a perbromocumulene (pbc) from a dibutylbromodiyne precursor (Figure 66). The reaction created two different products; namely, pbc and 1,1,2,3,4,4-hexabromobutadiene (hbbd). The presence

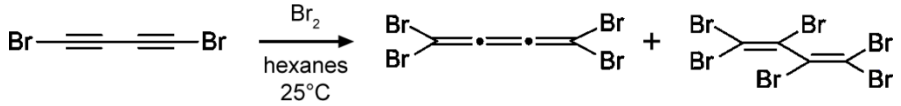

dibutylbromodiyne **pbc** **hbbd**

Figure 66. Schematic reaction involving formation of pbc and hbb products during the synthesis of pbc.

of two compounds was confirmed by ^{13}C NMR from two different sets of carbons, as well as differences in mass spectra data, and melting point. Owing to the ambiguous spectroscopic nature of pbc and hbbd, the growth of single-crystals was attempted to confirm the structure; however, crystals could not be obtained,

which is surprising given the high symmetry and the number of Br-atoms available for intermolecular (Br···Br) contacts.[155,156] However, when pbc was co-crystallized with phenazine, co-crystals of (pbc)·(phenazine) suitable for X-ray diffraction were obtained (Figure 67). Pbc and phenazine interact via N···Br and C-H···Br interactions. The phenazine stacks in plate-like arrangements around the pbc molecule, being sustained via π···π interactions. It is important to note that pbc decomposes in solution over time. The co-crystal may, thus, serve to stabilize the molecule from decomposition.

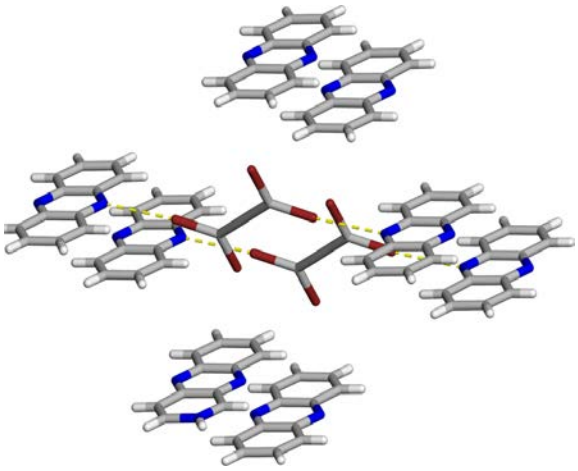

Figure 67. Wireframe model of single X-ray crystal structure of (pbc)·(phenazine).

3.1.3.4. Determination of Absolute Stereochemistry

The determination of absolute stereochemistry of chiral compounds can be obtained *via* means of chemical correlation, nuclear magnetic resonance in combination with chiral shift reagents, and circular dichroism.[24] Similar to Norton, Desiraju and co-workers set to establish the use of heavy atom co-crystals as means to provide the absolute stereochemistries of molecules.[24] In particular, steroids of known absolute stereochemistry, pregnenolone and cholesterol, were

incorporated into a co-crystal bearing 4-iodophenol (ip) and 2,4,6-trichlorophenol (tcp) as CCFs (Figure 68). The design of the co-crystal was to provide a hydroxyl site on the CCF to interact with either the hydroxyl or carbonyl group of the

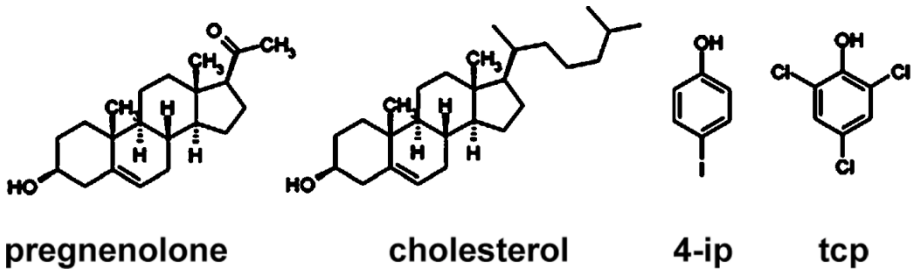

Figure 68. Schematic representations of steroids and hydroxyl-based CCFs.

steroid. Single crystals were obtained in the form of co-crystal (pregnenolone)·(4-ip), (pregnenolone)·(tcp), and 2(cholesterol)·(tcp). In each case, X-ray analysis confirmed the presence of a co-crystal. The flack parameters confirmed the absolute stereochemistries that matched well with the literature values. Co-crystal (pregnenolone)·(4-ip) contained individual steroid molecules interacting *via* hydroxyl-hydroxyl (O···H-O) and hydroxyl-carbonyl (O···H-O=C) hydrogen bonding arranged in a head-to-tail fashion (Figure 69). The CCF lies above and between the steroid molecules, forming hydrogen bonds *via* hydroxyl groups.

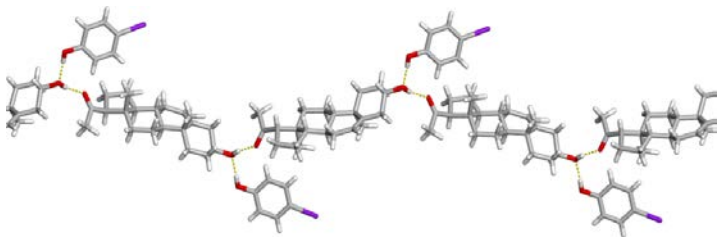

Figure 69. X-ray crystal structure of 1D assembly of (pregnenolone)·(4-ip) along the *c*-axis.

Lawrence *et al*. employed a co-crystallization to determine the absolute stereochemistries of a series of four 3-arylbutanoic acids derived from enzymatic hydrolysis reactions (Figure 70).[25] Due to the oily and viscous nature of the material as well as a limited amount of enanitopure material from

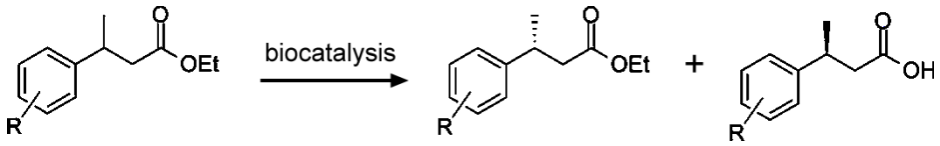

3-arylbutanoic acid **R = H, 2-Me, 3-Me, 4-F**

Figure 70. Schematic representation of enzymatic biotransformations of butanoic acid derivatives.

enantioselective biotransformations, chemical modification was avoided as well as salt precipitation to not compromise the structure. Given that each product contains a carboxylic acid, the compounds were readily suitable for being used as a supramolecular synthon. The authors chose isonicotinamide as a CCF owing to the number of single carboxylic acids known to readily crystallize with amides. Single-crystals suitable for X-ray diffraction were obtained and the absolute stereochemistries were confirmed using the Flack parameter. Figure 71 shows *(S)*-3-arylbutanoic acid co-crystal (isonicotinamide)·(3-arylbutanoic acid) stabilized by the pyridyl-carboxyl intermolecular hydrogen bonds, accompanied by amide-carbonyl (N-H···O=C) hydrogen bonds. It is important to note, as determined from chiral HPLC experiments, that the CCF did not interfere with the separation on the column.

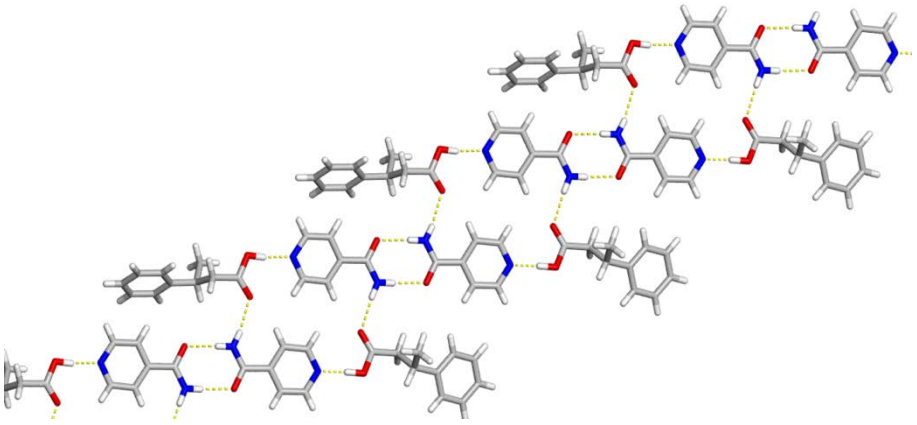

Figure 71. Wireframe 2D assembly of (isonicotinamide)·(*S*-3-arylbutanoic acid). The assembly arranges vertically along the *a*-axis.

3.1.3.5. Resolving Stereochemical Ambiguity

Brunklaus *et al*. set to establish co-crystallization as a means to resolve and isolate structurally similar stereoisomers with the assistance of the O-H···N heterosynthon acting as a 'molecular hook'.[16] To demonstrate the methodology, known stereoisomers quinidine and quinine were employed. It was determined using a variety of solid-state spectroscopic characterization techniques that the active pharmaceutical ingredient (API) methyl paraben (mp) can be used to isolate quinidine from an equimolar mixture of structurally-similar stereoisomer quinine (Figure 72a) in the form of a co-crystal of composition (quinidine)·(mp) (Figure 72b). In the context of the isolation of relevant biological products, this example demonstrated the importance of co-crystallization.

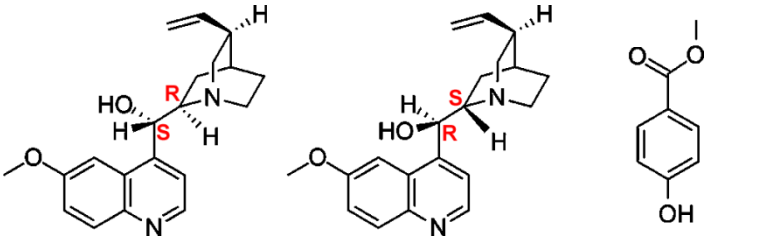

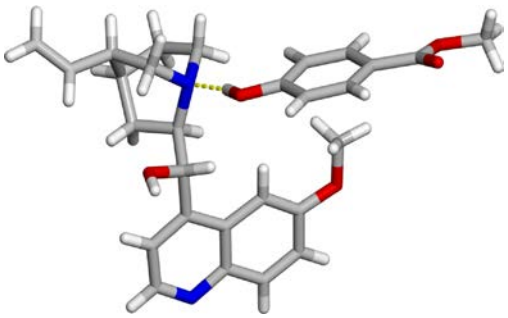

Figure 72. Schematic and wireframe representation of a) two stereoisomers quinidine and quinine and the co-crystal used for isolation; b) co-crystal of (quinidine)·(mp) stabilized by O-H···N 'molecular hook' interaction.

3.1.4. Chapter Overview: Determination of the Stereochemistry of a Chiral Ladderane Using a Co-crystal

In continuation of the ladderane studies from Chapter 2, it will be shown that a co-crystal strategy can be used to structurally-authenticate the chiral ladderane lad-1c. The ladderane lad-1c resisted crystallization by producing amorphous solids. We hypothesized that we could employ CCFs based on carboxylic acids to direct the assembly of the ladderane so as to achieve a well-ordered lattice. We expected that the formation of pyridine-carboxylic acid synthon would serve to stabilize the ladderane into a lattice for structural authentication.

In this chapter, we show that co-crystallization of the chiral ladderane lad-1c with carboxylic acids in the form of 3,5-dinitrobenzoic acid (3,5-DNBA) and trimesic acid (TMA) readily afforded single crystals that confirmed the stereochemistry of the ladderane. For our design strategy, we selected and employed acids as CCFs based on 1) the tendency of carboxylic acids to form neutral hydrogen bonds with pyridines,[157] 2) achiral symmetry of the CCF,[158,159] and 3) ability of the CCF to form ordered assemblies and/or insoluble solids. The rationale behind the approach is addressed in the order listed above. First, acids of moderate strength will generally facilitate neutral complexation with a moderately weak base.[26,146,157,160] By forming a neutral complex, possible isomerization of the cyclobutane rings can be avoided. Second, the use of a symmetrical CCF increases the ability of the target molecule to arrange in a 3D lattice.[6,135,155,161] Third, the fact that the certain CCFs have a tendency to form supramolecular multi-dimensional assemblies leads to relatively insoluble solids.[162-164] This allows for the possibility to insert the target molecule into the solid, considering that the CCF has complementary functionality. In particular, we will demonstrate that the acids and pyridines self-assemble *via* O-H(acid)···N(pyridyl) hydrogen bonds (Figure 73). In the monocarboxylic acid, the chiral ladderane and acid self-assemble to generate a five-component hydrogen-bonded complex (lad-1c)·4(3,5-DNBA)·5(CH_3NO_2), that packs to form large solvent-filled homochiral channels of nanometer-scale dimensions. The co-crystallization of lad-1c with the triacid TMA, affords co-crystal of composition (lad-1c)·2(TMA), a self-assembled pseudo-hexagonal shape, enantiomeric 3D network based on interpenetrating nets. The co-crystal involving 3,5-DNBA also represents the first porous solid containing a ladderane building block.

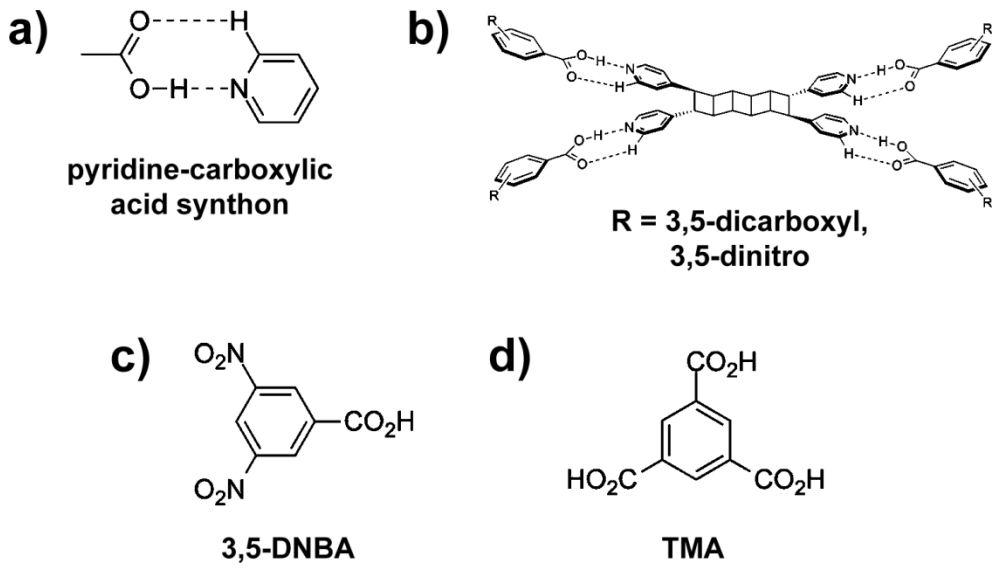

Figure 73. Schematic representations of a) pyridine-carboxylic acid synthon, b) primary interaction between lad-1c and CCF, c) 3,5-dinitrobenzoic acid and d) TMA.

3.2. Experimental

3.2.1. General Procedure

Reagents 3,5-DNBA (99%, Aldrich Chemical Co.), TMA (purum, ≥ 97.0%, Sigma-Aldrich), methanol (ACS reagent, ≥ 99.8%, Sigma-Aldrich), acetonitrile (ACS reagent, ≥ 99.5%, Sigma-Aldrich), and nitromethane (ACS reagent, ≥ 95%, Sigma-Aldrich) were used as received. Fourier transform infrared spectra were recorded from NaCl plates on a Nicolet 380 FT-IR spectrometer. OMNIC software was employed for data analysis using 4 cm^{-1} resolution and the averaging of 8 scans. All spectra were normalized and baseline-corrected.

All products were characterized using the DRX-400 NMR spectrometer (Billerica, MA) operating at 400 MHz, using deuterated dimethyl sulfoxide (DMSO-d_6) as solvent. ^{1}H and ^{13}C chemical shifts were referenced with the

residual proton and carbon chemical shifts of the solvents (DMSO-d_6, ^{1}H, 2.5 ppm). All of the NMR data were processed with the TOPSPIN 1.3 suite of software programs. One-dimensional ^{1}H data were processed with zero-filling to 64k data points and 0.2 Hz exponential line broadening. Relative numbers of proton signals multiplied by the integral areas were used for the quantification.

3.3.2. Synthesis of Co-crystal (lad-1c)·4(3,5-DNBA)·5(CH_3NO_2).

Co-crystals were obtained by a dissolving lad-1c (40.5 mg, 0.086 mmol) with 3,5-DNBA (73 mg, 0.346 mmol) in 1:3 (v:v) methanol:nitromethane, followed by hot filtration. The solution was allowed to evaporate slowly for a period of 3 days to afford colorless needles. (yield: 45 mg, 37.8%). ^{1}H NMR, (400 MHz; DMSO-d_6 δ/ppm): δ 9.01 (t, J = 2.4 Hz, 1H), 8.90 (d, J = 2 Hz, 1H), 8.51 (d, J = 6.0 Hz, 1H), 8.48 (d, J = 5.4 Hz, 1H), 7.37 (d, J = 5.4 Hz, 1H), 7.22 (d, J = 6.0 Hz, 1H), 4.18 (dd, J = 8.7 Hz, 8.6 Hz 1H) two peaks are overlapped, 4.00 (dd, J = 8.7 Hz, 3.2 Hz 1H), 3.17 (dd, J = 8.6 Hz, 3.6 Hz 1H), 2.90 (s, 1H), 2.87 (s, 1H), 2.48 (s, 1H). IR, ν/cm-1 (NaCl plate): 3096(w), 2923(m), 2843(w), 1708(m), 1628(m), 1534(s), 1450(w), 1338(s), 1174(w), 1067(m), 916(w), 822(w), 720(m).

3.3.3. Synthesis of Co-crystal (lad-1c)·2(TMA)

Co-crystals were obtained by a dissolving lad-1c (65 mg, 0.138 mmol) with TMA (58 mg, 0.276 mmol) in a 1:3 (v:v) methanol:acetonitrile solvent mixture. The solution was allowed to heat and sealed in a closed vessel for a period of 4 days. Single-crystals in the form of pale-yellow needles were observed (yield: 46.7 g, 38%). ^{1}H NMR, (400 MHz; DMSO-d_6 δ/ppm): δ 8.641 (s, 1H), 8.51 (d, J = 6.0 Hz, 1H), 8.48 (d, J = 5.4 Hz, 1H), 7.37 (d, J = 5.4 Hz, 1H), 7.22 (d, J = 6.0 Hz, 1H), 4.18 (dd, J = 8.7 Hz, 8.6 Hz 1H) two peaks are

overlapped, 4.00 (dd, J = 8.7 Hz, 3.2 Hz 1H), 3.17 (dd, J = 8.6 Hz, 3.6 Hz 1H), 2.90 (s, 1H), 2.87 (s, 1H), 2.48 (s, 1H). IR, ν/cm^{-1} (NaCl plate): 2932(m), 2853(w), 1698.80(s), 1634(w), 1605(m), 1504(w), 1416(w), 1259(br), 821(w), 752(w), 676(m).

3.2.4. X-ray Crystallography

All crystal data were collected on a Nonius KappaCCD single-crystal X-ray diffractometer using MoK_α radiation (λ = 0.7107 Å). Data collection, cell refinement and data reduction were performed using *Collect*[127] and *HKL Scalepack*/*Denzo*[128] respectively. Structure solution was accomplished with the aid of SHELXS-97, while refinement by full-matrix least-squares based on F^2 was conducted using SHELXL-97.[129] All non-hydrogen atoms were refined anisotropically. Hydrogen atoms attached to C- and O-atoms were fixed in geometrically constrained riding positions, and refined isotropically on the basis of corresponding C- and O-atoms [U(H) = 1.2 U_{eq}(C), U(H) = 1.5 U_{eq}(O)]. Structure solution and refinement for (lad-1c)·4(3,5-DNBA)·5(CH_3NO_2) revealed large channels. Further refinement uncovered relatively weak electron density (< 0.85 eA^{-3}) in the Fourier map. The peaks were attributed to diffuse solvent molecules. Even after all electron-density peaks were assigned to solvent molecules, the structure exhibited solvent-accessible voids, which suggested that partial desolvation occurred during the X-ray experiment. The ill-defined solvent peaks are in agreement with the poor diffraction quality. Since a reasonable model of the solvent could not be achieved, the data were treated with the SQUEEZE routine in PLATON[150] to remove electron density related to the diffuse solvent molecules. Four solvent-accessible voids that collectively account for 23% of the unit-cell volume (*i.e.* 1251 Å^3) and 483 electrons, which correspond to approximately 15 molecules of CH_3NO_2 per unit cell, were

identified. The sites of the disordered carboxylic acids were restrained to be the same as the ordered group. The occupancies of the disordered molecule refined to 0.62(1) and 0.38(1). Restraints were used on the thermal parameters of both the ordered and the disordered benzoic acids.

Table 4. Relevant general and crystallographic parameters for (lad-1c)·4(3,5-DNBA)·5(CH_3NO_2) and (lad-1c)·2(TMA).

compound reference	(lad-1c)·4(3,5-DNBA)·5(CH_3NO_2)	(lad-1c)·2(TMA)
chemical formula	$C_{32}H_{28}N_4$·4($C_7H_4N_2O_6$)·5($C_1H_3N_1O_2$)	$C_{32}H_{28}N_4$·2($C_9H_6O_6$)
formula Mass	1622.29	888.86
crystal system	Trigonal	Triclinic
a/Å	29.740(3)	9.1127(10)
b/Å	29.740(4)	16.9855(18)
c/Å	7.0681(8)	19.606(2)
α/°	90	76.889(5)
β/°	90	77.250(5)
γ/°	120	84.905(5)
unit cell volume/Å^3	5414.0(11)	2880.3(5)
temperature/K	150(2)	293(2)
space group	$P3_221$	$P\bar{1}$
no. of formula units per unit cell, *Z*	3	3
radiation type	MoK_α	MoK_α
absorption coefficient, μ/mm^{-1}	0.124	0.111
no. of reflections measured	29039	17385
no. of independent reflections	3379	10110
R_{int}	0.055	0.0742
final R_1 values ($I > 2\sigma(I)$)	0.0828	0.1893
final $wR(F^2)$ values ($I > 2\sigma(I)$)	0.2199	0.4818
final R_1 values (all data)	0.1095	0.2359
final $wR(F^2)$ values (all data)	0.2377	0.5065
goodness of fit on F^2	1.056	1.65

3.3. Results

3.3.1. X-ray Crystal Structure Analysis

3.3.1.1. Co-crystal (lad-1c)·4(3,5-DNBA)·5(CH_3NO_2)

The components of the co-crystal crystallized in the chiral trigonal space group $P3_221$. The asymmetric unit consists of one half of a molecule of lad-1c and two molecules of 3,5-DNBA, with one acid being disordered over two sites (occupancies: 0.62:0.38). As expected, the ladderane possesses C_2 symmetry. The acid interacts *via* four O-H(acid)···N(pyridyl) hydrogen bonds [O-H···N distances (Å): O(1)···N(1) 2.566(8), O(7a)···N(2) 2.58(1), O(7b)···N(2) 2.57(2)] (Figure 74a). The pyridyl groups of lad-1c point to the corners of a distorted tetrahedron (edges (Å): 6.57 and 7.81) with the C-C bond lengths and C-C-C angles being comparable to lad-1a (Figure 74b). The geometry of the carbonyl group of the ordered 3,5-DNBA also supports the acid being in the neutral form (d(C=O) = 1.185(9) Å; d(C-O) = 1.315(7) Å). The spontaneous resolution of the components to form a chiral solid presumably afforded a racemic conglomerate.[165]

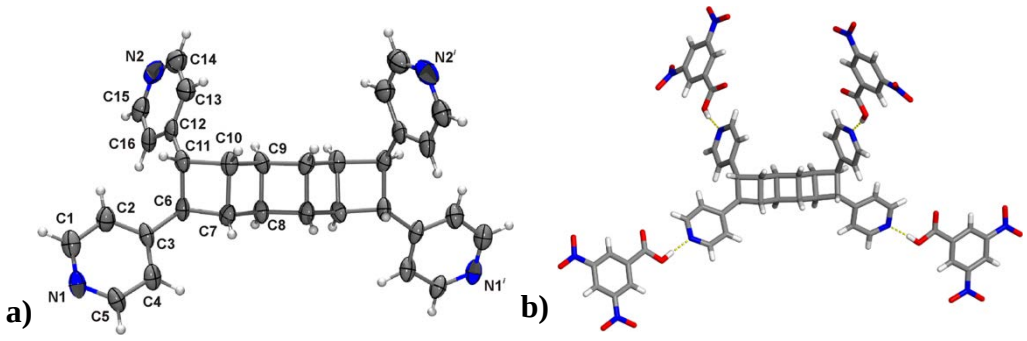

Figure 74. Single crystal X-ray structure of solid (lad-1c)·4(3,5-DNBA)·5(CH_3NO_2): a) ORTEP of chiral lad-1c. Selected C-C distances (Å): C6-C11 1.549(8), C7-C10 1.618(9), C8-C9 1.567(9).

Whereas the components of (lad-1c)·4(3,5-DNBA)·5(CH_3NO_2) assemble to form a discrete molecular array, the packing of the assemblies leads to a solid with large chiral channels. In particular, the five-component assemblies stack to form homochiral tubes parallel to the crystallographic *c*-axis that are sustained by a combination of C-H···π and π···π forces (Figure 75). The tubes are of nanometer-scale dimensions, being approximately 1.7 nm in diameter. Peaks from included solvent molecules were located in the channels, being highly diffuse so as to not allow the solvent to be modeled. The X-ray data were, thus, treated with the SQUEEZE routine[150] from Platon to remove the diffuse peaks and determined to correspond to a total of 15 CH_3NO_2 molecules per unit cell, with the solvent-accessible voids accounting for approximately 23% of the unit-cell volume (*i.e.* 1251 A^3). The walls of the channels are mainly composed of alternating aromatic groups in the form of the 4-pyridyl groups and acid molecules, with the polycyclobutane moieties being located at the corners. The resulting solid is a highly-porous channel framework composed of stacked tetrahedra that are sustained by intermolecular π···π forces. To our knowledge, (lad-1c)·4(3,5-DNBA)·5(CH_3NO_2) is the first example of a porous solid based on a ladderane.[166]

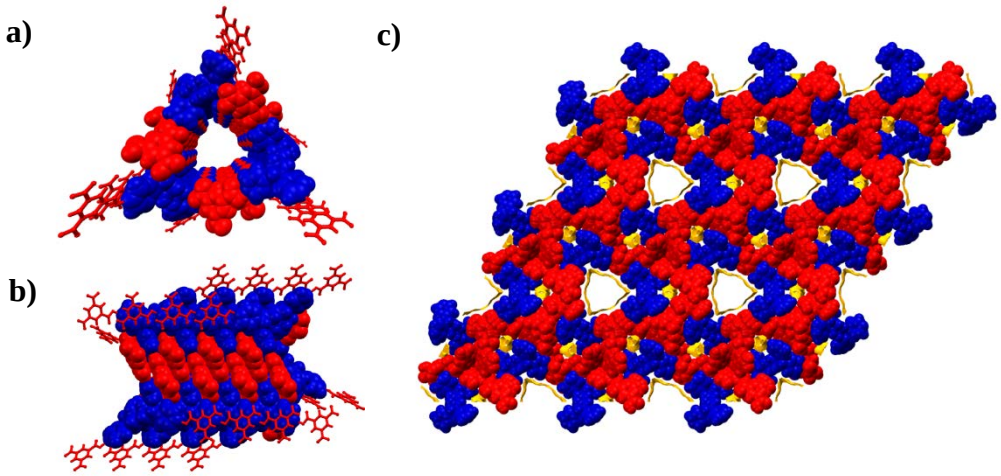

Figure 75. Space-filling views of channels: a) along crystallographic *c*-axis, b) sides along *b*-axis, and c) hexagonal arrangement [color scheme: lad-1c (blue), 3,5-DNBA (red), boundaries of void regions (yellow)].

3.3.1.1.1. Salt vs. Co-crystal

The formation of a salt of the solid (lad-1c)·4(3,5-DNBA)·5(CH_3NO_2) was ruled out by locating the relevant hydrogen atom in the Fourier difference map and IR spectroscopy. The Fourier difference maps showed that the acidic proton is positioned in close proximity to the O-atom of the carboxylic group at a distance that corresponds to a neutral carboxylic acid group. Specifically, the carbon-oxygen bond distances of the ordered 3,5-dinitrobenzoic acid were consistent with the formation of a co-crystal (*d*(C=O)=1.185(7) Å; *d*(C-O)=1.315 Å). The IR spectrum of solid (lad-1c)·4(3,5-DNBA)·5(CH_3NO_2) had shown a slight shift to a higher frequency of the carbonyl (C=O) stretch of 3,5-DNBA from 1703 cm^{-1} of the pure compound to 1708 cm^{-1}. Reported carboxylate salts of 3,5-DNBA show lower frequencies of C-O stretches between 1653 cm^{-1} and 1607 cm^{-1}.[167,168] The IR evidence further supported the formation of a co-crystal.

3.3.1.2. Co-crystal (lad-1c)·2(TMA)

The components of the co-crystal crystallize in the achiral space group $P\bar{1}$. The asymmetric unit contains one molecule of lad-1c and two molecules of TMA. The co-crystal bears both enantiomers of lad-1c with the C-C bond lengths and C-C-C angles being comparable to lad-1c (Figure 76). Similar to (lad-1c)·4(3,5-DNBA)·5(CH_3NO_2) each pyridyl of lad-1c forms a hydrogen bond with a carboxylic acid of TMA *via* pyridine-carboxylic acid synthon [O-

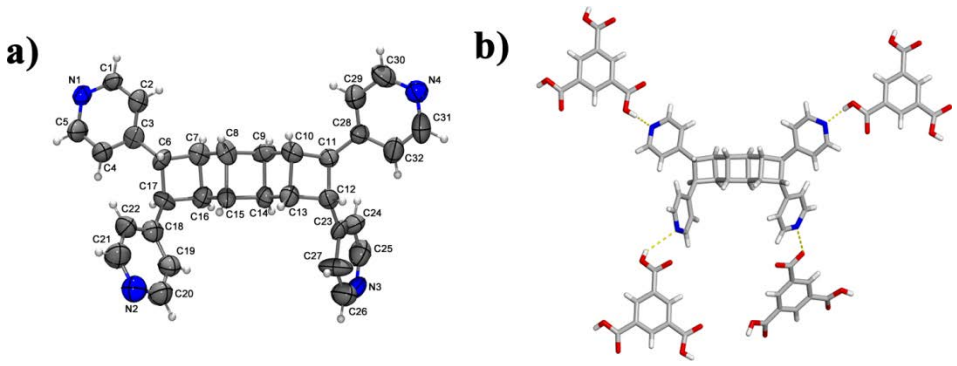

Figure 76. Single crystal X-ray structure of solid (lad-1c)·2(TMA): a) ORTEP of chiral lad-1c (displacement ellipsoids 70% probability) Selected C-C distances (Å): C6-C17 1.533(2), C7-C16 1.584(2), C8-C15 1.634(2), C9-C14 1.595(2), C10-C13 1.564(2), C11-C12 1.533(2); and b) hydrogen-bonded assembly.

H(carboxyl)···N]. Each ladderane molecule is surrounded by TMA molecules *via* C-H(cyclobutane)···π(TMA) interactions and as a result, the neighboring ladderane molecules are insulated by surrounding TMA (Figure 77).

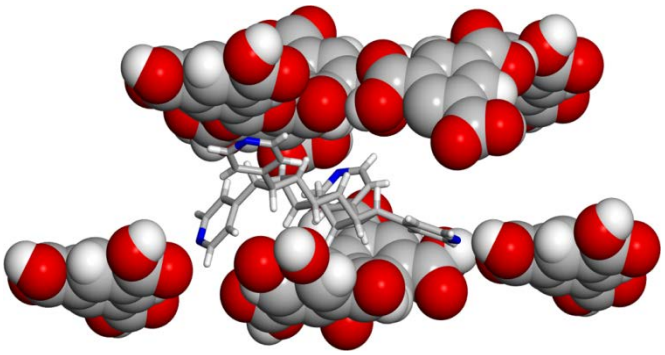

Figure 77. X-ray crystal structure wireframe and spacefill representation of chiral ladderane surrounded by TMA molecules.

The assembly of lad-1c and TMA affords an infinite 3D pseudo-hexagonal enantiomeric 4-fold interpenetrating network sustained *via* pyridine-carboxylic acid supramolecular synthon (Figure 78).[169] The networks are linked by two dimensional honeycomb planes in which each plane is a Shubinkov hexagonal plane (hcb) net topology with each ladderane enantiomer alternating between planes (Figure 78b).[170] The distance between the pseudohexagonal cavities of (lad-1c)·2(TMA) is 22 x 16 Å. The 2D planes are comprised of one trimesic acid and one ladderane enantiomer each acting as a three connector node forming a honeycomb pattern consistent with a hcb topology. The second trimesic acid then acts as two connector node linking every fourth plane creating a 3-D framework consisting of a single ladderane enantiomer, while the second trimesic acid links the two planes through the open pyridine site on the ladderane to a carbonyl on the trimesic acid forming the plane (Figure 78c).

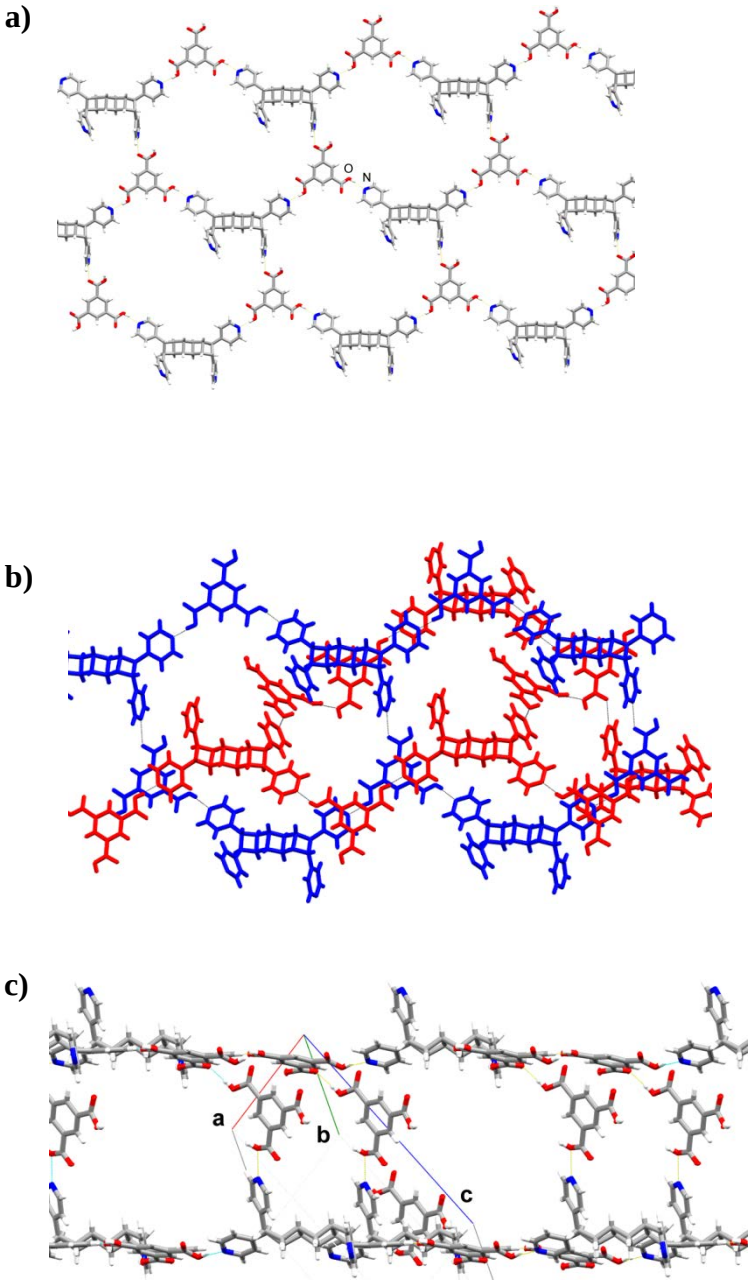

Figure 78. Wireframe representation of (lad-1c)·2(TMA): a) pseudo-honeycomb 2D-network; b) interpenetrating enantiomeric networks; c) TMA molecules connecting planes.

3.3.1.2.1. Salt vs. Co-crystal

The formation of a salt of the solid (lad-1c)·2(TMA) was ruled out by IR spectroscopy. The IR spectrum of solid (lad-1c)·2(TMA) had shown a carbonyl

(C=O) stretch of 1698 cm^{-1}. A slight shift from 1722 cm^{-1} of the pure solid of TMA which signifies hydrogen bonded dimers (1740 – 1650 cm^{-1}).[171] The frequency is indicative of aromatic carboxylic acid carbonyls involved in intermolecular hydrogen bonds (1700 – 1680 cm^{-1}).[171,172] Furthermore, a C=O stretch of an aromatic carboxylate anion generally exhibits stretching between 1610 – 1550 cm^{-1}.

3.4. Discussion

The results demonstrate the use of a co-crystal to structurally determine the stereochemistry of lad-1c that resists crystallization as a pure form. Our observations are, perhaps, not surprising given that, according to Carnelley's rule, molecules of relatively high symmetry tend to pack most favorably in a 3D lattice.[135,161] The results support Carnelley's rule such that use of an achiral CCF assists and enhances the crystal packing of lad-1c. 3,5-DNBA is trigonally substituted and possess C_{2v} symmetry, which facilitates a discrete assembly serving as a directional one-connecting spacer within solid (lad-1c)·4(3,5-DNBA)·5(CH_3NO_2). Moreover, TMA in solid (lad-1c)·2(TMA), possess C_3-symmetry which allows the formation of a pseudohexagonal grid acting as a three-connected node. In each case, the CCF serves to generate a supermolecular complex that packs efficiently to allow the stereochemistry of lad-1c to be determined. Moreover, it is reasonable to suggest that the presence of the achiral CCF increases the propensity for the chiral ladderane to crystallize in a well-packed environment.

Whereas lad-1c did not crystallize as a pure form, we managed to achieve single-crystals via neutral complexation with two carboxylic acids. Having the ability to form neutral complexes is an advantage of the use of a co-crystal. The pKa values of 3,5-DNBA and TMA are 2.82 and 2.12, respectively. The

formation of co-crystals and salts have been reported involving both acids, depending on the strength of the complementary base.[167,173] In our case, the pKa of the protonated pyridyl groups is likely comparable to 4-picoline (pKa = 5.98; pyridinium ion).[136] It is noted that the ladderane lad-1c is unique in that the stereochemistry is sensitive to the presence of acid. Nevertheless, the solids (lad-1c)·4(3,5-DNBA)·5(CH_3NO_2) and (lad-1c)·2(TMA) confirm the chiral structure.

Whereas a covalent derivatization of salt formation is relatively limiting, our results reinforce the enhanced modularity of co-crystallization. A derivatization of the lad-1c would likely require that the pyridyl groups be covalently functionalized. In comparison to other functional groups such as a carboxylic acid, synthetic transformations are limited. There are many covalent modifications involving the methylation of pyridines; however placing a charge on the pyridyl group or a bulky substituent may have similar isomerization effect as the acids that induce isomerization through protonation. Furthermore, chemists have at his/her disposal a wide range of neutral organic compounds that can be used as a CCF; however, precipitation by the use of a salt requires the presence of a strong base and/or acid which limits the availability of the crystallizing agent. Our results provide the first example of applying the use of a co-crystal for structural determination of a pH sensitive compound.

The co-crystallization to form (lad-1c)·4(3,5-DNBA)·5(CH_3NO_2) and (lad-1c)·2(TMA) resulted in a conglomerate and a racemate, respectively. Thus, the solids (lad-1c)·4(3,5-DNBA)·5(CH_3NO_2) and (lad-1c)·2(TMA)crystallize in a chiral $P3_221$ and achiral $P\bar{1}$ space group, respectively. The difference in chirality stems from one enantiomer being present in (lad-1c)·4(3,5-DNBA)·5(CH_3NO_2) and inducing chirality within the lattice, while both enantiomers are reside in (lad-1c)·2(TMA) likely crystallized as a racemic conglomerate.

The architecture of the assemblies of (lad-1c)·4(3,5-DNBA)·5(CH_3NO_2) and (lad-1c)·2(TMA) can be described as discrete and infinite, respectively. That the CCF 3,5-DNBA possesses a single carboxylic acid to interact with each pyridyl of lad-1c provided a discrete structure. The neighboring assemblies stack to form chiral channels. The formation of the channels may be attributed to the secondary interactions of the nitro groups which stack so as to achieve complementary interactions. In contrast, (lad-1c)·2(TMA) formed a 3D assembly that incorporates the ladderane into a honeycomb framework of TMA.[169] Unlike the empty channels of (lad-1c)·4(3,5-DNBA)·5(CH_3NO_2), the pores of the framework are occupied by an interpenetrating network of opposite handedness. An example of a 3D network based on TMA involves co-crystals of TMA and a linear pyridyl-based spacer 1,2-bis(4-pyridyl)ethane (4-bipy).[163] The network contains larger cavities of 35 x 26 Å in size as well as an 18-fold interpenetration (Figure 79). The potential applications for organic porous and interpenetrating networks lie in electric, optical, catalytic, and gas storage. These organic solids have received attention due to the structural modularity, the ability and predictability to self-assemble under mild conditions, and the flexibility of the weak interactions.[174,175]

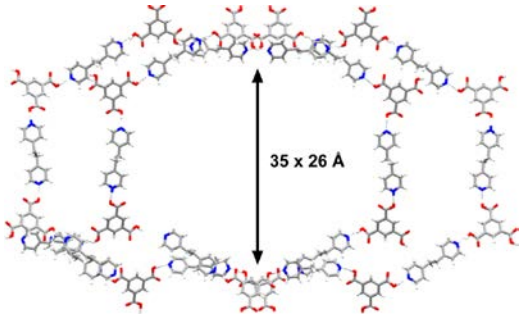

Figure 79. X-ray crystal structure of 2(TMA)·3(4-bipy) depicting cavity and neighboring interpenetrating network.

Neighboring secondary interactions contribute to the arrangement and stability of (lad-1c)·4(3,5-DNBA)·5(CH_3NO_2) and (lad-1c)·2(TMA). In particular, the oxygen of the nitro group of (lad-1c)·4(3,5-DNBA)·5(CH_3NO_2) interacts with the α-proton of the pyridyl group, the aromatic hydrogen of surrounding 3,5-DNBA molecules, as well as the N-atom of a neighboring nitro group in a perpendicular fashion. The neighboring ladderanes closely stack the inner cyclobutanes in a ladder type arrangement. The hydrogens of the ladderane scaffold and the aromatic hydrogens of the pyridyl interact with TMA *via* π-interactions. The interactions presumably provide secondary interactions so as to contribute to the rigidity of the structure.

3.5. Conclusion

We have described an application of a co-crystallization to determine the relative configuration of a diastereomer of a novel chiral [5]-ladderane that resists crystallization as a pure form. The ladderane is one of two isomers with relative configurations that could not be assigned using spectroscopy alone. Given that a wide variety of supramolecular synthons are now recognized to sustain the structures of multi-components solids, we expect co-crystallizations to experience more widespread applicability to problems of structure determination in organic synthetic chemistry.

CHAPTER 4. SOLID-STATE REACTIVITY OF A CARBOXYL-FUNCTIONALIZED POLYUNSATURATED OLEFIN

4.1. Introduction

The solid-state reactivity of unsaturated polyolefins continues to attract attention for the synthesis of complex molecules.[21,81,176,177] In particular, 1,3-dienes such as muconic acid are familiar reactants in organic solid-state photochemistry,[47,178-180] known to undergo cycloadditions, polymerizations,[181-185] and isomerizations (Figure 80).[186-188] The dienes can be arranged topochemically in either an 'in-phase' or 'out-of-phase' geometry to react.[66]

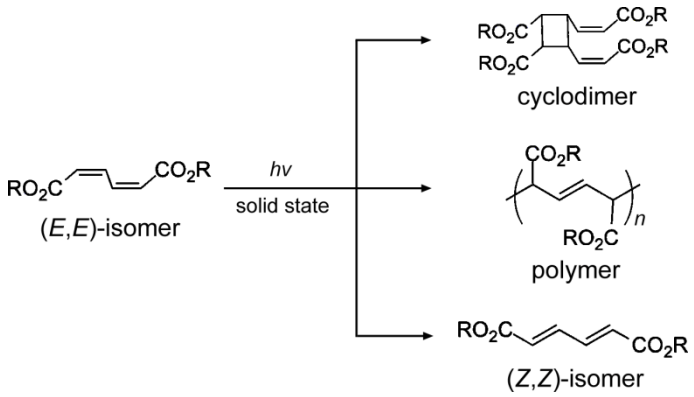

Figure 80. Solid-state reactivities of *E*,*E*-1,3-butadienes, where R = H (cyclodimer), ethyl (polymer), and methyl (isomerization).[176]

In this chapter, we will describe the solid-state reactivity of a hydrogen-bond donor 1,3-butadiene in the form of (*E*, *E*)-2,5-dimethylmuconic acid (dmma) with the use of a hydrogen-acceptor-based templates in the form of 1,2-bis(4-thiomethylenepyridyl)benzene (1,2-tmpb),[189] 2,3-bis(4-methylenethiopyridyl)naphthalene (2,3-nap),[63] and 1,8-bis(4-pyridyl)naphthalene (1,8-dpn) as well as the reactivity of dmma in pure form. A bicyclobutyl that

bears six carboxylic acid groups results from a trimerization of a diene diacid in the solid state. Powder X-ray diffraction and a co-crystallization are used to solve the structures of the diene and elucidate the stereochemistry of the bicyclobutyl, respectively. The hydrogen-bond-acceptor (HBA) templates 1,2-tmpb, 2,3-nap and 1,8-dpn are used to assemble dmma in the solid state for an intermolecular [2 + 2] photocycloaddition. Co-crystallization of 1,2-tmpb forms a shaped 0D hydrogen-bonded assembly, while 2,3-nap affords an 1D hydrogen-bonded polymer with dmma that are both photostable. A photoactive assembly is achieved with the use of the template 1,8-dpn with dmma that affords a 0D hydrogen-bonded solid. The diene stacks in-phase and reacts to give a *syn* monocyclobutane in up to 55% yield.

4.1.1. Early Solid-State Investigations of 1,3-Butadienes: Reactivity of Muconic Acid and Derivatives

Schmidt provided early detailed investigations of the solid-state reactivity of 1,3-butadienes.[47,48,50] Based on work with cinnamic acids, as well as mono- and dimethyl fumarate, diolefins in the form of butadienes, were determined to undergo [2 + 2] photodimerizations to afford various monocyclobutane derivatives. The first studies involved *E,E*-muconic acid.[48] The acid was shown to undergo a solid-state [2 + 2] photodimerization to the *syn*-monocyclized product (1*R*,2*S*)-3,4-bis((*E*)-2-carboxyvinyl)cyclobutane-1,2-dicarboxylic acid in 18-26% yield (Figure 81). Moreover, the packing arrangement of the solid according to X-ray analysis before photoreaction revealed parallel stacks of 1D-assemblies, separated by a distance of 3.7Å and sustained *via* hydrogen-bonded carboxylic acid dimers.

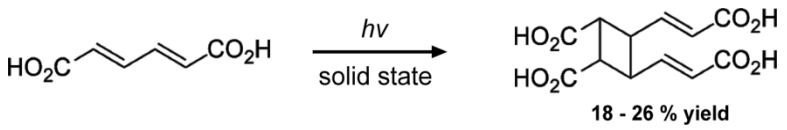

Figure 81. Solid-state photoreactivity of *E,E*-muconic acid.

Photoreactivity studies were also conducted with derivatives of *E,E*-muconic acid that included *Z,Z*-muconic acid, the all *trans* mono- and dimethyl esters, *E,E*-sorbic acid as well as 1,3-butadienes containing an acetyl- and phenyl-functionalized groups (Figure 82).[43,45,47,190] A common feature of the photoproducts derived from the reactive solids is the fact that all of the acids produced monocyclized products. It was also determined from later

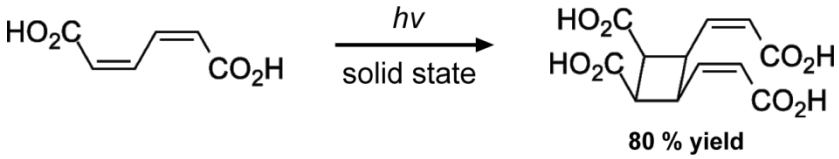

Figure 82. Solid-state photoreactions involving 1,3-butadienes.

work that 2,6-dichloro-4-phenyl-(*E,E*)-butadiene (dpe) arranges in a head-to-head fashion, which is likely due to chloro-chloro (Cl···Cl) interactions. Upon UV-irradiation, the solid produced a monocyclobutane in 80% yield (Figure 83).[49]

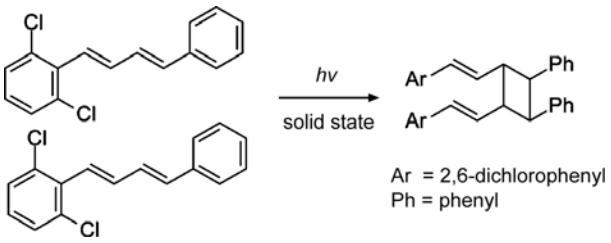

Figure 83. Solid-state photoreaction of dpe.

A mixed crystal with 1-(2,6-dichlorophenyl)-4-thienyl-(*E*,*E*)-1,3-butadiene (dtb) from a melt or growth *via* solution has also been studied.[50] UV-irradiation of the solid afforded a mixture of three different monocyclized photoproducts with the chiral molecule being the majority (Figure 84).

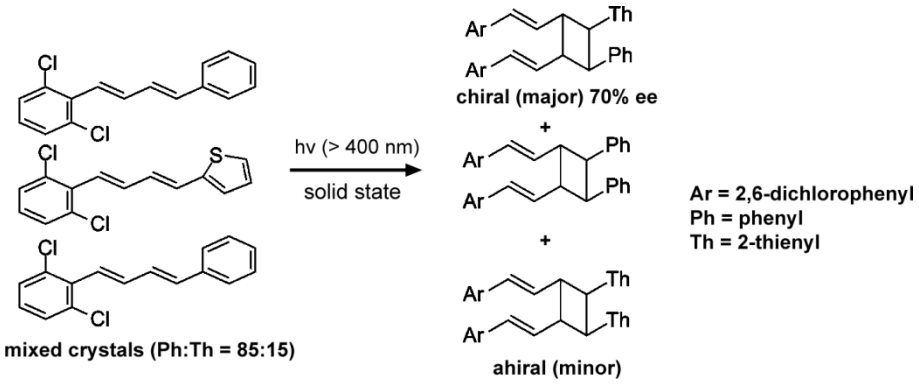

Figure 84. Schematic depiction of solid-state photodimerization of mixed crystals.

All of the photoproducts from reactions involving 1,3-butadienes afforded either *syn* or *anti*-monocyclized products. A possible explanation is the fact that once atoms move in solid, neighboring atoms for a photodimerization are placed out of position for reaction.[191,192]

4.1.2. Schmidt Revisited: Towards the Topochemical Control of 1,3-butadienes

Following the work of Schmidt involving 1,3-dienes, chemists set to further investigate the solid-state reactivity of dienes.[103,177,180,193] The reports here involved the use of non-covalent forces in the form of alkoxy-nitro, phenyl-fluoro, fluoro-fluoro and both covalently attached substituents and auxiliaries in the form of templates.

4.1.2.1. Alkoxy-Nitro Interactions

In 1993, Codding *et al*. used alkoxy-nitro interactions to control the organization of a diene, (*E*,*E*)-1-(2-methoxyphenyl)-4-(4-nitrophenyl)-1,3-butadiene, with aromatic alkoxy and nitro groups at opposite ends of the molecules (Figure 85).[54] The molecule arranged in a head-to-tail 'out-of-phase' fashion. Irradiation of the solid resulted in the formation of a *anti*-monocyclized product.

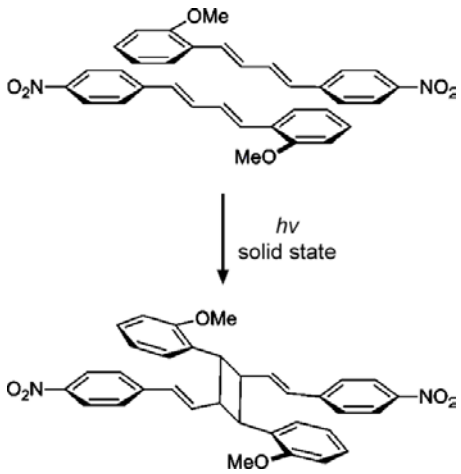

Figure 85. Solid-state reactivity of 1,3-butadienes stabilized *via* alkoxy-nitro interactions.

4.1.2.2. Phenyl-Fluorobenzene Interactions

Nine years later Vishnumurthy *et al*. induced the [2 + 2] photodimerization of all *trans* 1,3-butadiene derivatives (1*E*,3*E*)-1-pentafluorophenyl-4-(4-methoxyphenyl)buta-1,3-diene, (1*E*,3*E*)-1-pentafluorophenyl-4-(4-methylphenyl)buta-1,3-diene, and (1*E*,3*E*)-1-pentafluorophenyl-4-phenylbuta-1,3-diene by use of fluorine substitution.[57] The phenyl-perfluorophenyl arrangement dictates the head-to-tail conformations in each case (Figure 86). Exposure to UV-irradiation of the solids provides 23-25% yields of the photoproducts that resemble molecular ladders based on both mass and NMR spectra.

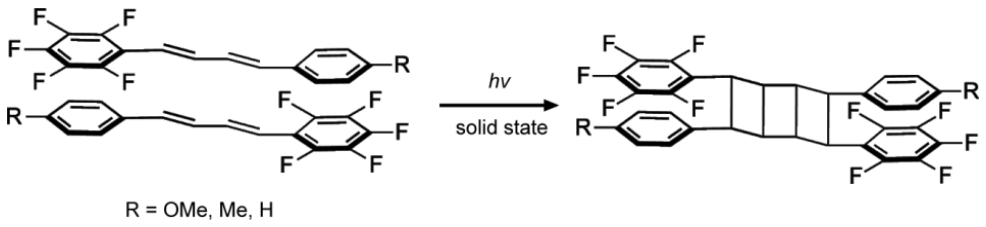

Figure 86. Schematic involving intermolecular construction of [3]-ladderane via phenyl-perfluorophenyl interactions.

4.1.2.3. Template Approach

In 2004, Gao *et al*. reported the syntheses of ladderanes in the organic solid state.[103] It was shown that small molecule templates based on resorcinol can assemble functionalized polyenes *via* hydrogen bonds into supramolecular architectures suitable for intermolecular [2+2] photodimerizations that generate [3]-ladderanes (Figure 87). Co-crystallization of 5-methoxyresorcinol (5-OMe-res) with 4-pyridyl-substituted 1,4-butadiene yielded four-component hydrogen-bonded molecular assemblies of general composition 2(template)·2(polyene).

UV-irradiation of the crystalline assemblies produced the corresponding end-functionalized ladderanes stereospecifically, in quantitative yield, and in gram amounts.

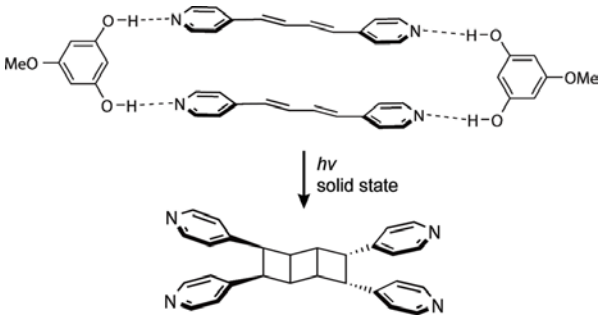

Figure 87. Schematic representation of reaction involving the arrangement of dienes in position for a photoreaction to obtain a [3]-ladderane.

4.1.2.4. Trifluoromethyl Groups

Following the work of MacGillivray *et al*., Liu and Boarman employed trifluoromethyl groups to direct the arrangement of a *E*,*E*-1,4-di(*o*-trifluoromethyl)phenyl-1,3-butadiene (tpb) in a position suitable for a photoreaction (Figure 88).[194] The tpb arranged in an offset 'out-of-phase' fashion with overlapping trifluoromethyl groups from neighboring molecules. UV-irradiation of the solid afforded the monocyclized product in 100% yield.

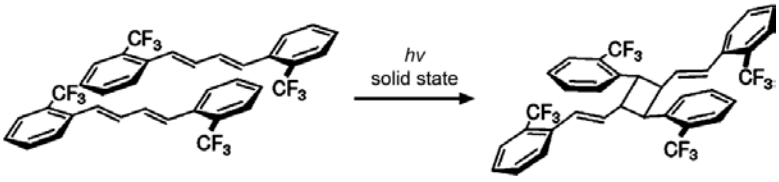

Figure 88. Schematic representation of trifluoromethyl-directed solid-state reaction.

4.1.2.5. Fluorine-Substituted Aromatics

Matsumoto *et al*. investigated the solid-state reactivity of 16 fluorine-substituted benzyl (*Z*,*Z*)- and (*E*,*E*)-muconates (Figure 89).[195] It was anticipated that aromatic stacking and C-H···F could orient the dienes in position that meet topochemical criteria for a photoreaction. Upon exposure to UV-irradiation, out of the eight *Z*,*Z* derivatives, four dimers were obtained in yields from 3-23%,

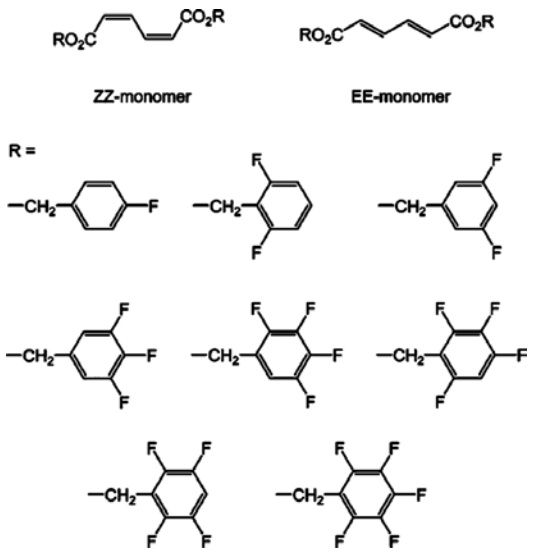

Figure 89. Schematic representations of muconate derivatives.

while out of the eight *E*,*E* derivatives four solids afforded dimers from 3 to 59% yield, all dimers being in the form of monocyclobutanes. Although an 'in-phase' arrangement of the muconates had been observed, the flexibility of the ester linkages likely decrease the ability for the double bonds to stack in a co-facial arrangement (Figure 90). It is also important to note that reactivity of the solids was also investigated in the presence of γ-ray radiation, with only three *E*,*E* derivatives producing dimers in no higher than 4% yield.

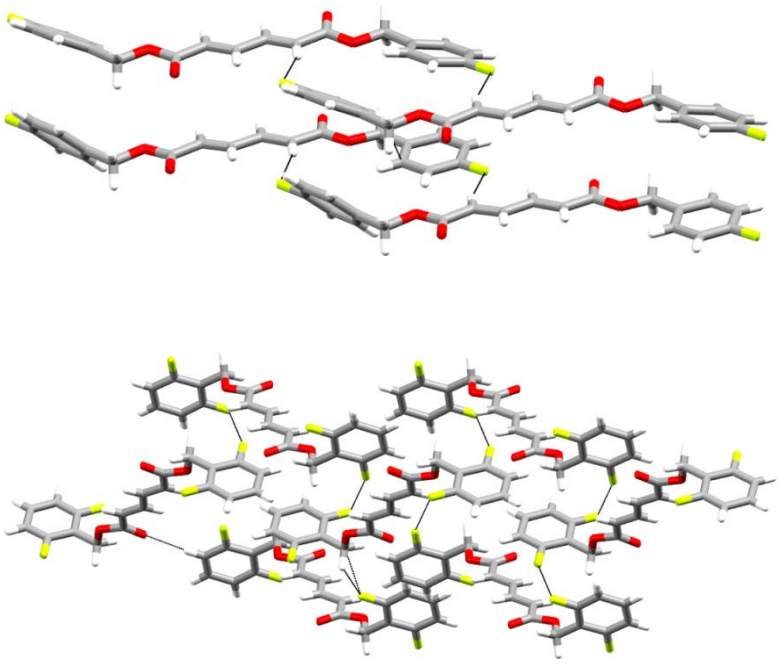

Figure 90. Wireframe X-ray crystal structures of muconates: a) photoactive solid b) photostable solid.

In a related study, a close examination of a single-to-single-crystal transformation of bis(3,4,5-trifluorobenzyl) (*E*,*E*)-muconate revealed a columnar assembly of monomer molecules that arrange to form what was likely a mixture of a *syn* dimer and a bicyclobutyl trimer in 27.9% yield.[196] The evidence from the photoreaction suggested that the dimer which is the majority product was obtained first followed by subsequent photodimerization from a single neighboring unreacted diene molecule.

4.1.2.6. Two-Dimensional Hydrogen-Bonds *via* Amide Groups

Mori and Matsumoto examined 14 *N*-substituted sorbamides and carbamates by stacking diene derivatives with amide functionalities.[197] Due to the NH group acting as a hydrogen-bond donor and the carbonyl as the hydrogen-

bond-acceptor, it was anticipated that 2D networks could be obtained that would place the double bond in position for a solid-state topochemical [2 + 2] photodimerization. Out of the 14 compounds, only one solid resulted in a [2 + 2] photodimerization. The *N*-sorbamides form 1D assemblies that interact *via* N-H···O=C hydrogen bonds. The molecules orient so as to cancel a dipole in alternating directions. As a consequence, the double bonds lie out of the topochemical criteria for a [2 + 2] photodimerization. In particular, *N*-benzylsorbamide formed 1D assemblies *via* 1D N-H···O=C hydrogen bonds and was photoactive (Figure 91). Later work by Odani *et. al*. included the investigation of the solid-state photoreactivity of various diynediammonium dienecarboxylates.[184] It was determined that the photodimerization of diene moieties in the crystals of 2,4-hexadiyne-1,6-diammonium (*E*,*E*)-muconate could be achieved.

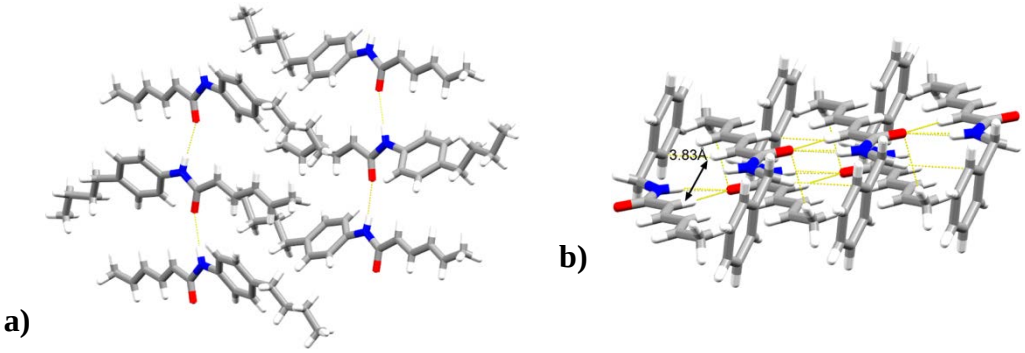

Figure 91. Wireframe X-ray crystal structures of sorbamides: a) photostable solid b) photoactive solid.

4.1.3. Chapter Overview: Application of Hydrogen-bond Acceptor Templates to a Diene Diacid

In this chapter, we describe the solid-state reactivity of the diene dmma with and without the use of three hydrogen-bond-acceptor (HBA) templates 1,2-tmpb,[189] 2,3-nap,[63] and 1,8-dpn (Figure 92). The ability of the bipyridines to

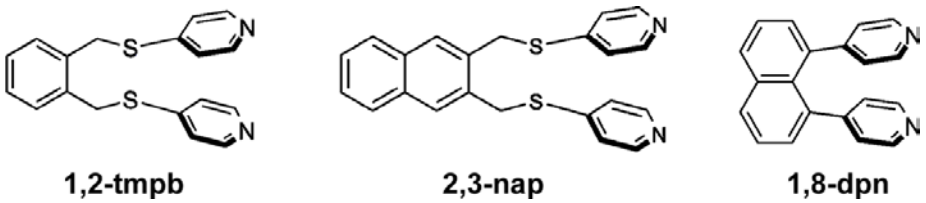

Figure 92. Schematic representation of hydrogen-bond acceptor templates.

enforce face-to-face stacking of fumaric acid (fum) for a photodimerization prompted us to determine whether each HBA template could be used to control the alignment of dmma in position for a [2 + 2] photodimerization. To employ the use of templates to dmma it was important to first determine the reactivity as a pure form. In our studies, we have discovered that dmma undergoes a trimerization in the solid state to generate the bicyclobutyl hexaacid diene, bis((*E*)-2-carboxyprop-1-en-1-yl)-2,2',4,4'-tetramethyl-[1,1'-bi(cyclobutane)]-2,2',4,4'-tetracarboxylic acid (bha) as well as a related *anti* dimer 2,4-bis((*E*)-2-carboxyprop-1-en-1-yl)-1,3-dimethylcyclobutane-1,3-dicarboxylic acid (cbta-1a) (Figure 93). A bicyclobutyl is a strained molecule composed of two cyclobutane rings connected at two corners *via* a carbon–carbon single (C–C) bond (Figure 93). To understand the origin of the photoreactivity, and to circumvent difficulties encountered to grow single crystals we used powder X-ray diffraction to determine the solid-state packing of the diene. Difficulties to isolate and grow

single crystals of the photoproduct have prompted us to apply co-crystallization to separate bha from cbta-1a and confirm the stereochemistry of the bicyclobutyl by single-crystal X-ray diffraction (Figure 93).

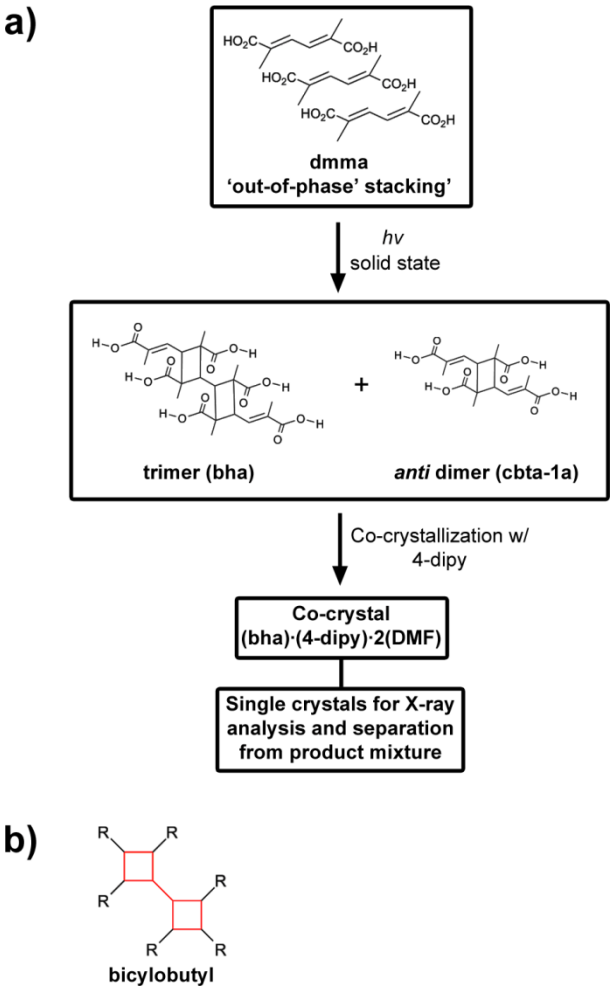

Figure 93. Schematic representation of a) reaction of dmma in pure form and b) bicyclobutyl.

Co-crystallization of dmma with templates 1,2-tmpb and 2,3-nap affords co-crystals (1,2-tmpb)·(dmma) and (2,3-nap)·(dmma) that form 1D hydrogen-bonded polymers that are both photostable, while 1,8-nap affords co-crystal 2(1,8-dpn)·2(dmma), a 0 D hydrogen-bonded assembly that is photoactive (Figure 94).

The diene stacks in-phase and reacts to give a *syn* monocyclobutane cbta-1b in up to 55% yield.

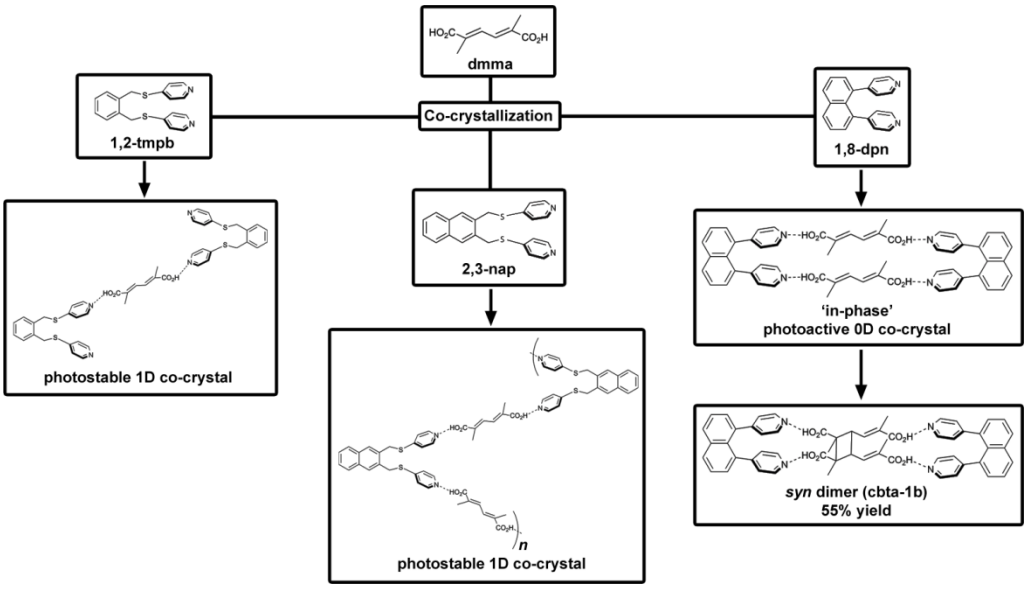

Figure 94. Schematic representation of reactivity of dmma with hydrogen-bond acceptor templates.

4.2. Experimental

4.2.1. Synthesis of Co-crystal (bha)·(4-dipy)·2(DMF)

A sample of the solid mixture from the photoreaction of dmma (100.0 mg) was combined with 4,4'-dipyridine (4-dipy) (21.0 mg) in DMF (1.0 mL) and allowed to sit for a period of one week; colourless single crystals of (bha)·(4-dipy)·2(DMF) were obtained (6 mg, 4.9% yield). ^{1}H NMR, (400 MHz; DMSO-d_6 δ/ppm): 8.72 (dd, J = 5.6 Hz, 6.8 Hz 1H), 7.95 (s, 1H), 7.83 (dd, J = 5.2 Hz, 6.8 Hz 1H), 5.72 (d, J = 9.6 Hz, 1H), 4.05 (d, J = 10.4 Hz, 1H), 2.89 (s, 1H), 2.73 (s, 1H), 1.79 (s, 1H), 1.26 (s, 1H), 1.21 (s, 1H).

4.2.2. Synthesis of Co-crystal (dmma)·2(1,2-tmpb)

A sample of 8 mg (0.025 mmol) of 1,2-tmpb and 4 mg (0.025 mmol) of dmma was dissolved in 2 mL of MeOH and the mixture heated to reflux, followed by a hot filtration. Cooling of the solution to room temperature and standing overnight provides the 2:1 co-crystals of (dmma)·2(1,2-tmpb) as light-brown crystals (7 mg, 58% yield). ^{1}H NMR, (400 MHz; DMSO-d_6 δ/ppm): 8.36 (dd, J = 1.6 Hz, 6.0 Hz 1H), 7.65 (dd, J = 2.0 Hz, 9,2 Hz 1H), 7.32 (dd, J = 3.2 Hz, 6.4 Hz 1H), 7.27 (dd, J = 2.0 Hz, 9.2 Hz 1H), 7.24 (s, 1H), 4.70 (s, 1H), 1.92 (s, 1H).

4.2.3. Synthesis of Co-crystal (dmma)·(2,3-nap)

A sample of 8 mg (0.21 mmol) of dmma and 3.7 mg (0.21 mmol) of 2,3-nap was dissolved in 2 mL of acetonitrile, heated to reflux, followed by hot filtration. Cooling of the solution to room temperature and standing overnight provides the 1:1 co-crystals of dmma with 2,3-nap (6 mg, 51% yield) as pale-brown crystalline solids. When 2,3-nap was co-crystallized with dmma (ratio: 1:1) from acetonitrile (2.0 mL), light-brown needles of (2,3-nap)·(dmma) formed during a period of 24 h. ^{1}H NMR, (400 MHz; DMSO-d_6 δ/ppm): 8.36 (dd, J = 1.6 Hz, 6.0 Hz 1H), 8.02 (s, 1H),7.85 (dd, J = 3.6 Hz, 5.6 Hz 1H), 7.49 (dd, J = 1.2 Hz, 6.0 Hz 1H), 7.35 (dd, J = 2.6 Hz, 3.6 Hz 1H), 7.29 (s, 1H), 4.70 (s, 1H), 1.92 (s, 1H).

4.2.4. Synthesis of Co-crystal 2(dmma)·2(1,8-dpn)

A sample of 31 mg (0.11 mmol) of dmma and 19 mg of 1,8-dpn (0.11 mmol) was dissolved in 2 mL of 1:10 (v/v) methanol:ethyl acetate and the mixture heated to reflux, followed by a hot filtration; light-yellow cubes of (1,8-dpn)·2(dmma) formed after a period of 24 h (19 mg, 38% yield). ^{1}H NMR, (400 MHz; DMSO-d_6 δ/ppm): 8.18 (dd, J = 8.14 Hz, J = 4.4 Hz, 4H), 8.15 (dd, J = 7.2

Hz, *J* = 8.2 Hz, 2H), 7.69 (dd, *J* = 1.1 Hz, *J* = 8.2 Hz, 2H), 7.47 (dd, *J* = 1.1 Hz, *J* = 7.2 Hz, 2H), 7.29 (s, 1H), 7.0 (dd, *J* = 1.7 Hz, *J* = 4.4 Hz, 4H), 1.92 (s, 1H).

4.2.5. Synthesis of Co-crystal 2(1,8-dpn)·(cbta-1b)

The reacted solid from 2(dmma)·2(1,8-dpn) was dissolved in 4:1 hexanes:ethyl acetate (v/v) and filtered to afford a white precipitate involving 1,8-dpn and the cyclobutane (ratio: 2:1). The filtered solid 2(1,8-dpn)·(cbta-1b) (10 mg, 0.011 mmol) was dissolved in 2mL of MeOH and allowed to evaporate slowly overnight to afford light-yellow needles (3 mg, 30% yield). ^{1}H NMR, (400 MHz; DMSO-d_6 δ/ppm): 8.18 (dd, *J* = 8.14 Hz, *J* = 4.4 Hz, 4H), 8.15 (dd, *J* = 7.2 Hz, *J* = 8.2 Hz, 2H), 7.69 (dd, *J* = 1.1 Hz, *J* = 8.2 Hz, 2H), 7.47 (dd, *J* = 1.1 Hz, *J* = 7.2 Hz, 2H), 7.0 (dd, *J* = 1.7 Hz, *J* = 4.4 Hz, 4H), 6.03 (d, *J* = 9.6 Hz, 1H), 3.39 (d, *J* = 10.4 Hz, 1H), 1.79 (s, 1H), 1.26 (s, 1H).

4.2.6. Photoreaction Experiments

Photoreaction experiments were performed using 30 mg samples of finely ground co-crystals of ma or dmma with either of 1,2-tmpb, 2,3-nap, or 1,8-dpn. The sample was placed between two Pyrex glass plates and exposed to ultraviolet radiation from a high-pressure broadband mercury lamp for 1 week or until no further reaction occurred.

4.2.7. NMR Spectroscopy

All products were characterized by the Avance-300, DRX-400, Avance-400, and Avance-600 Bruker NMR spectrometers (Billerica, MA) operating at 300, 400, and 600 MHz, respectively, using deuterated dimethyl sulfoxide (DMSO-d_6) as solvent. ^{1}H and ^{13}C chemical shifts were referenced with the residual proton and carbon chemical shifts of the solvents (DMSO-d_6, ^{1}H, 2.5 ppm; ^{13}C, 39.5 ppm). Fractions with milligram quantities of the product were

characterized with a battery of one- and two-dimensional heteronuclear experiments [^{1}H, 1D correlated spectroscopy (COSY), and heteronuclear multiple bond correlation (HMBC)]. Inverse detection were used for these 2D experiments. Typical parameters for the NMR experiments were as follows: ^{1}H (TD, 64k; NS, 4k), ^{13}C (TD, 128k; NS, 10000), 1D COSY (TD, 64k; NS, 512), NOESY (TD, 2k; TD1, 256; NS, 32; DS, 32; mixing times, 1.0, 1.5, and 2.0s), and ^{13}C-^{1}H HMBC (TD, 2k; TD1, 128; NS, 32; DS, 128). TD, NS, and DS refer to time domain data points, number of scans, and dummy scans, respectively. All of the NMR data were processed with the TOPSPIN 1.3 suite of software programs. One-dimensional ^{1}H data were processed with zero-filling to 64k data points and 0.2 Hz exponential line broadening, whereas ^{13}C spectra were processed with zero-filling to 128k data points and 1.0 Hz of exponential line broadening. The 2D NMR data were processed with the zero-filling to 2048 points and 1024 points in acquisition and second dimension, respectively. Relative numbers of proton signals multiplied by the integral areas were used for the quantification.

4.2.8. Powder X-ray Diffraction

The following PXRD structure solution data were provided in collaboration with Dr. Ivan Halasz and Dr. Robert E. Dinnebier of the Max-Planck-Institute for Solid State Research in Stuttgart, Germany. Structure solution of dmma by powder X-ray diffraction (PXRD) was accomplished on a Bruker D8 Advance powder diffractometer, equipped with Cu*K* α1 radiation from a primary Ge(111)-Johannson monochromator, Våntag-1 position sensitive detector with 6° angle opening; step mode with 0.0085° per step. The sample was gently crushed in an agate mortar into a fine powder and packed in a 0.5 mm borosilicate glass capillary. The capillary was rotated during data collection for

better particle statistics. The high-resolution pattern of dmma was collected in the angle region from 4° to 75° in *2*θ and the total data collection time was 18 h. Rietveld refinement was performed using restraints on bond lengths and valence angles as well as planarity restraints. All calculations (indexing, structure solution by simulated annealing in direct space and Rietveld refinement) were performed using the program Topas, version 4.1 (Bruker-AXS, Karlsruhe, Germany).

Table 5. Relevant general and crystallographic parameters for dmma.

Compound reference	Dmma
Chemical formula	$C_8H_{10}O_4$
Formula Mass	170.166
Crystal system	Monoclinic
a/Å	3.898360(63)
b/Å	7.87939(11)
c/Å	13.51483(35)
α/°	90
β/°	95.9652(16)
γ/°	90
Unit cell volume/Å3	412.883(14)
Temperature/K	293
Space group	*P*21/*c*
No. of formula units per unit cell, *Z*	2
*R*wp	0.0376
*R*p	0.0282
Goodness of fit on *F*2	1.72

4.2.9. X-ray Crystallography

Single-crystal X-ray diffraction studies of 2(1,2-tmpb)·(dmma), (2,3-nap)·(dmma), 2(1,8-dpn)·2(dmma), (bha)·(4-dipy)·2(DMF), and 2(1,8-dpn)·(cbta-1b) were performed on a Nonius Kappa CCD diffractometer. Data collection was conducted at 150 K using MoKα radiation (λ = 0.71073 Å). A total of 491

diffraction images were collected in two phi scans (frame-exposure times: 60 s and 240 s) and four omega scans (frame-exposure times: 240 s) with 2.0º per-frame rotations. Data reduction was accomplished using the *HKL Denzo*[128] and *HKL Scalepack* programs (Otwinowski & Minor, 1997). The structure was fully solved *via* direct methods using *SHELXS-97* (Sheldrick, 2008). Refinement by full-matrix least-squares based on F_2 was performed utilizing *SHELXL-97*[129] (Sheldrick, 2008). All hydrogen atoms were refined in geometrically constrained riding positions.

Table 6. Relevant general and crystallographic parameters for (bha)·(4-dipy)·2(DMF).

Compound reference	(bha)•(4-dipy)•2(DMF)
Chemical formula	$C_{50}H_{60}N_6O_{14}$
Formula Mass	969.04
Crystal system	Triclinic
a/Å	8.1654(9)
b/Å	11.7147(13)
c/Å	13.1518(14)
α/°	86.292(5)
β/°	77.546(5)
γ/°	78.982(5)
Unit cell volume/Å3	1205.4(2)
Temperature/K	293(2)
Space group	$P\bar{1}$
No. of formula units per unit cell, *Z*	1
Absorption coefficient, *μ*/mm-1	0.098
No. of reflections measured	8199
No. of independent reflections	4236
Rint	0.0182
Final *R1* values ($I > 2\sigma(I)$)	0.0462
Final *wR*(*F*2) values ($I > 2\sigma(I)$)	0.1239
Final *R1* values (all data)	0.0576
Final *wR*(*F*2) values (all data)	0.1294
Goodness of fit on *F*2	1.051

Table 7. Relevant general and crystallographic parameters for 2(1,2-tmpb)·(dmma), (2,3-nap)·(dmma), 2(1,8-dpn)·2(dmma), and 2(1,8-dpn)·(cbta-1b).

Compound reference	2(1,2-tmpb)•(dmma)	(2,3-nap)•(dmma)
Chemical formula	$C_{22}H_{21}N_2O_2S_2$	$C_{22}H_{18}N_2S_2$•$C_8H_{10}O_4$
Formula Mass	409.53	544.66
Crystal system	Triclinic	Monoclinic
a/Å	8.3642(9)	12.8295(14)
b/Å	11.0392(12)	14.5618(16)
c/Å	11.9678(13)	14.3340(15)
α/°	95.645(5)	90
β/°	106.936(5)	95.724(5)
γ/°	105.626(5)	90
Unit cell volume/Å3	999.11(19)	2664.5(5)
Temperature/K	293(2)	150(2)
Space group	$P\bar{1}$	*C*2/*c*
No. of formula units per unit cell, *Z*	2	4
Absorption coefficient, *μ*/mm-1	0.287	0.24
No. of reflections measured	6775	8919
No. of independent reflections	3502	2351
Rint	0.0191	0.0324
Final *R1* values ($I > 2\sigma(I)$)	0.0328	0.0361
Final *wR*(*F*2) values ($I > 2\sigma(I)$)	0.0823	0.0946
Final *R1* values (all data)	0.0414	0.047
Final *wR*(*F*2) values (all data)	0.0873	0.099
Goodness of fit on *F*2	1.083	1.053

Table 7. Continued.

Compound reference	2(1,8-dpn)•2(dmma)	2(1,8-dpn)•(cbta-1b)
Chemical formula	$C_{20}H_{14}N_2$•$C_8H_{10}O_4$	'$C_{16}H_{20}O_8$•2($C_{20}H_{14}N_2$)
Formula Mass	452.49	904.98
Crystal system	Monoclinic	Monoclinic
a/Å	14.5252(16)	31.686(4)
b/Å	6.9630(8)	9.6115(11)
c/Å	23.665(3)	29.601(3)
α/°	90	90
β/°	102.029(5)	93.685(5)
γ/°	90	90
Unit cell volume/Å3	2340.9(5)	8996.3(18)
Temperature/K	190(2)	150(2)

Table 7. Continued.

Space group	*P*21/*n*	*C*2/*c*
No. of formula units per unit cell, *Z*	4	8
Absorption coefficient, μ/mm-1	0.086	0.09
No. of reflections measured	15098	27238
No. of independent reflections	4117	7918
Rint	0.0388	0.0601
Final *R1* values ($I > 2\sigma(I)$)	0.0394	0.0579
Final *wR*(*F*2) values ($I > 2\sigma(I)$)	0.0994	0.1483
Final *R1* values (all data)	0.0597	0.0963
Final *wR*(*F*2) values (all data)	0.1078	0.1634
Goodness of fit on *F*2	1.046	1.07

4.3. Results and Discussion

4.3.1. Photoreactivity of dmma in Pure Form

When crystalline dmma was subjected to broadband UV-irradiation (450 W medium pressure Hg lamp) for a period of *ca* 60 h, a ^{1}H NMR spectrum (DMSO-d_6) revealed the diene to be consumed in a [2+2] photodimerization in near quantitative yield (Figure 95a). A photoreaction was evidenced by the near complete disappearance of the olefinic protons at 7.23 ppm and the emergence of three peaks, in the form of two doublets and a singlet, at 4.21, 4.04, and 3.35 ppm in the cyclobutane region, respectively (Appendix B). The signal for the methyl protons also disappeared and was replaced by five singlets in the region of 1.21-1.82 ppm, while two new peaks, in the form of two doublets, appeared in the vinyl region at 5.85 and 5.72. The NMR data were also consistent with the photoreaction having generated two products. The formation of two products was evidenced by a ^{1}H-^{1}H COSY spectrum, which revealed two groups of resonances in the cyclobutane region that correlated as two separate J-coupling networks in a 2:1 ratio (Appendix B). An electrospray ionization mass spectrum showed two

major peaks at *m/z* 339.11 and 509.17, which suggested the diacid reacted to give a trimer and a dimer as products (Figure 95b). From the combined NMR and mass spectrometry data, it was revealed that the solid-state reaction afforded a trimer and a dimer in 35% and 65% yield, respectively.

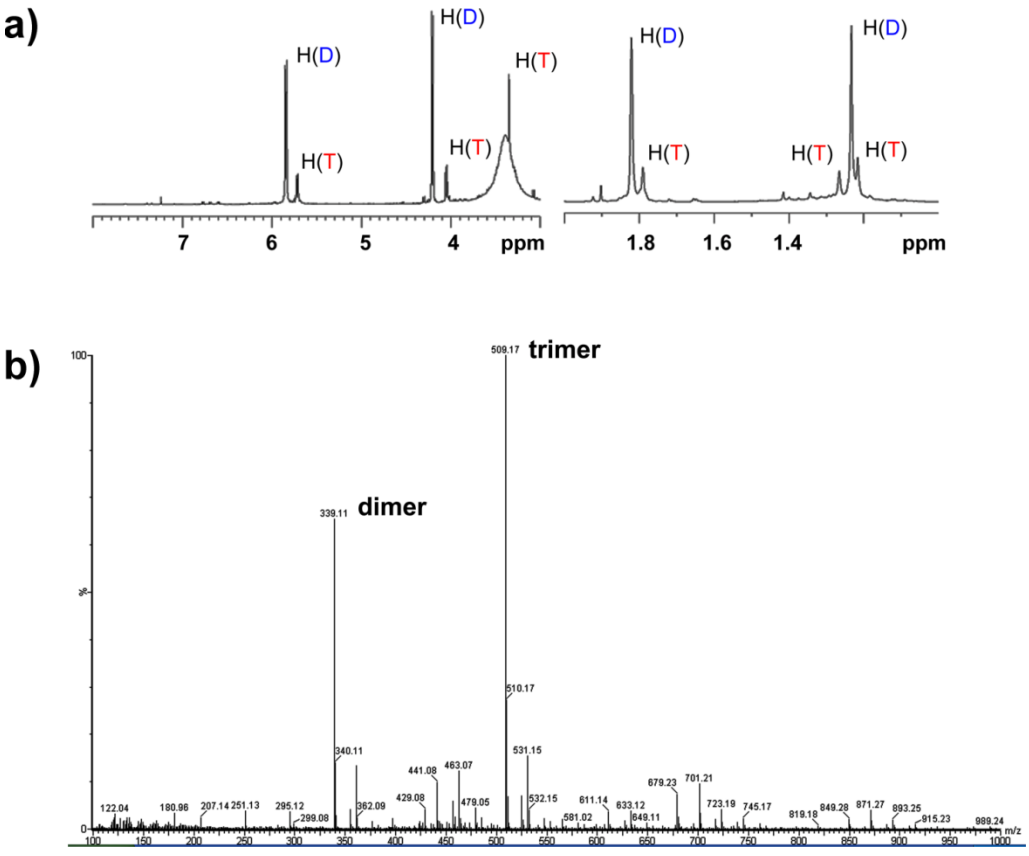

Figure 95. Spectroscopic data of dmma after photoreaction a) ^{1}H NMR spectrum after photoreaction; b) ESI-Mass Spectrum of photoreacted dmma after 60 hours. The fragment at 339.11 m/z represents the dimer. The fragment at 509.17 m/z represents the trimer.

In principle, a simple means to form a trimer or a bicyclobutyl is to arrange three dienes in a geometry for two intermolecular [2+2] photodimerizations (Figure 96). The bicyclobutyl framework has recently

emerged as an alternative high-energy hydrocarbon component of propellants and fuels.[198,199] Chemists have typically employed solution-based methods to synthesize bicyclobutyls.[200] Transformations based on metal-mediated couplings using Grignard and lithium reagents, as well as free radical and anionic-initiated polymerizations of functionalized cyclobutanes, have been reported. A trimerization of this type would be expected to bear a high energetic cost in solution owing to effects of solvation and entropy. Given that the [2+2] photodimerization readily proceeds in solids, the restricted yet flexible environment of the solid state has an inherent capacity to circumvent problems of solvation and entropy to make a trimerization of a diene possible.[196]

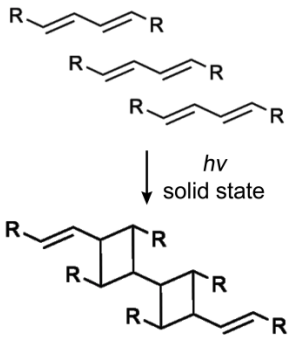

Figure 96. Schematic representation of a solid-state [2 + 2] photodimerization of three dienes to generate a bicyclobutyl.

A diagnostic peak in the NMR spectrum for the trimer is the lone cyclobutane singlet at 3.35 ppm, which is assigned to the two H-atoms that span the C–C bond that connect the cyclobutane rings of bha. Assignment of the peak to the network of bha was also verified by single-bond and multiple-bond ^{13}C–^{1}H correlation data (HMBC) of the photoreacted product mixture (Appendix B). A NOE experiment also demonstrated a close interaction between the methyl and

olefinic protons of cbta-1a, which is consistent with the *anti* geometry (Appendix B).

4.3.1.1. Crystallization Studies

4.3.1.1.1. Crystal Structure Analysis of dmma *via* PXRD

To understand the reactivity of dmma, we attempted to grow single crystals of the diacid. Although the diacid was soluble in common polar and apolar solvents, conventional methods of crystallization (*e.g.* supersaturation, slow cooling) afforded microcrystalline powders. Consequently, we turned to powder X-ray diffraction (PXRD) to elucidate the structure of dmma. PXRD has received increasing attention as a means to extract structural information from organic powder samples.[201-205] When a high-resolution powder diffraction pattern was collected on dmma, the data indexed to give a monoclinic unit cell with $P2_1/c$ as the most likely space group. According to volume increments, it was determined that the unit cell contained two molecules of dmma. The crystal structure was then solved by direct space global optimization assuming the asymmetric unit to consist of one half of molecule of dmma and confirmed by refinement according to the Rietveld method.

The diene was determined from the PXRD data to self-assemble, similar to the parent muconic acid,[48] in a one-dimensional (1D) hydrogen-bonded polymer sustained by carboxylic-acid dimers (O-H···O distance: 2.649(2) Å) (Figure 97a). The polymers lie stacked offset interacting *via* face-to-face π···π interactions along the crystallographic *a*-axis. The C=C bonds of nearest-neighbor dienes lie approximately parallel such that each C=C bond sits in close proximity to two adjacent C=C bonds at separations of 3.79 Å and 3.89 Å (Figure 97b). The geometry of dmma satisfies the criteria of Schmidt for a

photodimerization,[40] wherein the diene is able to react to give the trimer bha, the related photodimer cbta-1a, as well as higher oligomers and polymers.

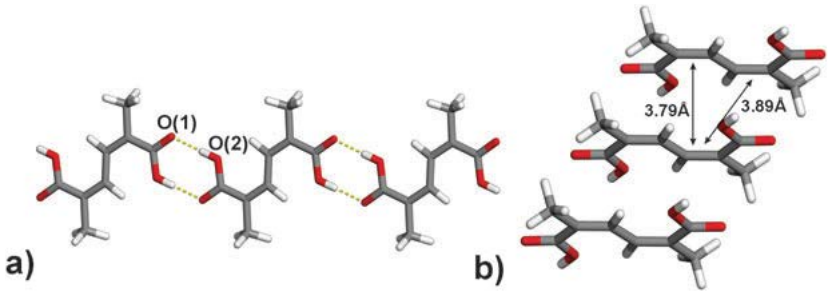

Figure 97. X-ray crystal structure of dmma as determined by PXRD: (a) hydrogen-bonded polymer and (b) stacked CQC bonds along *a*-axis.

Importantly, the structure from the PXRD experiment is consistent with three molecules of dmma having reacted in a trimerization to afford bha. The products arise from 'out-of-phase' stacking of the diene in the solid. In such a transformation, the diene undergoes two intermolecular [2+2] photodimerizations that produce a bicyclobutane composed of eight stereocenters, six carboxylic acid groups, and two unreacted C=C bonds. In addition to bha, the packing is consistent with dmma reacting to give the *anti* photodimer of dmma. The shortest C=C separation (3.79 Å) and a θ value of 96.5^{o} place the *p*-orbitals in a favorable position to react to give *anti* cbta-1a. The photodimer presumably serves as a precursor in a second cycloaddition that gives the trimer.

4.3.1.2.2. Co-crystal (bha)·(4-dipy)·2(DMF)

Whereas attempts to separate the trimer bha and dimer cbta-1a using chromatography were unsuccessful, bha was cleanly separated from cbta-1a and structurally characterized *via* a co-crystallization. Given that both photoproducts are decorated with acid groups, we hypothesized that co-crystallization of the

crude reacted solid mixture with a co-crystal former (CCF) lined with hydrogen-bond-acceptor functionality could be used to isolate and, possibly, confirm the structure of a photoproduct *via* a selective crystallization. A co-crystallization would be promoted by the specificity of the hydrogen bonds between the CCF and photoproduct, as well as crystal packing.

When a sample of the reaction mixture from dmma was combined with 4-dipy in DMF and allowed to sit for a period of one week, colourless single crystals suitable for X-ray diffraction were obtained. A ^{1}H NMR spectrum (DMSO-d_6) revealed signals that matched bha in the form of (bha)·(4-dipy)·2(DMF).

The co-crystal solid (bha)·(4-dipy)·2(DMF) crystallizes in the space group $P\bar{1}$. An X-ray analysis of (bha)·(4-dipy)·2(DMF) confirmed the structure of bha (Figure 98). The bicyclobutane bha sits around a center of inversion positioned at the central C-C bond [C-C distance (Å): 1.523(2)] with the C-C distances of the cyclobutane rings comparing well to experimentally-related structures [C-C distances (Å): C(2)-C(3) 1.583(2), C(3)-C(4) 1.575(2), C(4)-C(5) 1.574(2), C(5)-C(2) 1.579(2)]. The components self-assemble to form a 1D hydrogen-bond chain, which runs approximately parallel to the crystallographic *c*-axis, held together by O-H···N hydrogen bonds [O···N distances (Å): O(1)···N(1) 2.667(2), O(4)···N(2) 2.685(2)] (Figure 98). The four inner carboxylic acid groups (*i.e.* across cyclobutane rings) of bha participate in the hydrogen bonds to 4,4'-dipy with the bipyridine being propagated as stacked dimers along the chain. Each outer acid group participates in an O-H···O hydrogen bond to an included DMF molecule [O···O distance (Å): O(6)···O(7) 2.624(2)]. The co-crystal solid (bha)·(4-dipy)·2(DMF) represents, to our knowledge, the first structure confirmation of a bicyclobutyl obtained from the solid state.[196] Efforts are underway to employ a similar approach to elucidate the structure of cbta-1a.

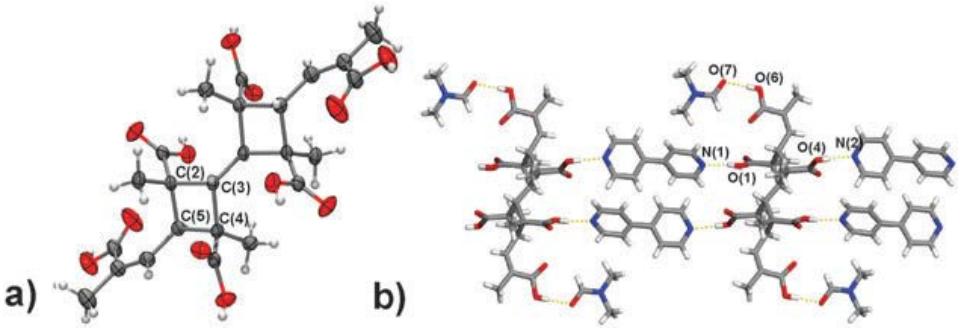

Figure 98. Single crystal X-ray structure of (bha)·(4-dipy)·2(DMF): a) trimer and b) 1D hydrogen-bonded assembly showing the stacked bipyridines.

4.3.2. Co-crystallization and Solid-State Reactivity of dmma with HBA Templates

4.3.2.1. Co-crystal (dmma)·2(1,2-tmpb)

Co-crystal (dmma)·2(1,2-tmpb) crystallizes in the space group $P\bar{1}$. The components dmma and 1,2-tmpb afford an S-shaped hydrogen-bonded assembly that is photostable (Figure 99). Each end of the diacid molecule is bound to a single 4-pyridyl group via O-H···N hydrogen bonds (O(1)···N(1) 2.634(2) from two different tmpb molecules, leaving a free pyridyl group on each tmpb molecule. The S-shaped assemblies alternate in stacked arrangements diagonal to the *ac*-plane interacting with the free pyridyl groups *via* co-facial pyridyl-pyridyl π···π interactions. The pyridyl groups from the neighboring stacks surround top and bottom of the diacid via C-H···π and C-H···carbonyl (C=O) interactions such that the diacid is insulated from the other molecules. Exposure of a powdered crystalline sample of the co-crystal to UV-irradiation (medium-pressure Hg lamp) revealed no photoreaction. The formation of the photostable 1D polymer is attributed to the conformational flexibility of 1,2-tmpb, which adopts an *anti* conformation in the solid.

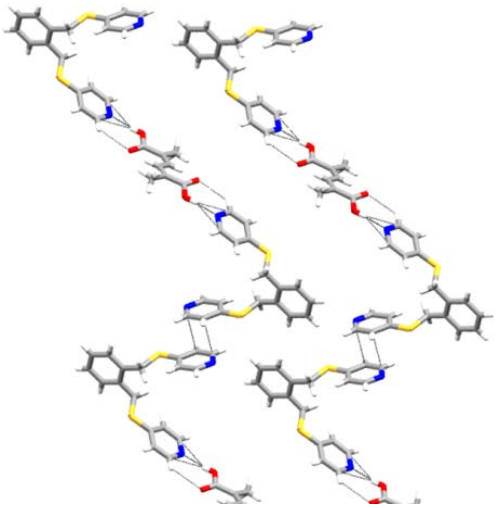

Figure 99. Single crystal X-ray wireframe structure of solid (dmma)·(2,3-nap) depicting a S-shaped assembly.

4.3.2.2. Co-crystal (dmma)·(2,3-nap)

The co-crystal (dmma)·(2,3-nap) crystallizes in the space group *C*2/*c*. The components of (2,3-nap)·(dmma) self-assemble to form a 1D polymer held together by O-H···N hydrogen bonds (O(1)···N(1) 2.584(2) Å) (Figure 100a). Neighboring 1D polymers lie parallel and offset, with the naphthalene units participating in edge-to-face π-π forces with 4-pyridyl groups. As a consequence of the assembly process, the C=C bonds of the dienes are separated by approximately 9.6 Å within and 9.7 Å between adjacent 1D polymers, respectively (Figure 100b). Exposure of a powdered crystalline sample of the co-crystal to UV-irradiation (medium-pressure Hg lamp) revealed no photoreaction.

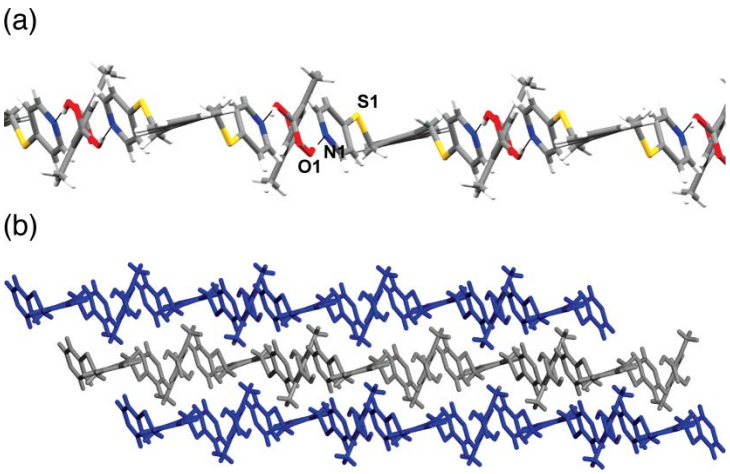

Figure 100. Perspective of (2,3-nap)·(dmma): a) 1D polymer and b) offset stacking along crystallographic *ac*-plane.

In contrast to the pure solid, the formation of the photostable 1D polymer is attributed to the conformational flexibility of 2,3-nap, which adopts an *anti* conformation in the solid. In this arrangement, 2,3-nap adopts, in contrast to (2,3-nap)·(fum) yet similar to the pure bipyridine,[5] an *anti* conformation (dihedral angle: 42.1^{o}) with the S-atoms pointing in opposite directions. The geometries lie well outside the criteria of Schmidt for a photodimerization in a solid. In line with the structure of (2,3-nap)·(dmma), the solid is photostable.

4.3.2.3. Co-crystal 2(dmma)·2(1,8-dpn)

Whereas (1,2-tmpb)·(dmma) and (2,3-nap)·(dmma) are photostable, the co-crystal 2(1,8-dpn)·2(dmma) is photoactive. The co-crystal 2(dmma)·2(1,8-dpn) crystallizes in the space group *P*21/*n*. In contrast to (1,2-tmpb)·(dmma) and (2,3-nap)·(dmma), 2(dmma)·2(1,8-dpn) is a discrete hydrogen-bonded assembly, which sits around a crystallographic center of inversion, sustained by four O-H···N hydrogen bonds (O(1)···N(1) 2.676(2) Å) (Figure 101a). In this arrangement, 1,8-dpn, being more rigid than 2,3-nap, enforces the diene into an

in-phase stacked geometry wherein the C=C bonds lie parallel and separated by 3.69 Å. The geometry places each C=C bond in a position suitable for [2+2] photodimerization. Nearest-neighbor assemblies lie orthogonal and separated at a distance > 10 Å (Figure 101b), which means the olefins within the 0 D hydrogen-bonded structures possess the C=C bonds able to undergo photoreaction.

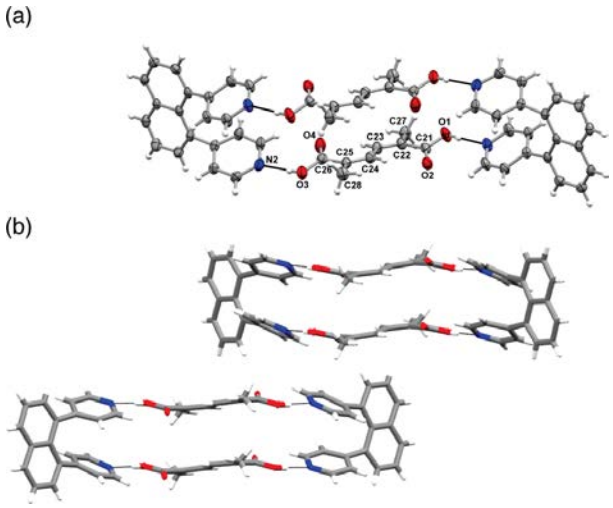

Figure 101. Perspective of (1,8-dpn)·(dmma): a) four-component assembly and b) nearest-neighbor assemblies.

To determine the reactivity of the solid, a powdered crystalline sample of 2(1,8-dpn)·2(dmma) was subjected to UV-irradiation (medium-pressure Hg lamp) for a period of approximately 70 h. As determined by ^{1}H NMR spectroscopy (solvent: DMSO-d_6), a monocyclobutane formed stereospecifically in 55% yield. The solid reacted to generate the monocyclized product that was evidenced by the emergence of both alkene and cyclobutane protons at 6.36 ppm and 3.70 ppm, respectively (ratios: 1:1). The chemical shift values of the peaks were different than the recently reported *anti* photodimer. Moreover, given that dmma was assembled in-phase in 2(1,8-dpn)·2(dmma) for reaction, the

cyclobutane product was assigned as the *syn* photodimer *rctt*-3,4-bis((*E*)-2-carboxyprop-1-enyl)-1,2-dimethylcyclobutane-1,2-dicarboxylic acid (cbta-1b).

4.3.2.4. Co-crystal 2(1,8-dpn)·(cbta-1b)

The structure of the photoproduct cbta-1b was confirmed *via* single-crystal X-ray diffraction. When the reacted solid was dissolved in 4:1 hexanes:ethyl acetate (v/v), a white precipitate involving 1,8-dpn and the cyclobutane (ratio: 2 : 1) immediately formed. Recrystallization from methanol afforded light-yellow needles after a period of 24 hours.

The co-crystal 2(1,8-dpn)·(cbta-1b) crystallizes in space group *C*2/*c*. The components of 2(1,8-dpn)·(cbta-1b) assemble to form a three-component complex sustained by four O-H···N hydrogen bonds (O(1)···N(1) 2.717(3) Å, O(3)···N(2) 2.661(3) Å) (Figure 102a). The pairs of acid groups attached to the unsymmetrical cyclobutane ring lie splayed, with each type of group interacting with an identical template molecule. The complexes pack in the crystallographic *ab*-plane to form 2D layers sustained by edge-to-face π-π interactions involving the pyridyl and naphthalene units of the templates (Figure 102b).

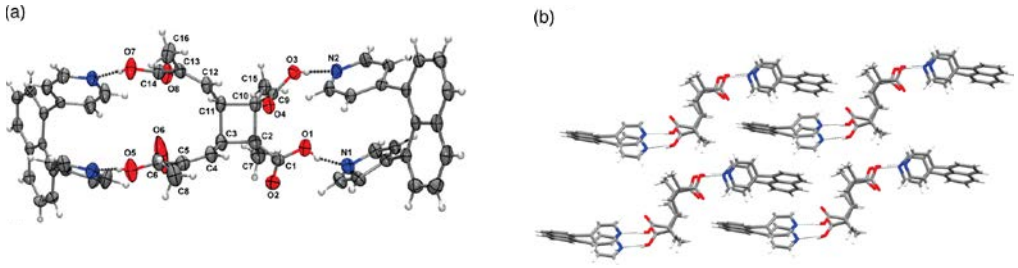

Figure 102. Perspective of 2(1,8-dpn)·(cbta-1b): a) discrete three-component assembly and b) packing of assemblies.

4.4. Conclusion

In summary, we have described a solid-state trimerization of a diene diacid that affords a bicyclobutane, as well as a related photodimer. An understanding of the origin of the trimerization has been provided by PXRD while the structure of the trimer has been authenticated *via* co-crystallization. This solid-state reaction represents, to our knowledge, the first case wherein an olefinic carboxylic acid has been determined to undergo a trimerization in a solid.[196] The approach described here may also be applied to additional dienes, and related polyenes, determined to form higher oligomers. In the future the hexaacid can potentially be reduced to a bicyclobutyl to hydrocarbon groups. The acid groups also make the resulting cyclobutanes attractive as ligands in coordination-driven self-assembly and amenable to a variety of post-synthetic transformations.[170,206] We have also demonstrated that 1,8-dpn assembles dmma for an in-phase intermolecular [2+2] photodimerization that generates *syn*-monocyclized product cbta-1b. The conformationally more flexible 2,3-nap results in a 1D hydrogen-bonded polymer that is photostable. With the reactivity of a diene diacid achieved, we are currently developing derivatives of both families of HBA templates so that libraries of bipyridines are available and can be applied in template switching[15] for the construction of more complex product molecules. Our results, thus, also further emphasize a critical role of template conformation in directing the reactivity of alkenes in co-crystalline solids.[14]

CHAPTER 5. MECHANOCHEMICAL PREPARATION OF TEMPLATE-DIRECTED REACTIVE SOLIDS

5.1. Introduction

The use of co-crystals is rapidly expanding in materials science, solid-state organic chemistry,[21] and pharmaceutics.[26,27,30] Traditional based approach to prepare a co-crystal is by dissolving the solid components in a solution and allowing crystallization between the two to occur via slow evaporation, cooling, and anti-solvent addition.[36,151] It is well established that solution-based crystallization provides well-defined and highly-ordered crystals with excellent opportunity for purification; however, there are disadvantages associated with this route to co-crystal formation.[151] Solution crystallizations may sometimes require the use of toxic solvents, which can be costly from both the purchase and waste disposal.[77] Moreover, the solvent can form solvates with the individual components rather than form the co-crystal or lead to undesired metastable polymorphs.[207,208] In this chapter the preparation of co-crystals *via* mechanochemical methods will be discussed in the context of forming reactive assemblies.

5.1.1. Preparation of Co-crystals: Mechanochemical vs. Solution

To circumvent the disadvantages of solution-based crystallizations mechanochemical methods have been employed to generate co-crystals with little or no solvent.[34,37] *Mechanochemistry* is the act of grinding or milling solids to induce the formation or breaking of a chemical bond.[33,37] Typically mechanochemical change is carried out by simple agitation of the solids in a vessel, with the use of mortar and pestle, or with the use of an electronic ball and mill. In each case, a substantial increase in heat and pressure is exerted on the

solid. In the case of co-crystal formation, non-covalent bonds are being broken and formed. An advantage of the preparation of co-crystals *via* mechanochemistry over solution is the fact that the yield obtained of co-crystal solid is generally greater than co-crystals grown from solution. Moreover, recent and rapid advances in structure solution from powder X-ray diffraction (PXRD),[205] solid-state NMR spectroscopy,[16,209] and terahertz spectroscopy[210] provide a means to characterize the molecular structure as well as phases of the solids.

5.1.2. Solvent-Free Grinding of Organic Solids

Typically, the first attempt to prepare a co-crystal by mechanochemical methods involves the act of grinding two solids to induce a change in a chemical bond without the assistance of solvent and is also known as solvent-free, dry, or neat grinding.[211] Although catalytic amounts of solvents can increase the rate of reaction,[33,207,212] the exclusion of solvent may be cost effective as well as free of toxic substances which can be a benefit in the case of pharmaceutics.[30,36,213]

5.1.2.1. Early Studies of Mechanochemical Preparation of Co-crystals

At the turn of the 20th century, the first known mechanochemical synthesis of a co-crystal was achieved by grinding the components metadichloroquinone and metachloroquinol to form a co-crystal in the form of tetrachloroquinhydrone.[33] It was not until the 1980's that studies involving the mechanochemical preparation of two-component organic solids that produce charge transfer complexes were continued. In particular, Paul *et al*. prepared complexes of unsymmetrically substituted quinhydrones that undergo self-oxidation-reduction in solution, with quinones *via* grinding with a mortar and pestle.[209,214,215] For instance, the grinding of benzoquinone (bq) with 1,4-

naphthohydroquinone (1,4-nhq) provides a stable complex, while the same components in solution afford redox-isomer products (Figure 103). These studies highlighted the fact that the solid-state can afford supramolecular

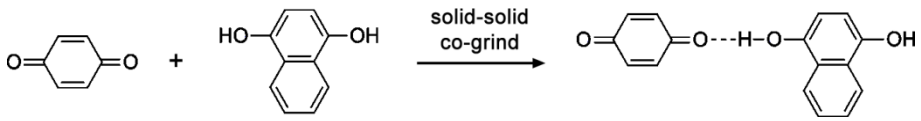

bq **1,4-nhq** **(bq)·(1,4-nhq)**

Figure 103. Solid-state grinding formation of (bq)·(nhq) complex.

assemblies that are difficult to obtain in solution.[33] Phase diagrams were later employed to complexes of hydroquinone and quinone derivatives to determine how variation of temperature or composition affects complexation.[216]

In 1987, Toda *et al.* determined the kinetics and solid-state interactions of host-guest complexes that generally undergo redox-isomerization.[217] As determined by IR spectroscopy and melting point, a variety of complexes could be obtained from grinding that did not produce charge-transfer interactions. For example, grinding 1,1-di(*o*-hydroxypheny1)cyclohexane (dhpch) and 1,4-naphthoquinone (1,4-nq) in a 2:1 ratio for 48 hours afforded a 2:1 complex, while solid-state grinding for 12 hours of *p*-cresol and *N*,*N*,*N*,*N*'-tetraisopropyloxamide (tipoa) produces a 1:1 complex (Figure 104). It is important to note that agitation of 1,1,6,6-tetraphenylhexa-2,4-diyne-1,6-diol (tphdd) and benzophenone (Ph_2CO) in an equimolar ratio produced a 1:1 complex in 12 minutes (Figure 104).

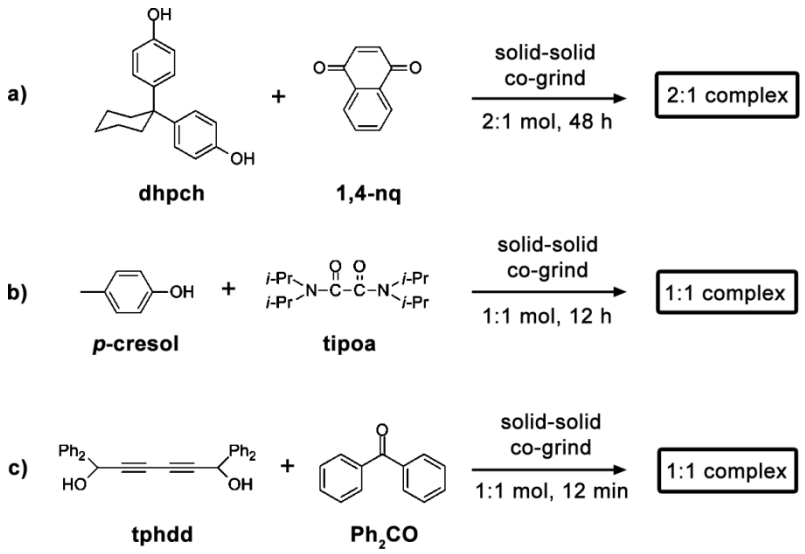

Figure 104. Solid-solid co-grinding formation of complexes that generally exhibit charge-transfer interactions in solution.

5.1.2.2. Combining Powder and Single X-ray Diffraction for Co-crystal Determination

Etter,[218-221] Kuroda,[222] and Hollingsworth[223] demonstrated the utility of combining both single crystal and powder X-ray diffraction (PXRD) characterization techniques to determine co-crystal formation from a mechanochemical preparation. Figure 105 shows compounds 3,5-dinitrobenzoic acid (3,5-DNBA) and 4-aminobenzoic acid (4-aba), which form co-crystals *via* solution and grinding. The co-crystal solid (3,5-DNBA)·(4-aba) was verified by a PXRD diffractogram that matched that of the simulated XRD diffractogram.[219]

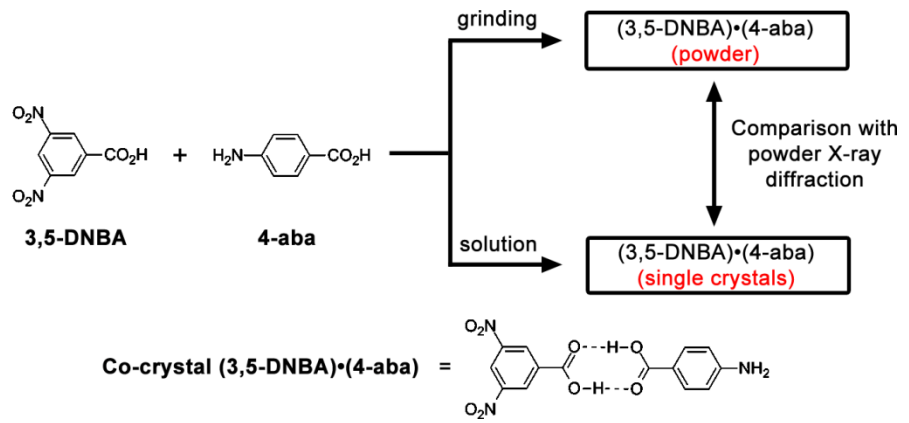

Figure 105. Co-crystal formation of (4-Cl-3,5-DNBA)·(4-aba) generated *via* solution or co-grinding pure components. The co-crystal powder obtained from grinding can be confirmed by the simulated powder pattern from the single-crystal X-ray diffraction data.

The application of mechanochemistry to generate pharmaceutical co-crystals was first reported by Ciara *et al.* in 1995.[173] Co-crystals of the drug sulfadimidine were prepared by individually grinding the active pharmaceutical ingredient (API) with various benzoic acid derivatives (Figure 106). By comparison of the PXRD patterns of co-crystals grown from solution it was determined that six co-crystals could be achieved by solvent-free grinding.

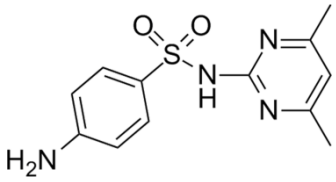

sulfadimidine

Figure 106. Schematic representation of sulfadimidine.

5.1.3. Liquid-Assisted Grinding

Whereas studies from the 1990's and early 2000's were aimed at determining the extent of obtaining co-crystals from grinding, it became apparent that a limitation of grinding was the fact that some co-crystals could not be obtained as a result of stronger intermolecular bonding of the individual solids.[33] A recent and significant advancement in mechanochemical grinding includes the process of adding small amount of solvent to enhance kinetics as well as control polymorphism. This method, namely, liquid-assisted grinding (LAG), is generally applied in the case where solvent-free grinding cannot provide the target co-crystal. The following sections will provide highlights of significant advancements in LAG.

5.1.3.1. First Example of LAG

Jones *et el.* demonstrated the first application of LAG. Co-crystals of (1s,3s,5s)-cyclohexane-1,3,5-tricarboxylic acid (CTA, $C_6H_9(CO_2H)_3$), with CCFs 4-dipy, hexamethyltetramine (HTMA), and 4,7-phenanthroline (fPh) were synthesized and analyzed using X-ray crystallography for the molecular structure and the simulated powder pattern (Figure 107).[224] When a mixture of CTA and HTMA were ground for 20 minutes, a PXRD revealed that the diffraction pattern differed from the individual patterns and matched that of the simulated co-crystal; however ground mixtures after one hour of CTA with 4-dipy or fPh resulted in partial change in the diffraction pattern indicative of limited amounts of co-crystal formation (Table 8). To facilitate co-crystal formation the addition of small amounts of solvent were added. PXRD analysis of the solvent-assisted samples revealed the co-crystals of the corresponding CCF had been achieved in periods of 10 minutes (Table 9).

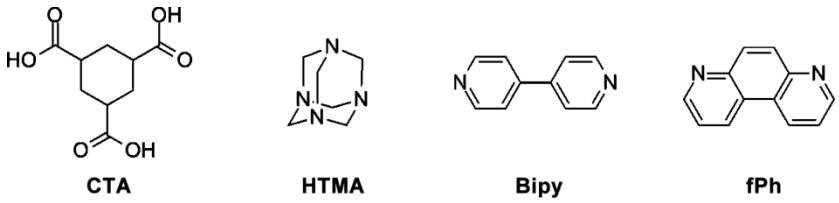

Figure 107. Compounds used to generate co-crystals *via* solvent-free or LAG.

Table 8. Solvent-free grinding of HBA compounds with CTA.

Solvent-free grinding		
Compound	**Co-crystal Formation**	**Time**
HTMA	Complete	20 min
Bipy	Partial	1 h
fPh	Partial	1 h

Table 9. LAG of HBA compounds with CTA.

LAG				
Compound	**Co-crystal Formation**	**Solvent**	**Amount of solvent**	**Time**
Bipy	Complete	MeOH	0.05 mL	20 min
fPh	Complete	MeOH or CH_3CN or EtOAc	0.05 mL	10 min

5.1.3.2. Control of Co-crystal Hydrates

An investigation involving co-crystal screening for hydrates by Jones *et al*. had shown that neat grinding with water or solid hydrates provided access to three-component co-crystals as well as demonstrated control of hydrate formation.[213] When theophylline, anhydrous citric acid, and water are ground, a co-crystal is obtained in equimolor ratios. Various combinations from the individual anhydrous forms with the monohydrate provided the same co-crystal; however neat grinding of only the anhydrous theophylline and citric acid affords an anhydrous co-crystal.

5.1.3.3. Polymorphic Control *via* LAG

The ability to control polymorphs is particularly important in pharmaceutics.[35,160] It is advantageous that chemists have used solvent-assisted grinding to enhance rates of supramolecular synthesis, but LAG has also been shown to control polymorphism. In 2002, Jones *et al*. demonstrated that liquid-assisted grinding provides access to the polymorph formation of model pharmaceutical co-crystals containing caffeine and glutaric acid (ga) (Figure 108).[207]

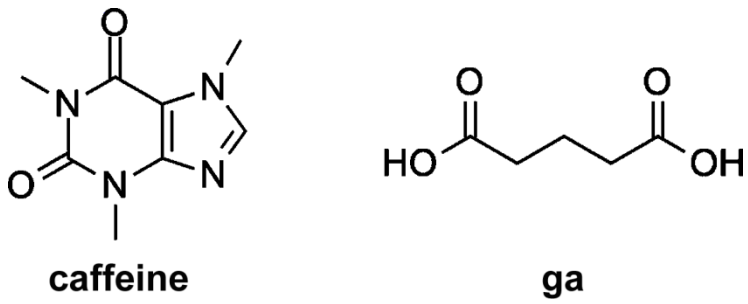

Figure 108. Schematic representations of caffeine and ga.

It was determined that slow evaporation of a mixture of caffeine and ga in chloroform affords two morphologically different crystals as monoclinic rods (solid 1) and triclinic blocks (solid 2). As confirmed by single-crystal X-ray diffraction the two crystals were different co-crystal polymorphs both in a 1:1 stoichiometric ratio. When caffeine and ga are ground solvent-free, solid 1 is the predominant form. Solid 1 was obtained with the use of small drops of non-polar solvents n-hexane, cyclohexane, and n-heptane. Solid 2 was obtained by the use of polar solvents such as chloroform, dichloromethane, acetonitrile, and water.

Such an application is highly desirable for co-crystal preparation such that it saves time opposed to slow evaporation as well as uses minimal amounts of solvents.

5.1.3.4. Systematic Three-Component Inclusion Solids *via* LAG

Inclusion compounds are important for the ability to trap gases or solvents *via* non-covalent interactions.[88] Typically, screening for inclusion of a guest compound is prepared *via* slow evaporation in solution.[225] The approach, however, can be limited to the solubilities of the molecular species involved. Friščić *et al*. demonstrated that screening for several solvents to act as guest in a multicomponent framework of caffeine and succinic acid can be achieved *via* solvent-assisted grinding.[225] It was determined that co-crystals of dioxane, caffeine, and succinic acid could be obtained from solution, neat grinding, as well as liquid-assisted grinding using acetonitrile as a catalyst in the reaction. Out of 25 solvents, attempts to obtain inclusion compounds from solution afforded 4, while neat and LAG were found to yield 15 and 18 complexes, respectively. These studies indicated that both neat and LAG is advantageous as opposed to solution-based crystallization, with LAG proving to be the most efficient technique.

5.1.4. Mechanisms of Mechanochemical Formation of Co-crystals

Given that the utility of mechanochemical methods towards the preparation of co-crystals is being realized, it is important to determine mechanisms associated with the mechanochemical synthesis.[226] To date few examples have focused on the study of mechanisms although several mechanisms have been proposed.[211] In particular, the mechanisms involve phase

transformations *via* 1) molecular diffusion, 2) eutectic formation, and 3) mediated amorphous phase.[211]

5.1.4.1. Molecular Diffusion

Molecular diffusion can readily occur when solids have relatively high vapor pressures.[227] This has been evidenced in the 1960's by Rastogi *et al*. in kinetic studies involving the complexation between picric acid and aromatic derivatives.[227-229] For example, when naphthalene and picric acid are placed in a capillary tube at opposite ends, it was determined that a complex forms at the interface that differs in color from the individual components in the absence of grinding (Figure 109). The kinetic results also suggested that the shape

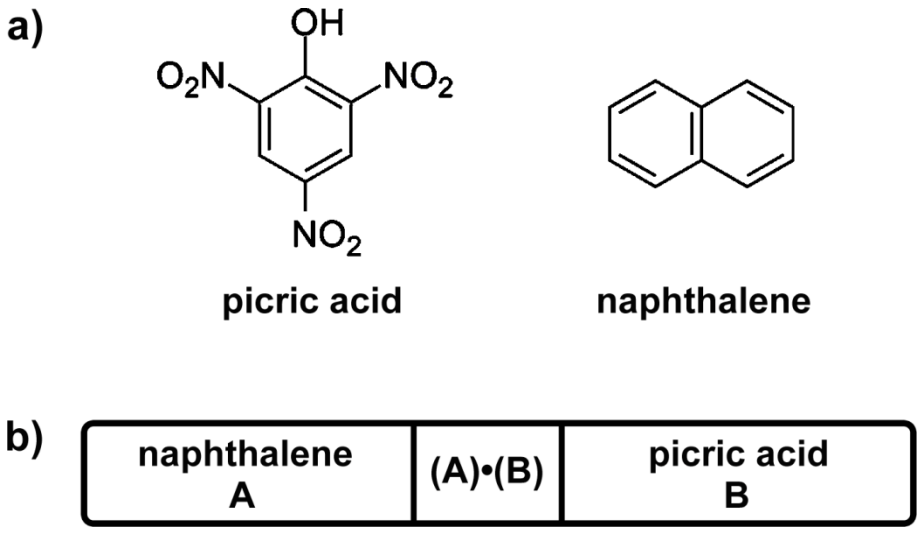

Figure 109. Schematic representations of a) structures of picric acid and naphthalene; b) complexation of naphthalene and picric acid in a closed capillary tube.

and symmetry of the molecules affected the rate of reaction. Specifically, flat and smooth molecules reacted faster than molecules containing larger or bulky substituents.[222] In essence, mechanochemical grinding increases the rate of surface diffusion through the gas phase. By mixing the pure solid components together once the surfaces undergo co-crystal formation, the co-crystal is removed from the surface of the pure solid exposing new surface available to react.[230-232] Evidence by Atwood *et al*. also suggests that gas can penetrate through the surface of solids.[88,233,234]

5.1.4.2. Eutectic-Mediated Phase

To better understand the mechanism of co-crystal formation by grinding, Davey *et al*. revisited a co-crystallization of a benzophenone (bzp) and diphenylamine (dpa) co-crystal which had been reported to change to a yellow color different from that of the pure white colored components upon co-crystallization (Figure 110).[235] Single crystals of the individual components were grown and brought into close proximity such that contact between the two separate surfaces was established at room temperature. Using real-time variable temperature microscopy and a cooling/heating stage, it was observed that upon contact, the solids began to melt and form a liquid phase. This liquid phase was likely a metastable eutectic mixture at room temperature given that the melting point was below that of the pure solids and the co-crystal. By confirmation by the yellow color, powder X-ray diffraction, and Raman microscopy, co-crystallization was only observed after agitation or seeding with crystals from one of the pure components. These results suggested that the force from grinding or remaining solid surfaces induces nucleation of the co-crystal. Later Lu *et al*. demonstrated the utility of differential scanning calorimetry (DSC) as a means to readily

identify eutectic melting and heating particularly for the use of pharmaceutical co-crystal screening.[236]

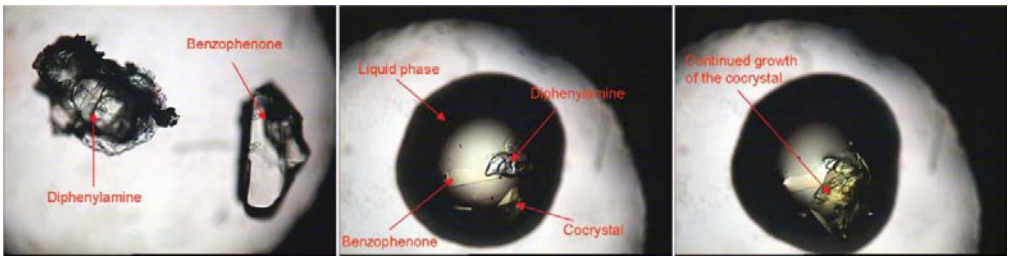

Figure 110. The solid state reaction of bzp and dpa at 25°C. (Mag x50). Starting crystals far left, growth of the co-crystal middle and far right.

5.1.4.3. Amorphous-Mediated Phase

Co-crystallization mediated by an amorphous phase is likely the result of grinding solids that are not volatile with robust intermolecular interactions.[237] Descamps *et al*. observed amorphous phases while investigating solid single-component transitions using lactose, trehalose, mannitol, and sorbitol.[237] Solids before and after grinding were observed using PXRD. While the solids before and 30 minutes afterward exhibited a clear powder pattern, the solid immediately after grinding had shown a noisy broad powder pattern, suggesting the presence of an amorphous intermediate phase before crystallization. The data supported the assertion that the amorphous phase likely occurred by grinding materials at temperatures below their glass transition point. These observations have also been observed with pharmaceutical co-crystals as demonstrated Rodríguez-Hornedo *et al*.[238]

5.1.4.4. Molecular Transitions: Bonding Effects on Mechanism

From a micromolecular perspective, Jones *et al*. provided significant insight on co-crystal molecular recognition.[239] It was determined from solution and neat grinding[240] for 30 minutes that 1:1 stoichiometric co-crystals of thiomorpholine (tmo) with tetrafluoro-1,4-diiodobenzene (1,4-tfib) could be obtained that consisted of linear halogen-bonded chains sustained by nitrogen-iodine (N···I) and sulfur-iodine (S···I) intermolecular interactions at opposite ends of 1,4-tfib (Figure 111). To better understand the mechanism, the components of the co-crystal reaction were ground and monitored at various times. After four minutes of grinding a powder pattern revealed the co-crystal; however an unknown crystalline solid was observed. Crystals from solution were grown to identify what was hypothesized to be an intermediate phase. Co-crystals of composition (1,4-tfib)·$(tmo)_2$ obtained from solution were shown to match the intermediate phase (Figure 111c). The crystal structure revealed a discrete assembly placing the two tmo molecules at the ends of 1,4-tfib sustained by nitrogen-iodine (N···I) halogen-bonds with the sulfur atoms of tmo now being free from bonding.

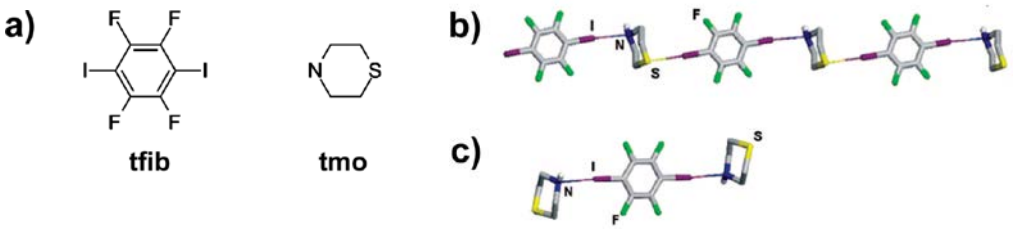

Figure 111. Schematic representations of a) structures of tfib and tmo; b) wireframe co-crystals (1,4-tfib)·(tmo); c) wireframe co-crystal (1,4-tfib)·$(tmo)_2$ from an intermediate phase.

The authors attributed this finding to the hierarchy of halogen bonds with the stronger N···I bond of the two forming the discrete assembly first, then forming the linear chain that involves the weaker S···I bonds. These studies provided the first systematic study of bonding competition among co-crystal reactants in the solid-state which adds to mechanistic insight of phase transformations. A similar report by Jones *et al*. has also explored this concept.[241]

5.1.4.5. Mechanisms of LAG

Presently, not much is known regarding the mechanism of liquid-assisted grinding,[211,242] however it is suggested that a significant increase in molecular collisions and the formation of co-crystal seeds can rapidly induce co-crystallization as described by Jones *et al*.[224] Recent evidence by Friščić and co-workers[225] as well as Bučar *et al*.[243] supports this hypothesis. Specifically, the co-crystal of caffeine and adipic acid could not be obtained from solution; however a LAG or slurry crystallization can achieve the formation of the co-crystal.[225,243]

5.1.5. Formation of Reactive Assemblies

Etter and co-workers activated a solid-state aromatic nucleophilic substitution reaction with the use of a co-crystal.[220] It was determined that 4-chloro-3,5-dinitrobenzoic acid (4-Cl-3,5-DNBA) and 4-aba form 1:1 co-crystals (4-Cl-3,5-DNBA)·(4-aba) by solution or grinding. When (4-Cl-3,5-DNBA)·(4-aba) is heated to 180°C, HCl gas is released to generate 4-((4-carboxyphenyl)amino)-3,5-dinitrobenzoic acid (4-a-4-cPh-3,5-DNBA) (Figure 112). Although single crystals for X-ray analysis could not be obtained, it is likely that the co-crystal permits the appropriate position for the nucleophilic substitution reaction to occur.

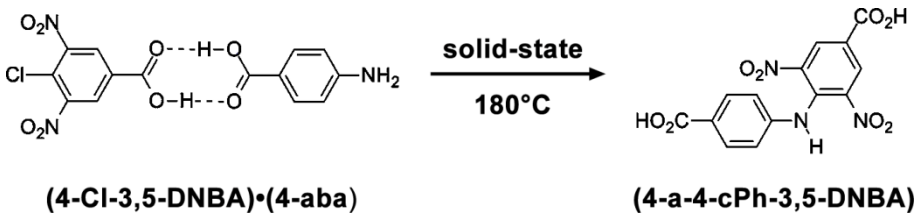

Figure 112. Schematic representation of solid-state reaction involving aromatic nucleophilic substitution reaction of (4-Cl-3,5-DNBA)·(4-aba).

Shan and Jones used LAG to prepare co-crystals of 1,2,4,5-benzenetetracarboxylic acid (bta) and 4,4'-bpe (Figure 113).[77] Solvent-free conditions did not facilitate the formation of (bta)·2(4,4'-bpe). The components formed an infinite 1D hydrogen-bonded polymer (bta)·2(4,4'-bpe) after grinding for 20 minutes with the subsequent addition of MeOH, which reacted to give 4,4'-tpcb in up to 100% yield after 48 hours.

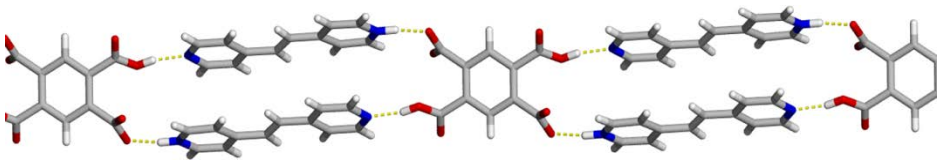

Figure 113. Wireframe representation of reactive co-crystal (bta)·2(4,4'-bpe) obtained via solution or grinding.

Zaworotko *et al*. also used LAG to achieve the synthesis of co-crystals that react to form imides by a heat assisted condensation reaction of the co-crystals containing 1,4,5,8-naphthalenetetracarboxylic dianhydride (NTCDA) and aromatic amine co-crystal formers.[244] A 1:2 co-crystal of NTCDA and 2-methyl-

4-nitroaniline (MNA) produced from LAG conditions produces the diamide in 75% yield after exposure to 180°C for 3 hours (Figure 114).

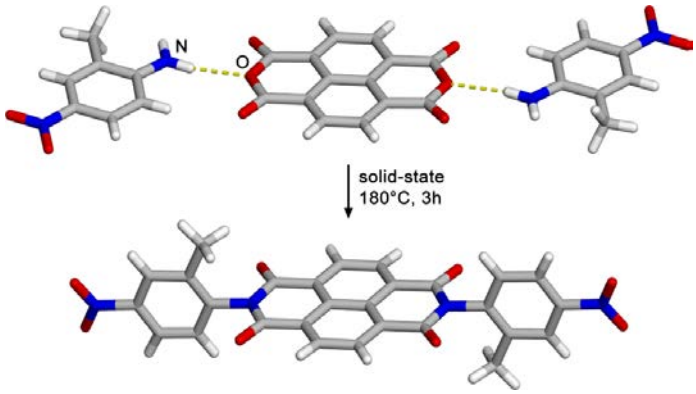

Figure 114. Condensation reaction of (NTCDA)·(MNA) derived from grinding.

5.1.6. Chapter Overview: Application of Mechanochemistry to Template-Directed Solid-State Synthesis

Given the significance of applications of co-crystals in the areas of pharmaceutics, materials science, and organic solid-state reactivity, combining mechanochemical methods is becoming increasingly important. Despite the few examples where mechanochemistry has been applied to prepare reactive co-crystals, a general methodology to apply mechanochemistry to systems that undergo reactions in the solid state has not been developed. In this chapter, we explore the generality of the application of mechanochemical methods to generate reactive supermolecules in template-directed syntheses. Indeed, combining mechanochemistry with methods that reliably direct the formation of reactive supermolecules can provide access to stereocontrolled and solvent-reduced routes for the covalent synthesis of a variety of organic molecules.[21]

We will show how supermolecules of general composition 2(res)·2(4,4'-bpe) form *via* solvent-free grinding within periods of minutes (Figure 115). In these solids, res acts as a hydrogen-bond donor template that assembles 4,4'-bpe for a stereocontrolled [2+2] photodimerization that generates 4,4'-tpcb in100% yield (Figure 115). In each HBD template-bpe reactant solid, the pyridine-hydroxyl synthon (O-H···N) facilitates the organization of a discrete assembly. In order to verify the general applicability of mechanochemistry to template-directed synthesis, we employed a systematic study in the ability of res-based templates to align olefins with 2- and 4-pyridyl substituents. We also describe two recently reported crystalline supermolecules 2,3-nap and 1,8-dpn to form *via* mortar-and-pestle co-grinding. In these solids, 2,3-nap and 1,8-dpn, in contrast to res, act as hydrogen-bond acceptor templates, assembling fumaric acid (fum) for a photodimerization that generates *rctt*-cbta stereospecifically, near 100% yield. The pyridine-carboxylic acid synthon assists with the formation of the discrete 4-component assembly. In contrast to 2(res)·2(4,4'-bpe), however, we have determined that liquid-assisted grinding is required to generate both supermolecules.

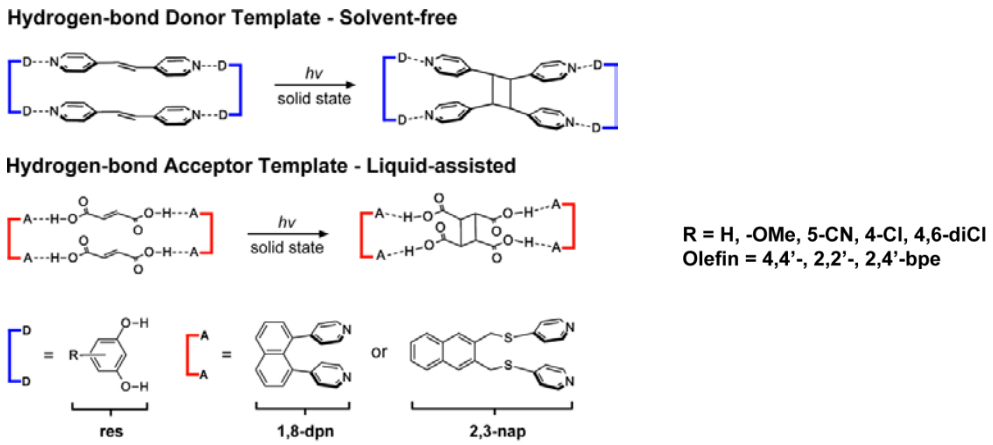

Figure 115. Schematic representation of templates and reactants.

5.2. Experimental

5.2.1. General Procedure

All reagents were purchased from Sigma-Aldrich Chemical Co. and used as received. All products were characterized by the Avance-300, a Bruker NMR spectrometer (Billerica, MA) operating at 300 MHz, using deuterated dimethyl sulfoxide (DMSO-d_6) as solvent. ^{1}H chemical shifts were referenced with the residual proton of the solvent (DMSO-d_6, ^{1}H, 2.5 ppm). Typical parameters for the NMR experiments were as follows: ^{1}H (TD, 64k; NS, 4k). TD, NS, and DS refer to time domain data points, number of scans, and dummy scans, respectively. All of the NMR data were processed with the TOPSPIN 1.3 suite of software programs. One-dimensional ^{1}H data were processed with zero-filling to 64k data points. Relative numbers of proton signals multiplied by the integral areas were used for the quantification. A melting point of 2,3-nap was examined using an Mel-Temp® Electrothermal apparatus.

5.2.2. Powder X-ray Diffraction

Powder X-ray diffraction was performed on a Siemens D5000 X-ray diffractometer using Cu K_α radiation on samples mounted on quartz slides.

5.2.3. Preparation of Co-crystals

The co-crystals were prepared under either solvent-free or LAG conditions. For solvent-free preparation, all co-crystallization experiments were performed using the same procedure exemplified below for the case of co-crystallization of the HBD res template, with 4,4'-bpe as the reactant. In a typical co-crystallization experiment a mixture of res (25 mg, 0.136 mmol) and 4,4'-bpe (15 mg, 0.136 mmol) was co-ground using a dry mortar-and-pestle for a period 15 minutes to achieve co-crystal 2(res)·2(4,4'-bpe). X-ray powder patterns included

the following peaks: 2θ = 10.0°, 11.9°, 16.3°, 17.4°, 18.26°, 19.3°, 20.12°, 21.82°, 22.78°, 24.32°, 25.9°, 26.84°, 27.59°, 29.8°, 30.2°, 31.7°, 32.92°, 36.0°. ^{1}H NMR, (400 MHz; DMSO-d_6 δ/ppm): 9.13 (s, 1H), 8.6 (d, *J* = 8.0 Hz, 1H), 7.6 (d, *J* = 7.6 Hz, 1H), 7.56 (s, 1H), 6.9 (t, *J* = 10.8 Hz, 1H), 6.19 (s, 1H), 6.17 (s, 1H). The following co-crystals were successfully prepared under the solvent-free conditions:

2(5-OMe-res)·2(4,4'-bpe): PXRD, 2θ = 9.08°, 10.02°, 11.74°, 13.98°, 14.96°, 15.52°, 16.42°, 17.04°, 18.02°, 18.3°, 19.16°, 19.94°, 21.1°, 22.32°, 24.24°, 24.6°, 25.66°, 26.76°, 27.16°, 29.74°, 31.72°, 36.66°, 41.36°. ^{1}H NMR, (400 MHz; DMSO-d_6 δ/ppm): 9.21 (s, 1H), 8.6 (d, *J* =8.0 Hz, 1H), 7.6 (d, *J* = 7.6 Hz, 1H), 7.56 (s, 1H), 5.81 (s, 1H), 5.78 (s, 1H), 5.77 (s, 1H).

2(5-CN-res)·2(4,4'-bpe): PXRD, 2θ = 7.24°, 8.18°, 10.42°, 12.6°, 14.64°, 15.88°, 16.8°, 17.44°, 19.04°, 19.84°, 20.86°, 21.94°, 23.04°, 24.46°, 26.04°, 27.02°, 27.66°, 28.18°, 28.78°, 30.16°. ^{1}H NMR, (400 MHz; DMSO-d_6 δ/ppm): 10.05 (s, 1H), 8.6 (d, *J* =8.0 Hz, 1H), 7.6 (d, *J* = 7.6 Hz, 1H), 7.56 (s, 1H), 6.57 (s, 1H), 6.52 (s, 1H).

2(4,6-dichloro-res)·2(4,4'-bpe): PXRD, 2θ = 13.0°, 14.1°, 15.68°, 16.78°, 20.56°, 21.92°, 23.32°, 24.2°, 25.74°, 26.92°, 28.24°, 29.6°, 30.88°, 31.92°, 33.5°. ^{1}H NMR, (400 MHz; DMSO-d_6 δ/ppm): 10.2 (s, 1H), 8.6 (d, *J* =8.0 Hz, 1H), 7.6 (d, *J* = 7.6 Hz, 1H), 7.56 (s, 1H), 7.24 (s, 1H), 6.64 (s, 1H).

2(res)·2(2,2'-bpe): PXRD, 2θ = 8.66°, 11.74°, 13.2°, 14.22°, 15.56°, 16.98°, 17.52°, 18.02°, 18.54°, 19.06°, 19.78°, 20.92°, 22.18°, 24.14°, 25.0°, 25.9°, 26.4°, 27.12°, 28.14°, 29.78°, 34.18°, 35.94°, 36.56°, 37.04°. ^{1}H NMR, (400 MHz; DMSO-d_6 δ/ppm): 9.13 (s, 1H), 8.61 (d, *J* = 4.8 Hz, 1H), 7.8 (m, 1H), 7.7 (s, 1H), 7.63 (s, 1H), 7.61 (s, 1H), 7.29 (m, 1H), 6.9 (t, *J* = 10.8 Hz, 1H), 6.19 (s, 1H), 6.17 (s, 1H).

2(4-Cl-res)·2(2,4'-bpe): PXRD, 2θ = 6.6°, 8.72°, 12.42°, 14.1°, 15.7°, 16.72°, 18.02°, 19.38°, 20.6°, 21.54°, 21.94°, 23.26°, 24.1°, 24.62°, 25.6°, 28.1°, 30.02°, 30.56°. ^{1}H NMR, (400 MHz; DMSO-d_6 δ/ppm): 9.94 (s, 1H), 9.46 (s, 1H), 8.61 (d, *J* = 4.0 Hz, 1H), 8.57 (d, *J* = 5.6 Hz, 1H), 7.83 (t, *J* = 6.8 Hz, 1H), 7.61 (m, 1H), 7.32 (m, 1H), 7.05 (s, 1H), 7.02 (s, 1H), 6.41 (d, *J* = 5.6 Hz, 1H), 6.02 (dd, *J* = 3.6 Hz, *J* = 3.6 Hz, 1H).

For LAG, both co-crystallization experiments were performed using the same procedure as shown below for the HBA template 2,3-nap and the fum reactant. A mixture of 2,3-nap (27.5 mg, 0.073 mmol) and fum (12.5 mg, 0.073 mmol) was co-ground using a dry mortar-and-pestle for a period of 10 minutes with the subsequent dropwise addition of 1.0 mL of ethyl acetate. X-ray powder patterns included the following peaks: 2θ = 9.4°, 11.82°, 12.32°, 13.16°, 16.2°, 18.88°, 22.2°, 22.8°, 23.9°, 25.28°, 26.66°, 27.6°, 28.72°, 29.32°, 38.22°. ^{1}H NMR, (400 MHz; DMSO-d_6 δ/ppm): 8.36 (dd, *J* = 1.6 Hz, 6.0 Hz 1H), 8.02 (s, 1H),7.85 (dd, *J* = 3.6 Hz, 5.6 Hz 1H), 7.49 (dd, *J* = 1.2 Hz, 6.0 Hz 1H), 7.35 (dd, *J* = 2.6 Hz, 3.6 Hz 1H), 6.61 (s, 1H), 4.70 (s, 1H).

The co-crystal 2(1,8-dpn)·2(fum) was successfully prepared using LAG conditions. PXRD, 2θ = 10.24°, 14.48°, 15.42°, 18.54°, 20.8°, 24.02°, 25.28°, 26.1°, 28.86°. ^{1}H NMR, (400 MHz; DMSO-d_6 δ/ppm): 8.18 (dd, *J* = 8.14 Hz, *J* = 4.4 Hz, 4H), 8.15 (dd, *J* = 7.2 Hz, *J* = 8.2 Hz, 2H), 7.69 (dd, *J* = 1.1 Hz, *J* = 8.2 Hz, 2H), 7.47 (dd, *J* = 1.1 Hz, *J* = 7.2 Hz, 2H), 7.0 (dd, *J* = 1.7 Hz, *J* = 4.4 Hz, 4H), 6.61 (s, 1H).

5.3. Results

We began our mechanochemical studies with the HBD templates and HBA reactants. Our experimental strategy was to began with the symmetrical reactants, particularly with res and 4,4'-bpe, as it is generally our simplest and

primary system of interest. Due to the fact that it is convenient and efficient to eliminate the use of solvent completely, we chose to explore solvent-free grinding as the initial approach to co-crystal formation. Liquid-assisted grinding was used in cases where attempts to synthesize the reactive assemblies were unsuccessful.

5.3.1. Model System and HBD templates

The co-crystal 2(res)·2(4,4'-bpe) served as a model system to determine grinding times that would afford co-crystallization of the template and reactant in the shortest time period. Initially, a mixture of res (25 mg, 0.136 mmol) and 4,4'-bpe (15 mg, 0.136 mmol) was co-ground using a dry mortar-and-pestle for a period of 1 hour. Our selection of the 1 h time period was based on the study of Shan and Jones where co-crystallization of 4,4'-bpe with 1,2,4,5-benzenetetracarboxylic acid (bta) by dry grinding was extremely slow, requiring periods greater than 2 h.[77,224] A powder X-ray diffraction (PXRD) analysis of the ground solid revealed that crystalline 2(res)·2(4,4'-bpe) formed in 1 hour (Figure 116). UV-irradiation produced, consistent with the structure of 2(res)·2(4,4'-bpe), tpcb-1a in near 100% yield.

Having achieved the formation of 2(res)·2(4,4'-bpe) *via* dry grinding in 1 hour, we turned to determine whether the co-crystal forms in shorter time periods. We monitored the grinding process using PXRD and ^{1}H NMR spectroscopy of the irradiated solids at intervals of 45, 30, 15, 14, 13, 12, 11, 10, 9, 8, 7, 6, 5, 4, 3, 2, and 1 minute. The shortest time period for the formation of 2(res)·2(4,4'-bpe) was determined to be 15 minutes (Figure 116). The diffractogram exhibited peaks at 2θ = 10.01, 11.91, and 25.91, which are consistent with the powder pattern from the co-crystal structure 2(res)·2(4,4'-bpe) from solution. UV-irradiation of the solid ground for 3 minutes generated 4,4'-tpcb stereospecifically in up to 55% yield (Appendix C).

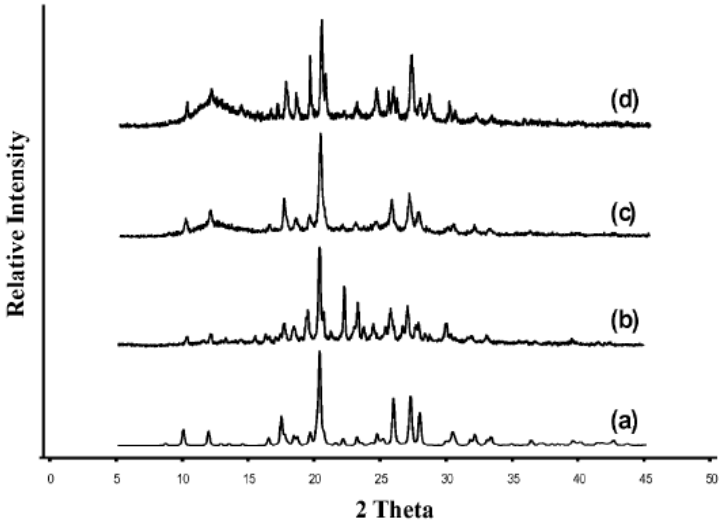

Figure 116. PXRD analysis of reactive 2(res)·2(4,4'-bpe): (a) simulated, (b) 1 h, (c) 15 min and (d) 3 min of dry grinding.

Our next entry into investigating such supramolecular reactivity led us to study the modularity by exploring derivatives of the res templates known to form reactive assemblies with 4,4'-bpe. Having established the conditions to obtain co-crystals of 2(res)·2(4,4'-bpe) from solvent-free grinding conditions, we applied a similar strategy to res derivatives. The derivatives were chosen based on existing single-crystal X-ray diffraction data. Moreover, having single-crystal data at hand, allowed to us to compare the powder diffractions patterns with the simulated pattern of the co-crystal. In particular, according to the diffraction patterns, all attempts to obtain co-crystals of dry co-grinding of R-res (where: R = 5-methoxy; 5-cyano; 4,6-dichloro) with 4,4'-bpe afforded the supermolecules 2(R-res)·2(4,4'-bpe) in approximately 15 minutes (Table 10). UV-irradiation of the solids afford tpcb-1a in 100% yield. Likewise, the co-crystals of 2(res)·2(2,2'-bpe), formed *via* dry grinding in 15 minutes. The solids reacted to give 2,2'-tpcb ≥ 98% yield. The co-crystals of 2(4-Cl-res)·2(2,4'-bpe) formed *via*

dry grinding in 15 minutes (Figure 117). The solid reacted to give *rctt*-2,4'-tpcb in near 100% yield.

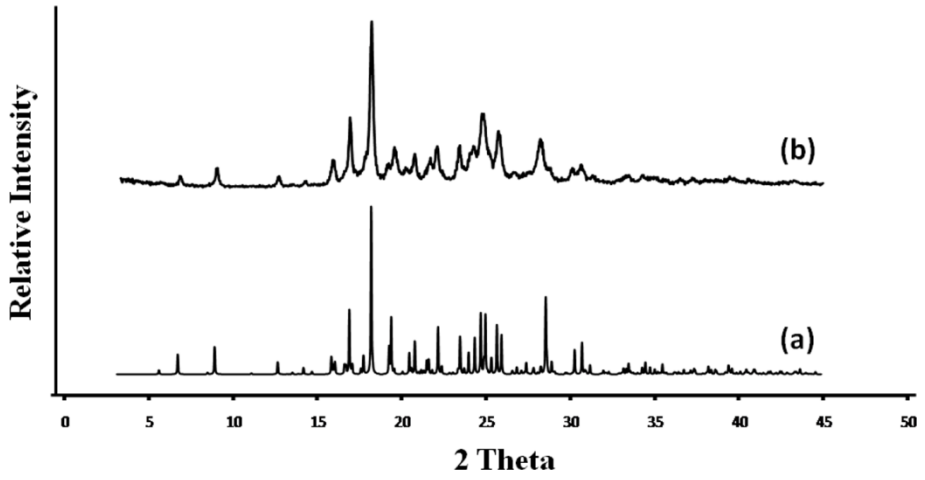

Figure 117. Co-crystals of 2(4-Cl-res)·2(2,4'-bpe): a) simulated powder pattern of 2(4-Cl-res)·2(2,4'-bpe), and b) co-crystals of 2(4-Cl-res)·2(2,4'-bpe) formed *via* dry grinding.

Table 10. Solvent-free conditions to obtain co-crystals (1:1 molar ratios) involving res and bpe derivatives.

Solvent-free grinding			
Template	**Reactant**	**Time**	**Co-crystal**
Res	4,4'-bpe	15 min	2(res)·2(4,4'-bpe)
4,6'-diCl-res	4,4'-bpe	15 min	2(4,6'-diCl-res)·2(4,4'-bpe)
5-CN-res	4,4'-bpe	15 min	2(5-CN-res)·2(4,4'-bpe)
5-OMe-res	4,4'-bpe	15 min	2(5-OMe-res)·2(4,4'-bpe)
Res	2,2'-bpe	15 min	2(res)·2(2,2'-bpe)
4-Cl-res	2,4'-bpe	15 min	2(4-Cl-res)·2(2,4'-bpe)

5.3.2. HBA templates

In contrast to the supermolecules based on res, the reactive assemblies 2(2,3 nap)·2(fum) and 2(1,8-dpn)·2(fum), did not form under dry conditions

(Figure 118). In particular, dry co-grinding of either 2,3-nap or 1,8-dpn and fum for up to 1 hour yielded mixtures of pure components. Liquid-assisted grinding, however, generated the assemblies. Thus, when 2,3-nap and fum were co-ground with a small aliquot (1.0 mL) of ethyl acetate for a period of approximately 10 minutes, crystalline 2(2,3-nap)·2(fum) cleanly formed, as determined by PXRD. UV-irradiation of the solid produced cbta, as reported.[64,245] Likewise, 2(1,8-dpn)-2(fum) was generated when 1,8-dpn and fum were ground in the presence of ethyl acetate (0.1 mL) for a period of approximately 10 minutes (Table 11).

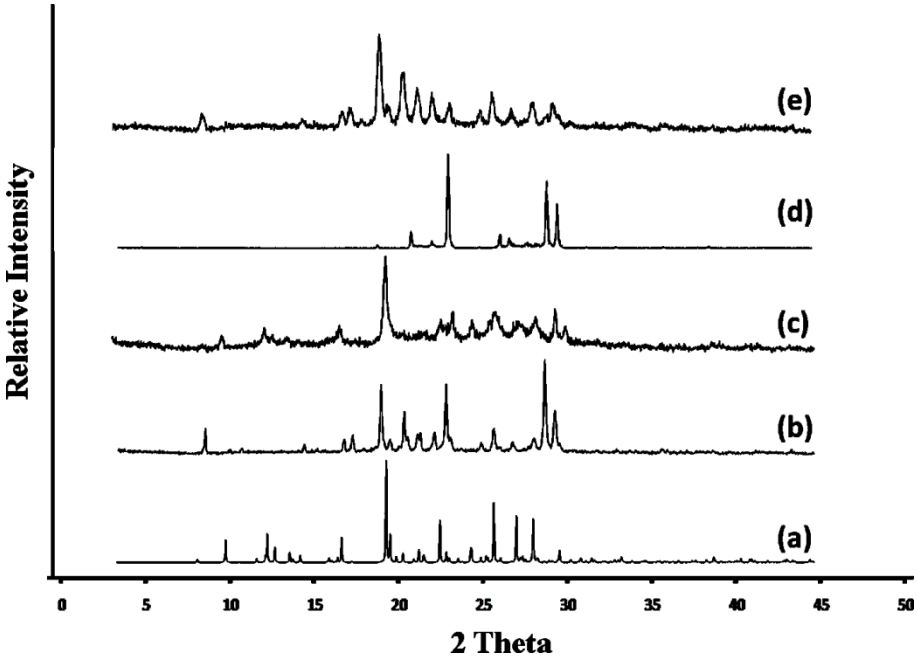

Figure 118. Powder X-ray diffraction pattern of (a) simulated pattern from single-crystal structure of 2(2,3-nap)·2(fum), (b) ground dry mixture of 2,3-nap + fum (1hr), (c) ground dry mixture of 2,3-nap + fum with EtOAc (10 min), (d) fum, (e) 2,3-nap.

Table 11. LAG experiments involving 2,3-nap, 1,8-dpn, and fum.

LAG					
Template	**Reactant**	**Time (min)**	**Solvent**	**Solvent (mL)**	**Co-crystal**
2,3-nap	Fum	10	EtOAc	0.1	2(2,3-nap)·2(fum)
1,8-dpn	Fum	10	EtOAc	0.1	2(1,8-dpn)·2(fum)

5.4. Discussion

That the reactive assemblies based on res form rapidly and under dry conditions is remarkable, particularly given that the mechanochemistry is general in both template and reactant. The HBD res-based supermolecules formed rapidly and without the use of solvent with bpe compounds, while the HBA templates formed under LAG conditions with fum. The reactivity may thus be attributed to 1) secondary intermolecular forces of the pure solid components, 2) synthons, and 3) melting points.

Prior to grinding, a solid mixture generally consists of pure template and olefinic components. To achieve the synthesis of a co-crystal, cohesive forces in both the pure solids of the template and reactant break to form non-covalent bonds associated with the co-crystal.[155] For res, and derivatives, single O–H(phenol)···O(phenol) hydrogen bonds predominate (Figure 119a).[246] The bond strength associated with these hydrogen bonds lies between 16 – 60 kJ mol^{-1}.[1,4,247] For the bpe derivatives C-H(pyridine)···H-C(pyridine), C-H(pyridine)···N(pyridine), and π(pyridine)···π(pyridine) interactions predominate (Figure 119b).[1,4,248] Bond strengths are generally weaker with these types of non-covalent interactions between 4 – 50 kJ mol^{-1}.[1,4] This contrasts the double O–H(acid)···O(carbonyl) hydrogen bonds of acid dimers with strength of 80 – 120

kJ mol^{-1} of a molecule such as bta.[4,77,224] Moreover, that bta is a tetraacid means that a dry grinding process will also be required to break apart a network of hydrogen bonds to afford crystalline (bta)·2(4,4'-bpe), which is likely facilitated by the addition of the liquid phase.[224,226] Our experiments involving 2(2,3-nap)·2(fum) and 2(1,8-dpn)·2(fum) support this assertion since fum forms a hydrogen-bonded network in the solid state sustained by acid dimers (Figure 119c).[249] This contrasts the structures of the pure bipyridines 2,3-nap and 1,8-dpn, as well as 4,4'-bpe which are sustained by weaker van der Waals and π···π forces.

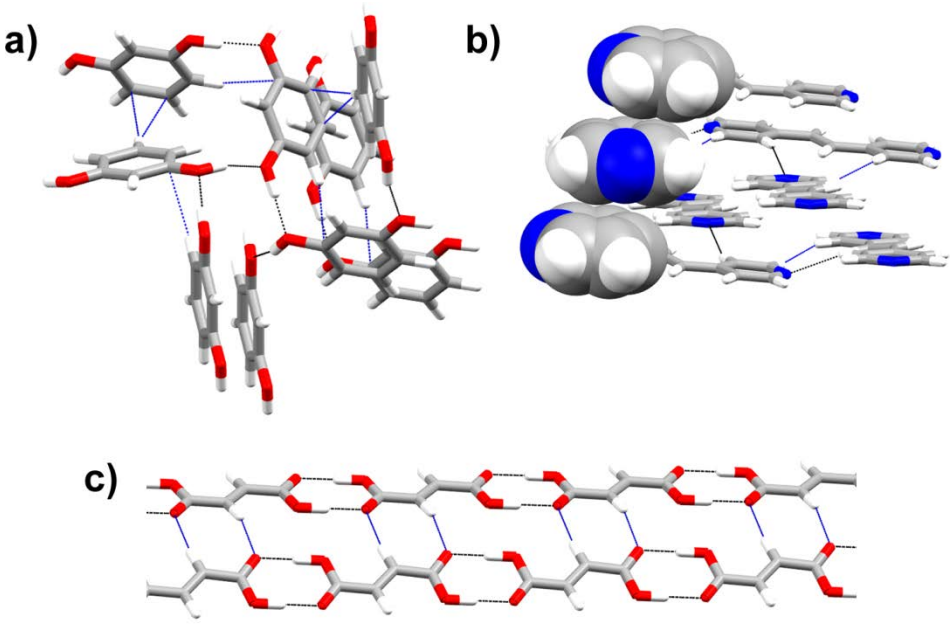

Figure 119. X-ray crystal structures of a) res depicting H(phenol)···O(phenol) bonds (black), C-H(phenol)···π(phenol) bonds (blue), b) 4,4'-bpe showing C-H(pyridine)···H-C(pyridine) bonds (blue), C-H(pyridine)···N(pyridine) bonds (black), and π(pyridine)···π(pyridine) interactions (space-filled region), and c) fum showing O–H(acid)···O(carbonyl) bonds (black) and C=O(carbonyl)···H-C(olefin) bonds (blue).

The molecular packing of the pure solids also contributes to an ability to break and form new bonds. This is evidenced by the molecular packing in the crystal structures of the individual components as well as the melting points of the templates and reactants (Table 12). In relation to the resorcinol based templates, alcohols in the solid state generally form networks and polymorphs.[246,250] This is due to the fact that alcohols bear a single hydrogen bond donor and two basic lone pairs, thus, limiting the ability to form saturated hydrogen-bonded assembles and decreasing the opportunity for efficient packing in the crystal lattice that would otherwise lead to high melting points. The bpe reactants differ by the position of the nitrogen on the pyridine as well as the symmetry. The bpe analog 2,4-bpe has both 2- and 4-pyridyl groups however, the molecule possess less symmetry than is symmetrical analogs 2,2'- and 4,4'- which likely inhibits the ability to pack efficiently. Out of the three reactants, 2,4'-bpe has the lowest melting point. In comparison, the HBD reactant fumaric acid has a much higher melting point (298-300°C) than the HBA reactants. The fumaric acid molecules assemble to form close packed 1D stacks sustained by $\pi\cdots\pi$ interactions. In addition, the HBA templates 2,3-nap and 1,8-dpn have melting points of 137-140°C and 279 – 280°C, respectively. Based on the high melting points values, excluding 2,3-nap, our results from the LAG experiments suggest that either fum and/or 1,8-dpn is inhibiting the solvent-free formation of the co-crystals.[135,155,161]

Table 12. Tables of melting points of a) HBD/HBA b) HBA/HBD templates and reactants.[245,251-259]

Template	mp °C
HBD	
res	109-112
5-Ome-res	40-43
4,6-diCl-res	104-106
5-CN-res	190-193
4-Cl-res	106-108
HBA	
2,3-nap	137-140
1,8-dpn	279-280

Reactant	mp °C
HBA	
4,4'-bpe	148-152
2,2'-bpe	118-119
2,4'-bpe	70-72 °C
HBD	
fum	298-300

5.5. Conclusion

In summary, we have demonstrated that mechanochemistry is generally applicable to templated solid-state reactivity. The res-based assemblies form both rapidly and solvent-free, which eliminates the use of solvent for co-crystallization. We have also generated reactive assemblies based on HBA templates via LAG, thus reducing the amount of solvent generally used for a typical solution-based co-crystallization. Our results also suggest that the structures of the individual components should be considered when planning such co-crystal syntheses. We now aim to determine how mechanochemistry can be employed to construct more complex molecules in organic solids. We are also planning to determine how interactions between functional groups involving templates and reactants further impact mechanochemistry and covalent-bond-forming reactions.

6. CONCLUSIONS

The work presented in this thesis demonstrates useful applications and preparations of co-crystals. We have shown that treatment by various acids of a tetra-pyridyl [5]-ladderane can afford a variety of ladderane derivatives based on isomerizations and oxidations. The stereoisomers generated from an acid-induced isomerization of a tetra-pyridyl [5]-ladderane described here detail the first cases of how chirality can be incorporated into a ladderane framework. In contrast to the natural products, which involve stereogenic centers, the chirality results from a change in the relative disposition of the terminal pyridyl groups of lad-1a. We have also generated *N*-oxides that are highly soluble in water. We anticipate that these compounds may be used as building blocks for MOFs.

We provide the first example, to our knowledge, in which the use of a co-crystal is applied to determine the stereochemistry of a compound that resists crystallization. Prior to our work, studies involving the use of a co-crystal for structural determination provided demonstrations using known compounds. In contrast, we used a co-crystal to obtain single-crystals to determine the relative configuration of a molecule that has not been reported.

We conducted the first reactivity study of a diacid diene that was determined to undergo dimer- and trimerization in pure form, *via* a [2 + 2] photodimerization in the solid-state. We also demonstrated the utility of using PXRD as a means to analyze the crystal packing of the molecules within the reactive solid. This was due to the fact that attempts to grow crystals suitable for X-ray diffraction afforded microcrystalline solids. To separate, isolate, and confirm the stereochemistry of the trimer, the use of a co-crystal was successfully applied. The co-crystal (bha)·(4-dipy)·2(DMF) represents, to our knowledge, the

first structure confirmation of a bicyclobutane obtained from the solid state. Efforts are underway to employ a similar approach to characterize cbta-1a.

We demonstrate the first study successfully applying templates to direct the synthesis of a diacid diene. With use of templates we demonstrate the ability to obtain a monocyclized product as well as generate photostable solids. Future work will consists of exploring the reactivity of dmma with a variety of HBA templates. This will require the development of 1,8-dpn derivatives.

We have demonstrated that mechanochemistry is generally applicable to templated solid-state reactivity. The res-based assemblies form both rapidly and solvent-free, which increases the practical value of the res system. Future work will focus on the formation of all template-directed assemblies, specifically, the remaining family of bpe molecules, as well as more complex co-crystal assemblies such as the ladderane precursors. We also anticipate exploring catalytic amounts of templates to reactants.

REFERENCES

1. Desiraju, G. R. *Angew. Chem., Int. Ed. Engl.* **1995**, *34*, 2311-2327.

2. Desiraju, Gautam R. *Angew. Chem. Int. Ed.* **2007**, *46*, 8342-8356.

3. Desiraju, G. R. *Nature* **2001**, *412*, 397-400.

4. Steed, J. W.; Atwood, J. L.; Editors *Supramolecular Chemistry, Second Edition*, **2009**.

5. Gavezzotti, A. *Acta Crystallogr., Sect. B: Struct. Sci* **1990**, *46*, 275-283.

6. Anderson, K. M.; Probert, M. R.; Goeta, A. E.; Steed, J. W. *CrystEngComm*, **2011**, *13*, 83-87.

7. Dunitz, J. D.; Filippini, G.; Gavezzotti, A. *Helv. Chim. Acta* **2000**, *83*, 2317-2335.

8. Dunitz, J. D.; Gavezzotti, A.; Schweizer, W. B. *Helv. Chim. Acta* **2003**, *86*, 4073-4092.

9. Gavezzotti, A.; Filippini, G. *Chem. Commun.* **1998**, 287-294.

10. Desiraju, G. *J. Chem. Sci.*, **2004**, *122*, 667-675.

11. Aakeroy, C. B.; Champness, N. R.; Janiak, C. *CrystEngComm*, **2011**, *12*, 22-43.

12. Adams, C. J.; Haddow, M. F.; Lusi, M.; Orpen, A. G. *Proc. Natl. Acad. Sci. USA* **2010**, *107*, 16033–16038.

13. Merz, K.; Vasylyeva, V. *CrystEngComm*, **2010**, *12*, 3989-4002.

14. Kavuru, P.; Aboarayes, D.; Arora, K. K.; Clarke, H. D.; Kennedy, A.; Marshall, L.; Ong, T. T.; Perman, J.; Pujari, T.; Wojtas, Å. u.; Zaworotko, M. J. *Cryst. Growth Des.*, **2007**,*10*, 3568-3584.

15. Shattock, T. R.; Arora, K. K.; Vishweshwar, P.; Zaworotko, M. J. *Cryst. Growth Des.* **2008**, *8*, 4533-4545.

16. Khan, M.; Enkelmann, V.; Brunklaus, G. *Cryst. Growth Des.* **2009**, *9*, 2354-2362.

17. Takusagawa, F.; Shimada, A. *Acta Crystallogr., Sect. B: Struct. Sci* **1976**, *32*, 1925-1927.

18. Desiraju, G. R. *CrystEngComm* **2003**, *5*, 466-467.

19. Dunitz, J. D. *CrystEngComm* **2003**, *5*, 506-506.

20. Friscic, T.; MacGillivray, L. R. *Croat. Chem. Acta* **2006**, *79*, 327-333.

21. MacGillivray, L. R. P., G.S.; Friščić, T.; Hamilton, T. D.; Bučar, D.-K; Chu, Q.; Varshney, D.B.; Georgiev, I.G. *Acc. Chem. Res.* **2008**, *41*, 280.

22. Sokolov, A. N.; Friščić, T.; MacGillivray, L. R. *J. Am. Chem. Soc.* **2006**, *128*, 2806–2807.

23. Eger, C.; Norton, D. A. *Nature* **1965**, *208*, 997-999.

24. Bhatt, P. M.; Desiraju, G. R. *CrystEngComm* **2008**, *10*, 1747-1749.

25. Eccles, K. S.; Deasy, R. E.; Fabian, L.; Maguire, A. R.; Lawrence, S. E. *J. Org. Chem.* **2011**, *76*, 1159-1162.

26. Schultheiss, N.; Newman, A. *Cryst. Growth Des.* **2009**, *9*, 2950-2967.

27. Vishweshwar, P.; McMahon, J. A.; Peterson, M. L.; Hickey, M. B.; Shattock, T. R.; Zaworotko, M. J. *Chem. Commun.* **2005**, 4601-4603.

28. Bučar, D.-K.; Henry, R. F.; Lou, X.; Duerst, R. W.; MacGillivray, L. R.; Zhang, G. G. Z. *Cryst. Growth Des.* **2009**, *9*, 1932-1943.

29. Blagden, N.; Berry, D. J.; Parkin, A.; Javed, H.; Ibrahim, A.; Gavan, P. T.; De Matos, L. L.; Seaton, C. C. *New J. Chem.* **2008**, *32*, 1659.

30. Babu, N. J.; Nangia, A. *Cryst. Growth Des., in press*.

31. Schultheiss, N.; Newman, A. *Cryst. Growth Des.* **2009**, *9*, 2950.

32. Remenar, J. F.; Morissette, S. L.; Peterson, M. L.; Moulton, B.; MacPhee, J. M.; GuzmÃ¡n, H. c. R.; Almarsson, Ã. r. *J. Am. Chem. Soc.* **2003**, *125*, 8456-8457.

33. Trask, A. V.; Jones, W. *Top. Curr. Chem.* **2005**, *254*, 41–70.

34. Friščić, T. *J. Mater. Chem.* **2011**, *20*, 7599-7605.

35. Weyna, D. R.; Shattock, T.; Vishweshwar, P.; Zaworotko, M. J. *Cryst. Growth Des.* **2009**, *9*, 1106-1123.

36. Chen, J.; Sarma, B.; Evans, J. M. B.; Myerson, A. S. *Cryst. Growth Des.* **2011**,*11*, 887-895.

37. Braga, D.; Giaffreda, S. L.; Grepioni, F.; Pettersen, A.; Maini, L.; Curzi, M.; Polito, M. *Dalton Trans.* **2006**, 1249-1263.

38. Cohen, M. D.; Schmidt, G. M. J.; Sonntag, F. I. *J. Chem. Soc.* **1964**, 2000-2013.

39. Schmidt, G. M. J. *J. Chem. Soc.* **1964**, 2014-2021.

40. Schmidt, G. M. J. *Pure Appl. Chem.* **1971**, *27*, 647.

41. Lahav, M.; Schmidt, G. M. J. *J. Chem. Soc. B* **1967**, 239-243.

42. Filippakis, S. E.; Leiserowitz, L.; Rabinovich, D.; Schmidt, G. M. J. *J. Chem. Soc., Perkin Trans. 2* **1972**, 1750-8.

43. Lahav, M.; Schmidt, G. M. J. *Tetrahedron Lett.* **1966**, *7*, 2957-2962.

44. Filippakis, S. E.; Leiserowitz, L.; Schmidt, G. M. J. *J. Chem. Soc. B* **1967**, 305-311.

45. Filippakis, S. E.; Leiserowitz, L.; Schmidt, G. M. J. *J. Chem. Soc. B* **1967**, 290-296.

46. Green, B. S.; Lahav, M.; Schmidt, G. M. J. *J. Chem. Soc. B* **1971**, 1552-1564.

47. Lahav, M.; Schmidt, G. M. J. *J. Chem. Soc. B* **1967**, 312-317.

48. Lahav, M.; Schmidt, G. M. J. *J. Chem. Soc. B* **1967**, 312-317.

49. Cohen, M. D.; Elgavi, A.; Green, B. S.; Ludmer, Z.; Schmidt, G. M. J. *J. Am. Chem. Soc.* **1972**, *94*, 6776-6779.

50. Elgavi, A.; Green, B. S.; Schmidt, G. M. J. *J. Am. Chem. Soc.* **1973**, *95*, 2058-2059.

51. Nagarathinam, M.; Peedikakkal, A. M. P.; Vittal, J. J. *Chem. Commun.* **2008**, 5277-5288.

52. Desiraju, G. R.; Kamala, R.; Kumari, B. H.; Sarma, J. A. R. P. *J. Chem. Soc., Perkin Trans. 2* **1984**, 181-189.

53. Coates, G. W.; Dunn, A. R.; Henling, L. M.; Ziller, J. W.; Lobkovsky, E. B.; Grubbs, R. H. *J. Am. Chem. Soc.* **1998**, *120*, 3641-3649.

54. Capparelli, M. V.; Codding, P. W. *Can. J. Chem.* **1993**, *71*, 942-950.

55. Sharma, C. V. K.; Panneerselvam, K.; Shimoni, L.; Katz, H.; Carrell, H. L.; Desiraju, G. R. *Chem. Mater.* **1994**, *6*, 1282-1292.

56. Sarma, J. A. R. P.; Desiraju, G. R. *J. Chem. Soc., Chem. Commun.* **1984**, 145-147.

57. Vishnumurthy, K.; Guru Row, T. N.; Venkatesan, K. *Photochem. Photobiol. Sci.* **2002**, *1*, 427-430.

58. Ito, Y.; Borecka, B.; Trotter, J.; Scheffer, J. R. *Tetrahedron Lett.* **1995**, *36*, 6083-6086.

59. MacGillivray, L. R.; Reid, J. L.; Ripmeester, J. A. *J. Am. Chem. Soc.* **2000**, *122*, 7817-7818.

60. Friščić, T.; Drab, D. M.; MacGillivray, L. R. *Org. Lett.* **2004**, *6*, 4647-4650.

61. Varshney, D. B.; Gao, X.; Friščić, T.; MacGillivray, L. R. *Angew. Chem., Int. Ed.* **2006**, *45*, 646-650.

62. MacGillivray, L. R.; Reid, J. L.; Ripmeester, J. A.; Papaefstathiou, G. S. *Ind. Eng. Chem. Res.* **2002**, *41*, 4494-4497.

63. Friščić, T.; MacGillivray, L. R. *Chem. Commun.* **2003**, 1306-1307.

64. Friscic, T.; MacGillivray, L. R. *Chem. Commun.* **2005**, 5748-5750.

65. Gao, X.; Friscic, T.; MacGillivray, L. R. *Angew. Chem., Int. Ed.* **2004**, *43*, 232.

66. Liu, D.; Ren, Z.-G.; Li, H.-X.; Lang, J.-P.; Li, N.-Y.; Abrahams, B. F. *Angew. Chem., Int. Ed.*, **2011**, *49*, 4767-4770.

67. Hopf, H. *Angew. Chem., Int. Ed.* **2003**, *42*, 2822-2825.

68. Greiving, H.; Hopf, H.; Jones, P. G.; Bubenitschek, P.; Desvergne, J.-P.; Bouas-Laurent, H. *Eur. J. Org. Chem.* **2005**, *2005*, 558-566.

69. Hopf, H.; Greiving, H.; Jones, P. G.; Bubenitschek, P. *Angew. Chem., Int. Ed.* **1995**, *34*, 685-7.

70. Sinninghe Damste Jaap, S.; Strous, M.; Rijpstra, W. I. C.; Hopmans Ellen, C.; Geenevasen Jan, A. J.; van Duin Adri, C. T.; van Niftrik Laura, A.; Jetten Mike, S. M. *Nature* **2002**, *419*, 708-712.

71. Kuypers Marcel, M. M.; Sliekers, A. O.; Lavik, G.; Schmid, M.; Jorgensen Bo, B.; Kuenen, J. G.; Sinninghe Damste Jaap, S.; Strous, M.; Jetten Mike, S. M. *Nature* **2003**, *422*, 608-11.

72. Kaliappan, R.; Kaanumalle, L. S.; Natarajan, A.; Ramamurthy, V. *Photochem. Photobiol. Sci.* **2006**, *5*, 925-930.

73. Maddipatla, M. V. S. N.; Kaanumalle, L. S.; Natarajan, A.; Pattabiraman, M.; Ramamurthy, V. *Langmuir* **2007**, *23*, 7545-7554.

74. Xu, Y.; Smith, M. D.; Krause, J. A.; Shimizu, L. S. *J. Org. Chem.* **2009**, *74*, 4874-4877.

75. Amirsakis, D. G.; Garcia-Garibay, M. A.; Rowan, S. J.; Stoddart, J. F.; White, A. J. P.; Williams, D. J. *Angew. Chem. Int. Ed.* **2001**, *40*, 4256-4261.

76. Shan, N.; Jones, W. *Tetrahedron Lett.* **2003**, *44*, 3687-3689.

77. Shan, N.; Jones, W. *Green Chem.* **2003**, *5*, 728-730.

78. Bhogala, B. R.; Captain, B.; Parthasarathy, A.; Ramamurthy, V. *J. Am. Chem. Soc.*, **2003**, *132*, 13434-13442.

79. Caronna, T.; Liantonio, R.; Logothetis, T. A.; Metrangolo, P.; Pilati, T.; Resnati, G. *J. Am. Chem. Soc.* **2004**, *126*, 4500-4501.

80. Felloni, M.; Blake, A. J.; Hubberstey, P.; Wilson, C.; Schroder, M. *CrystEngComm* **2002**, *4*, 483-495.

81. Kole, G. K.; Tan, G. K.; Vittal, J. J. *Org. Lett.* **2009**, *12*, 128-131.

82. Nagarathinam, M.; Vittal, J. J. *Angew. Chem. Int. Ed.* **2006**, *45*, 4337-4341.

83. Peedikakkal, A. M. P.; Peh, C. S. Y.; Koh, L. L.; Vittal, J. J. *Inorg. Chem.*, **2010**, *49*, 6775-6777.

84. Hill, R. J.; Long, D.-L.; Champness, N. R.; Hubberstey, P.; Schroder, M. *Acc. Chem. Res.* **2005**, *38*, 335-348.

85. Jung Soo, S.; Dongmok, W. *Nature* **2000**, *404*, 982.

86. Hamilton, T. D.; Papaefstathiou, G. S.; MacGillivray, L. R. *J. Am. Chem. Soc.* **2002**, *124*, 11606-11607.

87. Ma, L.; Mihalcik, D. J.; Lin, W. *J. Am. Chem. Soc.* **2009**, *131*, 4610-4612.

88. Thallapally, P. K.; Peter McGrail, B.; Dalgarno, S. J.; Schaef, H. T.; Tian, J.; Atwood, J. L. *Nat. Mat.* **2008**, *7*, 146-150.

89. Tranchemontagne, D. J.; Mendoza-Cortes, J. L.; O'Keeffe, M.; Yaghi, O. M. *Chem. Soc. Rev.* **2009**, *38*, 1257-1283.

90. Papaefstathiou, G. S.; Hamilton, T. D.; Friscic, T.; MacGillivray, L. R. *Chem. Commun.* **2004**, 270-271.

91. Papaefstathiou, G. S.; Friščić, T.; MacGillivray, L. R. *J. Am. Chem. Soc.* **2005**, *127*, 14160-14161.

92. Hamilton, T. D.; Bucar, D.-K.; MacGillivray, L. R. *Chem. Commun.* **2007**, 1603-1604.

93. Bucar, D.-K.; Papaefstathiou, G. S.; Hamilton, T. D.; MacGillivray, L. R. *New. J. Chem.* **2008**, *32*, 797-799.

94. Hamilton, T. D.; Papaefstathiou, G. S.; Friščić, T.; BucÌŒar, D.-K.; MacGillivray, L. R. *J. Am. Chem. Soc.* **2008**, *130*, 14366-14367.

95. Hamilton, T. D.; Buĉar, D.-K.; MacGillivray, L. R. *New J. Chem.*, **2010** *34*, 2400-2402.

96. Hamilton, T. D.; Buĉar, D.-K.; Baltrusaitis, J.; Flanagan, D. R.; Li, Y.; Ghorai, S.; Tivanski, A. V.; MacGillivray, L. R. *J. Am. Chem. Soc.*, **2010**, *133*, 3365-3371.

97. Nouri, D. H.; Tantillo, D. J. *Curr. Org. Chem.* **2006**, *10*, 2055-2074.

98. Boumann Henry, A.; Longo Marjorie, L.; Stroeve, P.; Poolman, B.; Hopmans Ellen, C.; Stuart Marc, C. A.; Sinninghe Damste Jaap, S.; Schouten, S. *Biochim. Biophys. Acta* **2009**, *1788*, 1444-1451.

99. Santos, J. C.; Fuentealba, P. *Chem. Phys. Lett.* **2003**, *377*, 449-454.

100. Mascitti, V.; Corey, E. J. *J. Am. Chem. Soc.* **2004**, *126*, 15664-15665.

101. Mascitti, V.; Corey, E. J. *J. Am. Chem. Soc.* **2006**, *128*, 3118-3119.

102. Mascitti, V.; Corey, E. J. *Tetrahedron Lett.* **2006**, *47*, 5879-5882.

103. Gao, X.; Friščić, T.; MacGillivray, L. R. *Angew. Chem. Int. Ed.* **2004**, *43*, 232-236.

104. Mehta, G.; Viswanath, M. B.; Sastry, G. N.; Jemmis, E. D.; Reddy, D. S. K.; Kunwar, A. C. *Angew. Chem. Int. Ed.* **1992**, *31*, 1488-1490.

105. Avram, M.; Dinulescu, I. G.; Marica, E.; Mateescu, G.; Sliam, E.; Nenitzescu, C. D. *Chem. Ber.* **1964**, *97*, 382-389.

106. Mehta, G.; Viswanath, M. B.; Sastry, G. N.; Jemmis, E. D.; Reddy, D. S.; Kunwar, A. C. *Angew. Chem.* **1992**, *104*, 1557-8

107. Fitzpatrick, D. *Chem. Eng. News* **1965**, *43*, 38-39.

108. Martin, H.-D.; Hekman, M. *Angew. Chem. Int. Ed.* **1973**, *12*, 572-574.

109. Martin, H.-D.; Hekman, M. *Tetrahedron Lett.* **1978**, *19*, 1183-1186.

110. Martin, H.-D.; Mayer, B.; Pütter, M.; Höchstetter, H. *Angew. Chem. Int. Ed.* **1981**, *20*, 677-678.

111. Warrener, R. N.; Abbenante, G.; Solomon, R. G.; Russell, R. A. *Tetrahedron Lett.* **1994**, *35*, 7639-7642.

112. Warrener, R. N.; Pitt, I. G.; Nunn, E. E.; Kennard, C. H. L. *Tetrahedron Lett.* **1994**, *35*, 621-624.

113. Warrener, R. N.; Abbenante, G.; Kennard, C. H. L. *J. Am. Chem. Soc.* **1994**, *116*, 3645-6.

114. Warrener, R. N.; Russell, R. A.; Margetic, D. *Synlett* **1997**, 38-40.

115. Mehta, G.; Viswanath, M. B.; Kunwar, A. C. *J. Org. Chem.* **1994**, *59*, 6131-6132.

116. Mehta, G.; Viswanath, M. B.; Kunwar, A. C.; Kumar, K. R.; Reddy, S. K. *J. Chem. Soc., Chem. Commun.* **1994**, 739-40.

117. Li, W.; Fox, M. A. *J. Am. Chem. Soc.* **1996**, *118*, 11752-11758.

118. Weigert, F. J. *J. Fluorine Chem.* **1991**, *52*, 125-131.

119. Kazmina, N. B.; Antipin, M. Y.; Sereda, S. V.; Struchkov, Y. T.; Mysov, E. I.; Leites, L. A. *J. Fluorine Chem.* **1993**, *61*, 57-83.

120. Rachel, R. *Mol. Microbiol.* **2009**, *73*, 978-981.

121. Hopf, H.; Greiving, H.; Beck, C.; Dix, I.; Jones, P. G.; Desvergne, J.-P.; Bouas-Laurent, H. *Eur. J. Org. Chem.* **2005**, *2005*, 567-581.

122. Paradies, J.; Greger, I.; Kehr, G.; Erker, G.; Bergander, K.; Fröhlich, R. *Angew. Chem. Int. Ed.* **2006**, *45*, 7630-7633.

123. Peedikakkal, A. M. P.; Koh, L. L.; Vittal, J. J. *Chem. Commun.* **2008**, 441-443.

124. Coperet, C.; Adolfsson, H.; Khuong, T.-A. V.; Yudin, A. K.; Sharpless, K. B. *J. Org. Chem.* **1998**, *63*, 1740-1741.

125. Robinson, D.; McMorn, P.; Bethell, D.; Bulman-Page, P.; Sly, C.; King, F.; Hancock, F.; Hutchings, G. J. *Catal. Lett.* **2001**, *72*, 233-234.

126. Dolain, C.; Zhan, C.; Léger, J.-M.; Daniels, L.; Huc, I. *J. Am. Chem. Soc.* **2005**, *127*, 2400-2401.

127. Hooft, R. W. W.; Nonius, B. V. Delft, The Netherlands, 1998.

128. Otwinowski, Z.; Minor, W. *Processing of X-ray Diffraction Data Collected in Oscillation Mode*, 1997.

129. Sheldrick, G. M. *SHELXTL*, 1997.

130. Becke, A. D. *Phys. Rev. A* **1988**, *38*, 3098.

131. Schaefer, A.; Huber, C.; Ahlrichs, R. *J. Chem. Phys.* **1994**, *100*, 5829-5835.

132. Ahlrichs, R.; Baer, M.; Haeser, M.; Horn, H.; Koelmel, C. *Chem. Phys. Lett.* **1989**, *162*, 165-169.

133. Gao, X.; Friščić, T.; MacGillivray, L. R. *Angew. Chem. Int. Ed.* **2004**, *43*, 232-236.

134. Gérard Zuber, M.-R. G., David N. Beratan, Peter Wipf, *Chirality* **2005**, *17*, 507-510.

135. Pinal, R. *Org. Biomol. Chem.* **2004**, *2*, 2692-2699.

136. *Fundamentals of analytical chemistry*; 8th ed. ed.; Skoog, D. A.; West, D. M.; Holler, F. J., Eds., 2004.

137. Barchiesi, E.; Bradamante, S.; Carfagna, C.; Ferraccioli, R.; Pagani, G. A. *J. Chem. Soc., Perkin Trans. 2* **1987**, 1009-1013.

138. Tomooka, K.; Ezawa, T.; Inoue, H.; Uehara, K.; Igawa, K. *J. Am. Chem. Soc.*, **1971**, *133*, 1754-1756.

139. Moore, R. E.; Bartolini, G.; Barchi, J.; Bothner-By, A. A.; Dadok, J.; Ford, J. *J. Am. Chem. Soc.* **1982**, *104*, 3776-3779.

140. Wang, A. H. J.; Paul, I. C.; Rinehart, K. L.; Antosz, F. J. *J. Am. Chem. Soc.* **1971**, *93*, 6275-6276.

141. Harada, N.; Koumura, N.; Feringa, B. L. *J. Am. Chem. Soc.* **1997**, *119*, 7256-7264.

142. Bagal, S. K.; Davies, S. G.; Lee, J. A.; Roberts, P. M.; Scott, P. M.; Thomson, J. E. *J. Org. Chem.*, **2010**, *75*, 8133-8146.

143. Nicolaou, K. C.; Snyder, S. A. *Angew. Chem. Int. Ed.* **2005**, *44*, 1012-1044.

144. Smith, A. B.; Duffey, M. O.; Basu, K.; Walsh, S. P.; Suennemann, H. W.; Frohn, M. *J. Am. Chem. Soc.* **2007**, *130*, 422-423.

145. Hu, D. X.; Clift, M. D.; Lazarski, K. E.; Thomson, R. J. *J. Am. Chem. Soc.*, **2011**, *133*, 1799-1804.

146. Aakeroy, C.; Fasulo, M. E.; Desper, J. *Mol. Pharmaceutics* **2007**, *4*, 317-322.

147. Mohamed, S.; Tocher, D. A.; Vickers, M.; Karamertzanis, P. G.; Price, S. L. *Cryst. Growth Des.* **2009**, *9*, 2881.

148. Bernal, J. D. *Nature* **1932**, *129*, 277-8.

149. Bernal, J. D. *Nature* **1932**, *129*, 721.

150. Spek, A. *Acta Cryst. D* **2009**, *65*, 148-155.

151. Etter, M. C.; Jahn, D. A.; Donahue, B. S.; Johnson, R. B.; Ojala, C. *J. Cryst. Growth* **1986**, *76*, 645-655.

152. Ashwini, W.; Momany, C. *Cryst. Growth Des.* **2007**, *7*, 2219-2225.

153. Duax, W. L.; Eger, C.; Pokrywiecki, S.; Osawa, Y. *J. Med. Chem.* **1971**, *14*, 295-300.

154. Liu, P.-H.; Li, L.; Webb, J. A.; Zhang, Y.; Goroff, N. S. *Org. Lett.* **2004**, *6*, 2081-2083.

155. Gavezzotti, A. *J. Chem. Soc., Perkin Trans. 2* **1995**, 1399-404.

156. Dunitz, J. D.; Gavezzotti, A. *Angew. Chem. Int. Ed.* **2005**, *44*, 1766-1787.

157. Shattock, T. R.; Arora, K. K.; Vishweshwar, P.; Zaworotko, M. J. *Cryst. Growth Des.* **2008**, *8*, 4533–4545.

158. Burchell, C. J.; Glidewell, C.; Lough, A. J.; Ferguson, G. *Acta Cryst. B* **2001**, *57*, 201-212.

159. Aakeroy, C. B.; Desper, J.; Urbina, J. F. *CrystEngComm* **2005**, *7*, 193-201.

160. Childs, S. L.; Zaworotko, M. J. *Cryst. Growth Des.* **2009**, *9*, 4208-4211.

161. Brown, R. J. C. *J. Chem. Educ.* **2000**, *77*, 724-731.

162. Krishnamohan Sharma, C. V.; Zaworotko, M. J. *Chem. Commun.* **1996**, 2655-2656.

163. Shattock, T. R.; Vishweshwar, P.; Wang, Z.; Zaworotko, M. J. *Cryst. Growth Des.* **2005**, *5*, 2046-2049.

164. Zhou, H.; Dang, H.; Yi, J.-H.; Nanci, A.; Rochefort, A.; Wuest, J. D. *J. Am. Chem. Soc.* **2007**, *129*, 13774-13775.

165. Pérez-García, L.; Amabilino, D. B. *Chem. Soc. Rev.* **2002**, *31*, 342–356.

166. Trolliet, C.; Poulet, G.; Tuel, A.; J.D., W.; Sautet, P. *J. Am. Chem. Soc.* **2007**, *129*, 3621–3626.

167. Tan, T.-F.; Han, J.; Pang, M.-L.; Song, H.-B.; Ma, Y.-X.; Meng, J.-B. *Cryst. Growth Des.* **2006**, *6*, 1186-1193.

168. Anderson, K. M.; Probert, M. R.; Whiteley, C. N.; Rowland, A. M.; Goeta, A. E.; Steed, J. W. *Cryst. Growth Des.* **2009**, *9*, 1082–1087.

169. Abrahams, B. F.; Batten, S. R.; Hamit, H.; Hoskins, B. F.; Robson, R. *Chem. Commun.* **1996**, 1313-1314.

170. Thuéry, P. *Inorg. Chem.*, *50*, 1898-1904.

171. *Structure Determination of Organic Compounds: Tables of Spectral Data* 3rd ed. ed.; Prestch, E.; Buhlmann, P.; Affolter, C., Eds.; Berlin ; New York : Springer 2000.

172. *Spectrometric Identification of Organic Compounds*; 7th ed. ed.; Silverstein, R. M.; Webster, F. X.; Kiemle, D. J., Eds.; John Wiley & Sons, Inc., 2005.

173. Caira, M. R.; Nassimbeni, L. R.; Wildervanck, A. F. *Journal of the Chemical Society, Perkin Transactions 2* **1995**, 2213-2216.

174. Batten, S. R.; Robson, R. *Angew. Chem., Int. Ed.* **1998**, *37*, 1461-1494.

175. Basu, T.; Sparkes, H. A.; Mondal, R. *Cryst. Growth Des.* **2009**, *9*, 5164-5175.

176. Matsumoto, A. *Topp. Curr. Chem.* **2005**, *254*, 263-305.

177. Sonoda, Y. *Molecules* **2011**, *16*, 119-148.

178. Kaufmann, H. P.; Sen Gupta, A. K. *Justus Liebigs Ann. Chem.* **1965**, *681*, 39-44.

179. Schmidt, G. M. J.; Green, B. S.; Lahav, M. *J. Chem. Soc. B* **1971**, 1552-64.

180. Matsumoto, A. *Top. Cur. Chem.* **2005**, *254*, 263.

181. Oshita, S.; Matsumoto, A. *Chem. Eur. J.* **2006**, *12*, 2139-2146.

182. Matsumoto, A.; Furukawa, D.; Nakazawa, H. *J. Polym. Sci., Part A, Polym. Chem.* **2006**, *44*, 4952.

183. Furukawa, D.; Matsumoto, A. *Macromolecules* **2007**, *40*, 6048-6056.

184. Odani, T.; Okada, S.; Kabuto, C.; Kimura, T.; Shimada, S.; Matsuda, H.; Oikawa, H.; Matsumoto, A.; Nakanishi, H. *Cryst. Growth Des.* **2009**, *9*, 3481-3487.

185. Kitamura, T.; Tanaka, N.; Mihashi, A.; Matsumoto, A. *Macromolecules* **2010**, *43*, 1800-1806.

186. Saltiel, J.; Krishna, T. S. R.; Laohhasurayotin, S.; Fort, K.; Clark, R. J. *The J. Phys. Chem. A* **2007**, *112*, 199-209.

187. Furukawa, D.; Kobatake, S.; Matsumoto, A. *Chem. Commun.* **2008**, 55-57.

188. Nishizawa, N.; Furukawa, D.; Kobatake, S.; Matsumoto, A. *Cryst. Growth Des.*, *10*, 3203-3210.

189. Friščić, T. Thesis, University of Iowa, Iowa City, IA 2006.

190. Filippakis, S. E.; Leiserowitz, L.; Schmidt, G. M. J. *J. Chem. Soc. B* **1967**, 297-304.

191. Peachey, N. M.; Eckhardt, C. J. *J. Phys. Chem.* **1993**, *97*, 10849-10856.

192. Peachey, N. M.; Eckhardt, C. J. *J. Phys. Chem.* **1994**, *98*, 685-691.

193. MacGillivray, L. R. *J. Org. Chem.* **2008**, *73*, 3311-3317.

194. Liu, J.; Boarman, K. J. *Chem. Commun.* **2005**, 340-341.

195. Mori, Y.; Matsumoto, A. *Cryst. Growth Des.* **2007**, *7*, 377-385.

196. Mori, Y.; Matsumoto, A. *Chem. Lett.* **2007**, *36*, 510-511.

197. Mori, Y.; Chiba, T.; Odani, T.; Matsumoto, A. *Cryst. Growth Des.* **2007**, *7*, 1356-1364.

198. Eaton, P. E.; Gilardi, R. L.; Zhang, M.-X. *Adv. Mater.* **2000**, *12*, 1143-1148.

199. Savos'kin, M. V.; Kapkan, L. M.; Vaiman, G. E.; Vdovichenko, A. N.; Gorkunenko, O. A.; Yaroshenko, A. P.; Popov, A. F.; Mashchenko, A. N.; Tkachev, V. A.; Voloshin, M. L.; Potapov, Y. F. *Russ. J. Appl. Chem.* **2007**, *80*, 31-37.

200. *Cubanes, fenestranes, ladderanes, prismanes, staffanes, and other oligocyclobutanoids in Chemistry of Cyclobutanes*; Hopf, H.; Liebman, J. F.; Perks, H. M., Eds.; Wiley, 2005.

201. Harris, K. D. M.; Tremayne, M.; Lightfoot, P.; Bruce, P. G. *J. Am. Chem. Soc.* **1994**, *116*, 3543.

202. Harris, K. D. M.; Tremayne, M.; Kariuki, B. M. *Angew. Chem. Int. Ed.* **2001**, *40*, 1626.

203. David, W. I. F.; Shankland, K. *Acta Crystallogr., Sect. A: Found. Crystallogr.* **2008**, *64*, 52-64.

204. Harris, K. D. M.; Cheung, E. Y. *Chem. Soc. Rev.* **2004**, *33*, 526-538.

205. Karki, S.; Fabian, L.; Friščić, T.; Jones, W. *Organic Lett.* **2007**, *9*, 3133-3136.

206. Thuéry, P.; Masci, B. *Cryst. Growth Des.* **2008**, *8*, 3430-3436.

207. Trask, A. V.; Motherwell, W. D. S.; Jones, W. *Chem. Commun.* **2004**, 890-891.

208. Lu, J.; Rohani, S. *Curr. Med. Chem.* **2009**, *16*, 884-905.

209. Scheffer, J.; Wong, Y. F.; Patil, A. O.; Curtin, D. Y.; Paul, I. C. *J. Am. Chem. Soc.* **1985**, *107*, 4898-4904.

210. Lien Nguyen, K.; Friščić, T.; Day, G. M.; Gladden, L. F.; Jones, W. *Nat. Mater.* **2007**, *6*, 206-209.

211. Friščić, T.; Jones, W. *Cryst. Growth Des.* **2009**, *9*, 1621-1637.

212. Friščić, T.; Fabian, L.; Burley, J. C.; Jones, W.; Motherwell, W. D. S. *Chem. Commun.* **2006**, 5009-5011.

213. Karki, S.; FriÅ¡cÌŒiÄ‡, T.; Jones, W.; Motherwell, W. D. S. *Mol. Pharm.* **2007**, *4*, 347-354.

214. Patil, A. O.; Curtin, D. Y.; Paul, I. C. *J. Am. Chem. Soc.* **1984**, *106*, 4010-4015.

215. Patil, A. O.; Curtin, D. Y.; Paul, I. C. *J. Am. Chem. Soc.* **1984**, *106*, 348-353.

216. Guarrera, D.; Taylor, L. D.; Warner, J. C. *Chem. Mater.* **1994**, *6*, 1293-1296.

217. Toda, F.; Tanaka, K.; Sekikawa, A. *J. Chem. Soc., Chem. Commun.* **1987**, 279-280.

218. Etter, M. C.; Frankenbach, G. M.; Bernstein, J. *Tetrahedron Lett.* **1989**, *30*, 3617.

219. Etter, M. C.; Frankenbach, G. M. *Chem. Mater.* **1989**, *1*, 10.

220. Etter, M. C.; Frankenbach, G. M.; Bernstein, J. *Tetrahedron Lett.* **1989**, *30*, 3617-3620.

221. Etter, M. C. *J. Am. Chem. Soc.* **1982**, *104*, 1095.

222. Kuroda, R.; Higashiguchi, K.; Hasebe, S.; Imai, Y. *CrystEngComm* **2004**, *6*, 463-468.

223. Hollingsworth, M. D.; Brown, M. E.; Santarserio, B. D.; Huffmann, J. C.; Goss, C. R. Chem. Mater. 1996, 6.

224. Shan, N.; Toda, F.; Jones, W. *Chem. Commun.* **2002**, *20*, 2372-2373.

225. Friščić, T.; Trask, A. V.; Jones, W.; Motherwell, W. D. S. *Angew. Chem. Int. Ed.* **2006**, *45*, 7546-7550.

226. Friščić, T.; Jones, W. *Cryst. Growth Des.* **2009**, *9*, 1621-1637.

227. Rastogi, R. P.; Singh, N. B. *J. Phys. Chem.* **1966**, *70*, 3315-3324.

228. Rastogi, R. P.; Bassi, P. S.; Chadha, S. L. *J. Phys. Chem.* **1962**, *66*, 2707-2708.

229. Rastogi, R. P.; Bassi, P. S.; Chadha, S. L. *J. Phys. Chem.* **1963**, *67*, 2569-2573.

230. Kaupp, G.; Schmeyers, J.; Hangen, U. D. *J. Phys. Org. Chem.* **2002**, *15*, 307-313.

231. Kaupp, G. *CrystEngComm* **2003**, *5*, 117-133.

232. Kaupp, G. *CrystEngComm* **2006**, *8*, 794-804.

233. Atwood, J. L.; Barbour, L. J.; Agoston, J.; Schottel, B. L. *Science* **2002**, *298*, 1000-1002.

234. Dalgarno, S. J.; Thallapally, P. K.; Barbour, L. J.; Atwood, J. L. *Chem. Soc. Rev.* **2007**, *36*, 236-245.

235. Chadwick, K.; Davey, R.; Cross, W. *CrystEngComm* **2007**, *9*, 732-734.

236. Lu, E.; Rodriguez-Hornedo, N.; Suryanarayanan, R. *CrystEngComm* **2008**, *10*, 665-668.

237. Willart, J. F.; Descamps, M. *Mol. Pharm.* **2008**, *5*, 905-920.

238. Jayasankar, A. S., A.; Shao, Z. J.; Rodrı´guez-Hornedo, N. *Pharm. Res.* **2006**, *23*, 2381–2392.

239. Cincic, D.; Friscic, T.; Jones, W. *J. Am. Chem. Soc.* **2008**, *130*, 7524.

240. Cinčić, D.; Friščić, T.; Jones, W. *Chem.– Eur. J.* **2008**, *14*, 747-753.

241. Karki, S.; Friscic, T.; Jones, W. *CrystEngComm* **2009**, *11*, 470-481.

242. Friscic, T.; Jones, W. *Faraday Disc.* **2007**, *126*, 167.

243. Bučar, D.-K.; Henry, R. F.; Lou, X.; Borchardt, T. B.; Zhang, G. G. Z. *Chem. Commun.* **2007**, 525-527.

244. Cheney, M. L.; McManus, G. J.; Perman, J. A.; Wang, Z.; Zaworotko, M. J. *Cryst. Growth Des.* **2007**, *7*, 616-617.

245. Mei, X.; Liu, S.; Wolf, C. *Org. Lett.* **2007**, *9*, 2729-2732.

246. Bacon, G. E.; Jude, R. J. Z. *Z. Kristallogr.* **1973**, *138*, 19.

247. Desiraju, G. R. *Angew. Chem., Int. Ed.* **1995**, *34*, 2311.

248. Vansant, J.; Smets, G.; Declercq, J. P.; Germain, G.; Meerssche, M. *J. Org. Chem* **1980**, *45*, 1557-1559.

249. Roldan, L. G.; Rahl, F. J.; Paterson, A. R. *Acta Crytallogr.* **1965**, *19*, 1055.

250. Grosshans, P.; Jouaiti, A.; Bulach, V.; Planeix, J.-M.; Hosseini, M. W.; Nicoud, J.-F. *Chem. Commun.* **2003**, *5*, 414-416.

251. Bennett, C. T. *Pharm. J.* **1909**, *80*, 758.

252. Wagner, C. R.; Hamner, C. L.; Sell, H. M. *J. Am. Chem. Soc.* **1953**, *75*, 4861-2.

253. Faith, H. E. *J. Am. Chem. Soc.* **1950**, *72*, 837-9.

254. Reddy, R. A.; Sadashiva, B. K. *Liq. Cryst.* **2004**, *31*, 1069-1081.

255. Moszew, J.; Wojiechowski, J. *Rocz. Chem.* **1954**, *28*, 445-54.

256. Bertani, R.; Chaux, F.; Gleria, M.; Metrangolo, P.; Milani, R.; Pilati, T.; Resnati, G.; Sansotera, M.; Venzo, A. *Inorg. Chim. Acta* **2007**, *360*, 1191-1199.

257. Li, C.-P.; Chen, J.; Yu, Q.; Du, M. *Cryst. Growth Des.* **2011**, *10*, 1623-1632.

258. Konakahara, T.; Takagi, Y. *Tetrahedron Lett.* **1980**, *21*, 2073-6.

259. Craig, D. *J. Am. Chem. Soc.* **1951**, *73*, 4889-92.

APPENDIX A. SUPPORTING NMR SPECTROSCOPY DATA AND CARTESIAN COORDINATES FOR CHAPTER 2

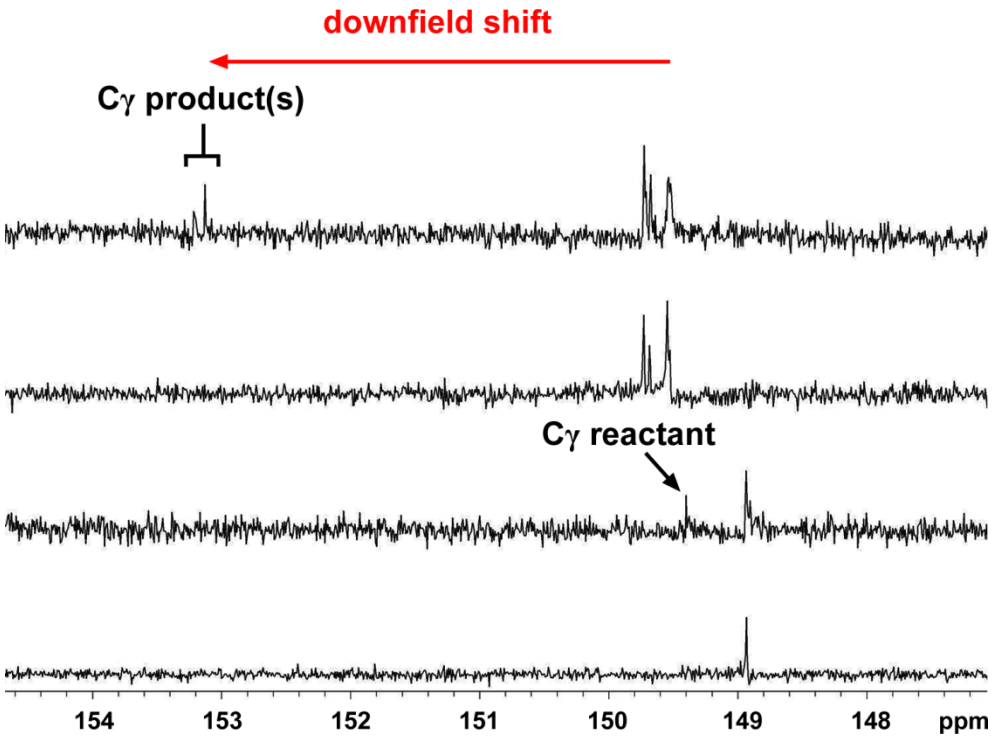

Figure A1. Expansion of NMR spectra of 1a showing downfield shift of γ-C on pyridyl substituent: (a) DEPT of lad-1c (reactant), (b) ^{13}C spectrum of lad-1c showing γ-C, (c) DEPT of reaction mixture of product(s), and (d) ^{13}C of reaction mixture showing downfield shift of γ-C.

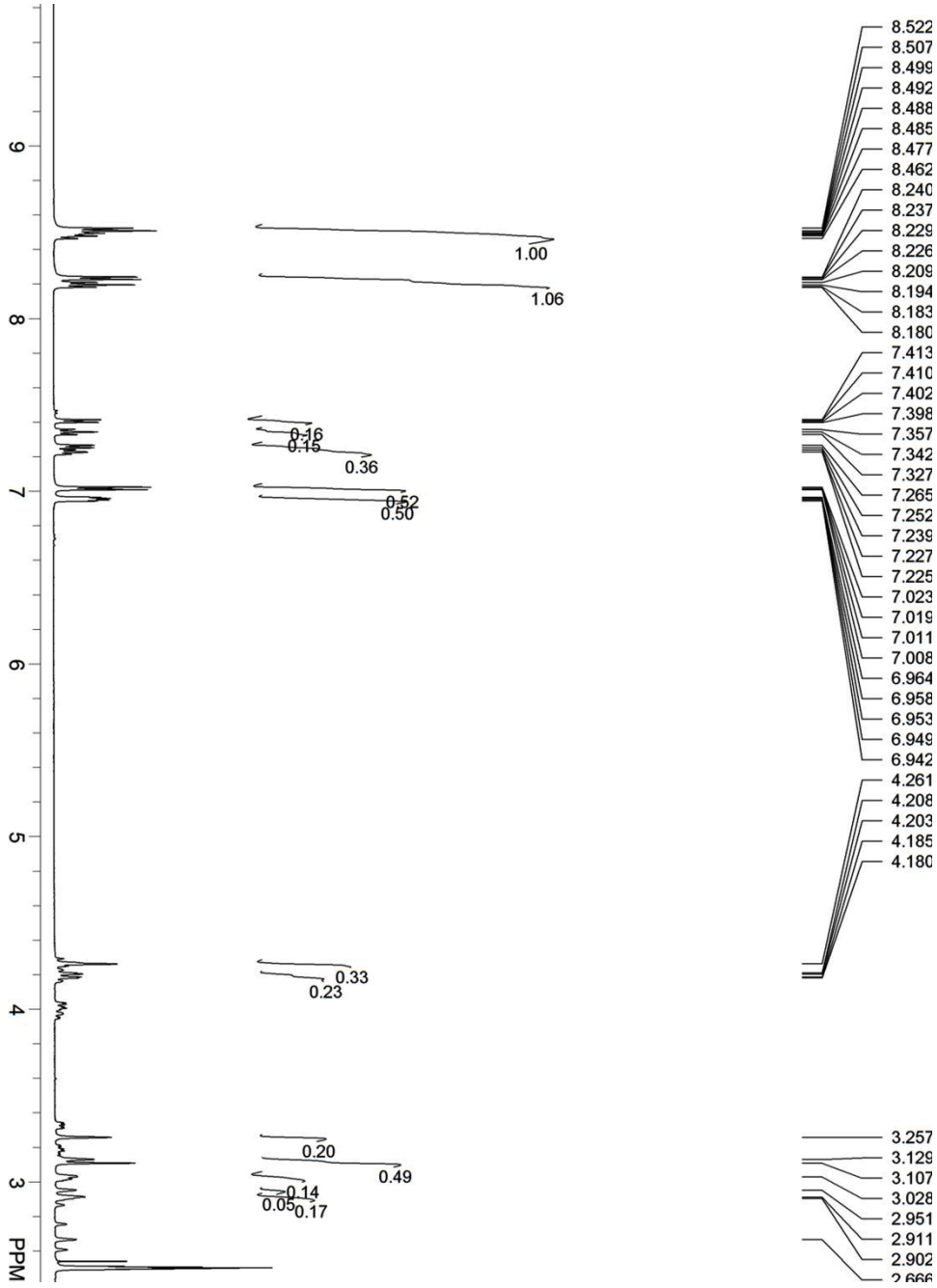

Figure A2. ^{1}H NMR spectrum of lad-1a in AcOH at 25 ºC after 12 hours.

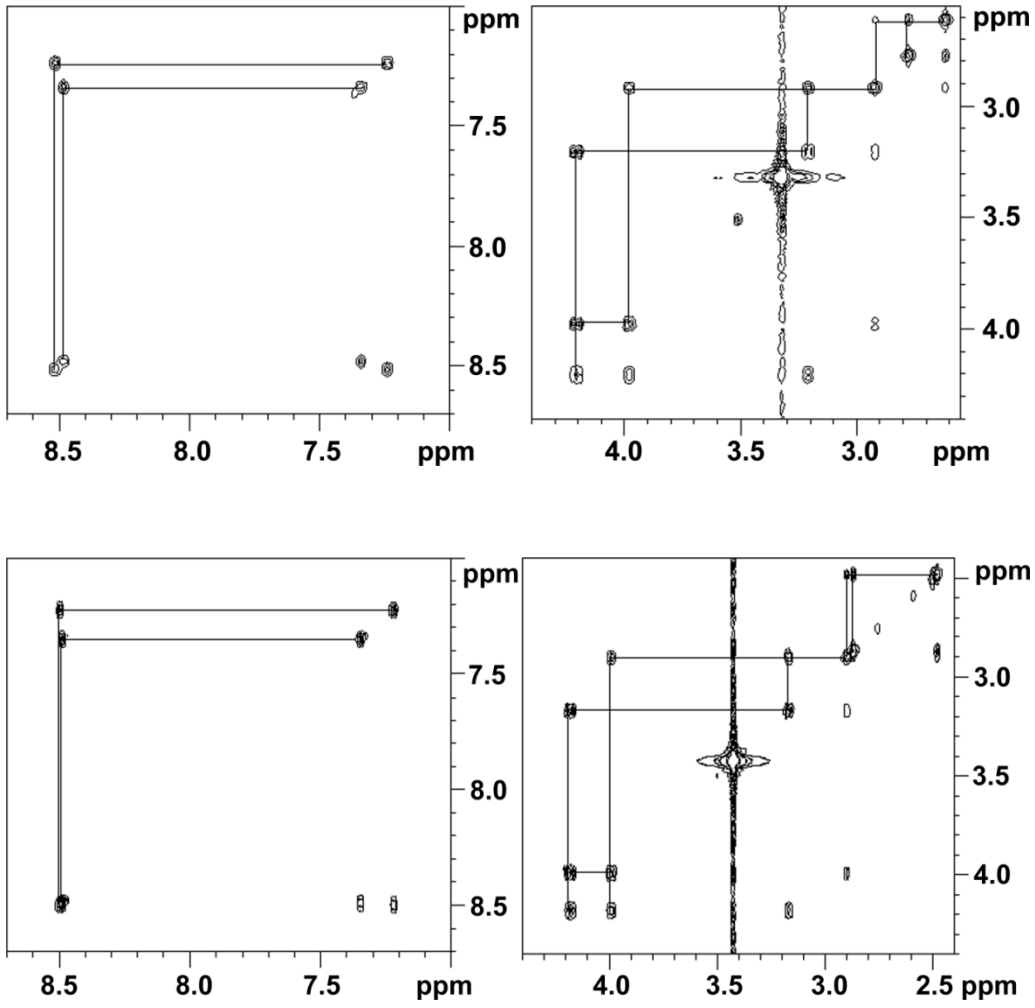

Figure A3. Expansion of ^{1}H-^{1}H COSY spectra of (a) filtrate (b) supernatant. Connected lines within the each spectrum reveal presence of one product.

Table A1. Chemical shift assignment table of lad-1a, lad-1b, lad-1c.

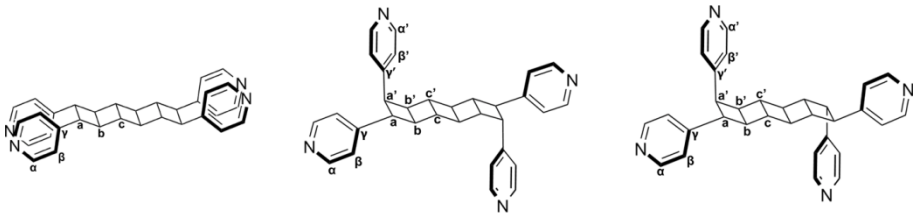

lad-1a (C_{2h}) **lad-1b** (C_i) **lad-1c** (C_2)

No.	Atom	lad-1a (C_{2h})			lad-1b (C_i)			lad-1c (C_2)		
		^{1}H (δ)	$^3J_{H-H}$	^{13}C (δ)	^{1}H (δ)	$^3J_{H-H}$	^{13}C (δ)	^{1}H (δ)	$^3J_{H-H}$	^{13}C (δ)
1	α	8.25	$J_{\alpha-\beta}$=5.8	148.9	8.52	$J_{\alpha-\beta}$=5.6	149.2	8.51	$J_{\alpha-\beta}$=6.0	149.8
2	α'				8.48	$J_{\alpha'-\beta'}$=5.4	149.4	8.48	$J_{\alpha'-\beta'}$=5.4	149.6
3	β'				7.34		121.6	7.37		122.1
4	β	7.02		123.4	7.24		122.0	7.22		122.4
5	γ'						153.2			153.3
6	γ			149.4			149.5			149.7
7	a	4.26	non resolvable	48.7	4.20	$J_{a-a'}$=8.7, J_{a-b}=8.7	46.9	4.18	$J_{a-a'}$=8.7, J_{a-b}=8.6	47.2
8	a'				3.97	$J_{a'-a}$=8.9, $J_{a'-b'}$=3.1	46.1	4.00	$J_{a'-a}$=8.7, $J_{a'-b'}$=3.2	46.1
9	b	3.27	non resolvable	47.5	3.20	J_{b-a}=8.4, $J_{b-b'}$=3.8	41.8	3.17	J_{b-a}=8.6, $J_{b-b'}$=3.6	42.1
10	b'				2.91	non resolvable	43.1	2.90	non resolvable	43.8
11	c	3.12	non resolvable	42.1	2.77	non resolvable	48.3	2.87	non resolvable	48.1
12	c'				2.61	non resolvable	41.4	2.48	non resolvable	42.4

Table A2. List of Cartesian coordinates for RI-BP/TZVP optimized ladderane structures.

lad-1f (C_1)

C	3.968652808	5.762307084	8.049027961
H	4.425266034	4.949400477	8.634282356
C	3.550423072	8.454481145	10.963276668
C	3.302700284	6.905783399	8.833981255
H	2.214403816	6.852566540	8.976818720
C	3.722921933	4.122264126	6.013070810
C	4.721874200	5.105201520	5.251090380
C	4.778146771	6.828141624	7.177684025
H	5.875331454	6.894085084	7.120258218
C	4.038842010	6.335857480	5.920413291
H	3.605170782	7.090599103	5.250698091
C	3.166519499	5.354567197	6.788335059
H	2.072446208	5.414188793	6.864983806
C	4.049666892	7.974676049	7.914665909
H	3.545448129	8.724002776	7.285630934
C	4.797895581	8.493178480	9.150656113
H	5.877795044	8.681352301	9.079285269
C	3.971139888	9.570791046	9.940857661
C	4.160150301	7.359760676	10.045037013
H	4.742355545	6.570019064	10.539969647
H	4.196982101	8.543495468	11.853357590
H	3.112281545	9.908834748	9.340397580
H	5.733971711	4.963577670	5.666883979
H	4.251079431	3.402353219	6.656390242
C	2.702073830	3.373733837	5.199448978
N	0.757456641	1.915822697	3.726507410
C	1.780019522	4.017305231	4.357370296
C	2.612561837	1.976136526	5.275603410
C	1.639092958	1.302890326	4.532311431
C	0.844936462	3.255644229	3.654547147
H	1.784839337	5.102409370	4.240790336
H	3.295638975	1.413113783	5.916226468
H	1.559819190	0.212926478	4.587497263
H	0.123112881	3.745415898	2.994408430
C	4.852799324	5.026825374	3.751050270
N	5.217400877	4.838177749	0.938253620
C	4.707708538	6.140572702	2.913918279
C	5.190885080	3.812803874	3.129133354
C	5.357565637	3.770849268	1.745120282
C	4.899267474	5.996276274	1.535558704
H	4.457321072	7.121763029	3.319543568
H	5.320914604	2.902507884	3.717347490
H	5.617835630	2.830190553	1.251059907
H	4.790689695	6.861418194	0.874292495
C	2.122550531	8.359196479	11.430318967
N	-0.548828283	8.161875014	12.369224465
C	1.299539692	9.488432073	11.544222470

Table A2. Continued

C	1.563227440	7.126891090	11.802644476
C	0.244284998	7.082379774	12.259371068
C	-0.008435879	9.339007368	12.013520239
H	1.670870464	10.480056849	11.279098345
H	2.148307508	6.207109650	11.737610963
H	-0.205101990	6.128511657	12.551612183
H	-0.660782027	10.212135086	12.109823995
C	4.706749970	10.775258161	10.458437720
N	6.099975949	13.068308649	11.396310460
C	5.830884089	10.665444864	11.293812198
C	4.311247588	12.074713730	10.107407812
C	5.027405257	13.171390519	10.594941272
C	6.480559835	11.822292652	11.728124974
H	6.208170148	9.688999093	11.605882701
H	3.448888733	12.232808894	9.455424097
H	4.725393255	14.188797176	10.328890611
H	7.356688136	11.749122880	12.379279267

lad-1g (C_1)

C	4.204716148	6.229606663	7.742481830
H	4.412644082	5.390751274	8.419983017
C	3.721298920	8.998385270	10.570773626
C	3.610766159	7.498339196	8.391913900
H	2.528445340	7.660124387	8.292048495
C	4.229420783	4.648740623	5.633092292
C	5.163650994	5.644462025	4.821793157
C	5.319131488	7.118954473	7.032709314
H	6.402289466	6.959021826	7.123959728
C	4.652982773	6.845660264	5.657812352
H	4.367922836	7.741831730	5.088951223
C	3.605317105	5.899204502	6.369955138
H	2.517406062	5.998783410	6.253571095
C	4.733302550	8.386264880	7.688543491
H	4.531987331	9.236542602	7.018688074
C	5.310556224	8.723676861	9.072373261
H	6.395506504	8.654168604	9.228900605
C	4.607422353	9.973314144	9.714659020
C	4.257984104	7.777798670	9.772377393
H	4.529066082	6.889359780	10.359260617
H	4.007826487	10.505013600	8.959538633
C	5.472879355	10.968432273	10.436245016
N	7.120189658	12.865464680	11.765360097
C	6.331156227	10.594956179	11.483926522
C	5.475594955	12.324528461	10.076946385
C	6.302035529	13.220013479	10.761310890
C	7.120353962	11.564624201	12.105156662
H	6.394697302	9.556829969	11.817785047
H	4.836756432	12.682656917	9.266157007
H	6.309204785	14.280066149	10.490393459
H	4.700254499	5.730303481	3.824173268

Table A2. Continued

C	6.629917848	5.410669548	4.573972074
N	9.372541060	5.010730189	3.950043755
C	7.120911408	4.154089015	4.183917196
C	7.558961123	6.460563010	4.631482386
C	8.897599817	6.212706493	4.314148659
C	8.477782867	4.008907051	3.889098967
H	6.455698400	3.292191396	4.111116864
H	7.245106874	7.468111322	4.909201210
H	9.630715331	7.024170509	4.353723773
H	8.872511815	3.034504698	3.586561243
H	3.480605659	4.215090885	4.955843935
C	4.764921594	3.521544975	6.474355824
N	5.637924363	1.351038439	8.095832323
C	4.031377769	2.327554951	6.576792548
C	5.958240749	3.583981011	7.213313958
C	6.342904724	2.490138278	7.993262082
C	4.497569114	1.290872896	7.387933428
H	3.097330679	2.205791467	6.022866119
H	6.596583989	4.466492788	7.177955519
H	7.273730447	2.528326937	8.566876070
H	3.930094879	0.359220307	7.472532190
H	4.148389966	8.948650668	11.587160881
C	2.240825424	9.239504524	10.697401609
N	-0.549729626	9.668625992	10.993822594
C	1.686438002	10.526017566	10.644816985
C	1.350750588	8.173944907	10.904907756
C	-0.013292266	8.437203577	11.045932779
C	0.306249749	10.684957027	10.797840361
H	2.319770468	11.402170659	10.494332411
H	1.715204680	7.145812711	10.956375192
H	-0.718368165	7.616168972	11.207230216
H	-0.139168616	11.683717276	10.761199149
H	7.792228608	11.285573056	12.922225713

lad-1b (C_2)

C	0.757240663	0.134363824	0.642435293
H	1.127697255	0.939650029	1.292495168
C	-3.133339905	1.024669382	0.690030935
C	-0.757240663	-0.134363824	0.642435293
H	-1.127697255	-0.939650029	1.292495168
C	3.133339905	-1.024669382	0.690030935
C	3.195238049	-0.658464353	-0.826199295
C	0.751803779	0.179988835	-0.952957101
H	1.051538568	1.050377670	-1.556709093
C	1.682842015	-1.041774708	-0.976249949
H	1.463598250	-1.866223279	-1.668259837
C	1.586352073	-1.175139212	0.592517940
H	1.144781621	-2.041423256	1.103312122
C	-0.751803779	-0.179988835	-0.952957101
H	-1.051538568	-1.050377670	-1.556709093

Table A2. Continued

C	-1.682842015	1.041774708	-0.976249949
H	-1.463598250	1.866223279	-1.668259837
C	-3.195238049	0.658464353	-0.826199295
C	-1.586352073	1.175139212	0.592517940
H	-1.144781621	2.041423256	1.103312122
H	-3.553128025	2.036389325	0.826082839
H	-3.315907496	-0.429823035	-0.970064444
H	3.553128025	-2.036389325	0.826082839
H	3.315907496	0.429823035	-0.970064444
C	4.197305217	-1.360491328	-1.707317844
N	6.085278918	-2.626450120	-3.410752606
C	3.985354282	-1.468178374	-3.091448562
C	5.386598661	-1.908287181	-1.207376558
C	6.285288334	-2.519243583	-2.087724042
C	4.942827382	-2.099996345	-3.886295238
H	3.079956785	-1.064281527	-3.549629402
H	5.623134303	-1.861227999	-0.142588064
H	7.217677305	-2.948678265	-1.709035156
H	4.788352139	-2.191975125	-4.965533033
C	3.731984892	-0.117223085	1.732344800
N	4.851177290	1.550121249	3.740662219
C	3.326512477	-0.206224454	3.074498210
C	4.715523882	0.834804717	1.432294685
C	5.236679497	1.631103487	2.457557322
C	3.906974506	0.635073983	4.024466249
H	2.562307070	-0.925065846	3.378236955
H	5.083132966	0.959732025	0.412034588
H	6.006475446	2.376506492	2.236059844
H	3.600347707	0.576148376	5.073111058
C	-4.197305217	1.360491328	-1.707317844
N	-6.085278918	2.626450120	-3.410752606
C	-5.386598661	1.908287181	-1.207376558
C	-3.985354282	1.468178374	-3.091448562
C	-4.942827382	2.099996345	-3.886295238
C	-6.285288334	2.519243583	-2.087724042
H	-5.623134303	1.861227999	-0.142588064
H	-3.079956785	1.064281527	-3.549629402
H	-4.788352139	2.191975125	-4.965533033
H	-7.217677305	2.948678265	-1.709035156
C	-3.731984892	0.117223085	1.732344800
N	-4.851177290	-1.550121249	3.740662219
C	-4.715523882	-0.834804717	1.432294685
C	-3.326512477	0.206224454	3.074498210
C	-3.906974506	-0.635073983	4.024466249
C	-5.236679497	-1.631103487	2.457557322
H	-5.083132966	-0.959732025	0.412034588
H	-2.562307070	0.925065846	3.378236955
H	-3.600347707	-0.576148376	5.073111058
H	-6.006475446	-2.376506492	2.236059844

Table A2. Continued

lad-1a (C_{2h})

C	-0.582681736	0.504397948	-0.798364583
H	-0.467661113	1.397508340	-1.431203935
C	3.155414963	-0.835456251	-0.805732032
C	0.582681736	-0.504397948	-0.798364583
H	0.467661113	-1.397508340	-1.431203935
C	-3.155414963	0.835456251	-0.805732032
H	-2.852560574	1.825443012	-1.179608098
C	-3.155414963	0.835456251	0.805732032
C	-0.582681736	0.504397948	0.798364583
H	-0.467661113	1.397508340	1.431203935
C	-1.970890760	-0.171042205	0.788324206
H	-2.084746050	-1.072704293	1.405073839
C	-1.970890760	-0.171042205	-0.788324206
H	-2.084746050	-1.072704293	-1.405073839
C	0.582681736	-0.504397948	0.798364583
H	0.467661113	-1.397508340	1.431203935
C	1.970890760	0.171042205	0.788324206
H	2.084746050	1.072704293	1.405073839
C	3.155414963	-0.835456251	0.805732032
H	2.852560574	-1.825443012	1.179608098
C	1.970890760	0.171042205	-0.788324206
H	2.084746050	1.072704293	-1.405073839
H	-2.852560574	1.825443012	1.179608098
H	2.852560574	-1.825443012	-1.179608098
C	-4.425602971	0.446306785	-1.510400893
N	-6.857156222	-0.199515174	-2.835121490
C	-4.811035322	-0.883285498	-1.737157286
C	-5.305556107	1.439924934	-1.969735275
C	-6.488523555	1.073889401	-2.613494512
C	-6.016166549	-1.148198280	-2.393876243
H	-4.183237193	-1.715985174	-1.417258669
H	-5.063927621	2.496869122	-1.835196505
H	-7.177164251	1.841276625	-2.979376732
H	-6.323166905	-2.181885159	-2.579415566
C	4.425602971	-0.446306785	-1.510400893
N	6.857156222	0.199515174	-2.835121490
C	4.811035322	0.883285498	-1.737157286
C	5.305556107	-1.439924934	-1.969735275
C	6.488523555	-1.073889401	-2.613494512
C	6.016166549	1.148198280	-2.393876243
H	4.183237193	1.715985174	-1.417258669
H	5.063927621	-2.496869122	-1.835196505
H	7.177164251	-1.841276625	-2.979376732
H	6.323166905	2.181885159	-2.579415566
C	4.425602971	-0.446306785	1.510400893
N	6.857156222	0.199515174	2.835121490
C	4.811035322	0.883285498	1.737157286
C	5.305556107	-1.439924934	1.969735275
C	6.488523555	-1.073889401	2.613494512

Table A2. Continued

C	6.016166549	1.148198280	2.393876243
H	4.183237193	1.715985174	1.417258669
H	5.063927621	-2.496869122	1.835196505
H	7.177164251	-1.841276625	2.979376732
H	6.323166905	2.181885159	2.579415566
C	-4.425602971	0.446306785	1.510400893
N	-6.857156222	-0.199515174	2.835121490
C	-5.305556107	1.439924934	1.969735275
C	-4.811035322	-0.883285498	1.737157286
C	-6.016166549	-1.148198280	2.393876243
C	-6.488523555	1.073889401	2.613494512
H	-5.063927621	2.496869122	1.835196505
H	-4.183237193	-1.715985174	1.417258669
H	-6.323166905	-2.181885159	2.579415566
H	-7.177164251	1.841276625	2.979376732

lad-1d (C_{2h})

C	-0.767158413	-0.088213826	0.798304225
H	-1.155765885	-0.884728728	1.445081788
C	3.063421186	-1.291622767	0.802457197
C	0.767158413	0.088213826	0.798304225
H	1.155765885	0.884728728	1.445081788
C	-3.063421186	1.291622767	0.802457197
C	-3.063421186	1.291622767	-0.802457197
C	-0.767158413	-0.088213826	-0.798304225
H	-1.155765885	-0.884728728	-1.445081788
C	-1.498467581	1.268293692	-0.792014614
H	-1.034815858	2.057398582	-1.400989326
C	-1.498467581	1.268293692	0.792014614
H	-1.034815858	2.057398582	1.400989326
C	0.767158413	0.088213826	-0.798304225
H	1.155765885	0.884728728	-1.445081788
C	1.498467581	-1.268293692	-0.792014614
H	1.034815858	-2.057398582	-1.400989326
C	3.063421186	-1.291622767	-0.802457197
C	1.498467581	-1.268293692	0.792014614
H	1.034815858	-2.057398582	1.400989326
H	3.362695776	-2.308664334	1.093279207
H	3.362695776	-2.308664334	-1.093279207
H	-3.362695776	2.308664334	-1.093279207
H	-3.362695776	2.308664334	1.093279207
C	3.896265138	-0.372091649	-1.657348340
N	5.543402828	1.221865786	-3.357594545
C	4.848743514	-0.936818851	-2.524585103
C	3.808993919	1.030501481	-1.677248685
C	4.637189181	1.765691545	-2.529473293
C	5.633454143	-0.118289351	-3.338559467
H	4.976626075	-2.021137230	-2.565941692
H	3.107515987	1.564628374	-1.040723180
H	4.569540141	2.857623959	-2.547728056

Table A2. Continued

H	6.373903811	-0.558626296	-4.012964586
C	3.896265138	-0.372091649	1.657348340
N	5.543402828	1.221865786	3.357594545
C	3.808993919	1.030501481	1.677248685
C	4.848743514	-0.936818851	2.524585103
C	5.633454143	-0.118289351	3.338559467
C	4.637189181	1.765691545	2.529473293
H	3.107515987	1.564628374	1.040723180
H	4.976626075	-2.021137230	2.565941692
H	6.373903811	-0.558626296	4.012964586
H	4.569540141	2.857623959	2.547728056
C	-3.896265138	0.372091649	1.657348340
N	-5.543402828	-1.221865786	3.357594545
C	-4.848743514	0.936818851	2.524585103
C	-3.808993919	-1.030501481	1.677248685
C	-4.637189181	-1.765691545	2.529473293
C	-5.633454143	0.118289351	3.338559467
H	-4.976626075	2.021137230	2.565941692
H	-3.107515987	-1.564628374	1.040723180
H	-4.569540141	-2.857623959	2.547728056
H	-6.373903811	0.558626296	4.012964586
C	-3.896265138	0.372091649	-1.657348340
N	-5.543402828	-1.221865786	-3.357594545
C	-3.808993919	-1.030501481	-1.677248685
C	-4.848743514	0.936818851	-2.524585103
C	-5.633454143	0.118289351	-3.338559467
C	-4.637189181	-1.765691545	-2.529473293
H	-3.107515987	-1.564628374	-1.040723180
H	-4.976626075	2.021137230	-2.565941692
H	-6.373903811	0.558626296	-4.012964586
H	-4.569540141	-2.857623959	-2.547728056

lad-1c (C_i)

C	-0.689507721	0.804045808	-0.329565082
H	-0.958745734	1.818041145	-0.003086527
C	3.252727807	0.702770443	0.207616433
C	0.804524052	0.506523668	-0.572645472
H	1.142491490	0.518170426	-1.620380107
C	-3.109456300	0.393290580	-1.324413256
C	-3.252727807	-0.702770443	-0.207616433
C	-0.804524052	-0.506523668	0.572645472
H	-1.142491490	-0.518170426	1.620380107
C	-1.759395664	-1.117574676	-0.464345903
H	-1.601322731	-2.155408554	-0.787097002
C	-1.579509060	0.134590820	-1.408667757
H	-1.146378471	0.082827469	-2.417340857
C	0.689507721	-0.804045808	0.329565082
H	0.958745734	-1.818041145	0.003086527
C	1.579509060	-0.134590820	1.408667757
H	1.146378471	-0.082827469	2.417340857

Table A2. Continued

C	3.109456300	-0.393290580	1.324413256
C	1.759395664	1.117574676	0.464345903
H	1.601322731	2.155408554	0.787097002
H	3.566970953	-0.002145427	2.249440239
H	-3.357833278	-0.249026067	0.790159986
H	-3.566970953	0.002145427	-2.249440239
H	3.357833278	0.249026067	-0.790159986
C	-3.641816539	1.781832594	-1.090787925
N	-4.661366898	4.404083613	-0.712790816
C	-4.758201048	2.025220224	-0.278388636
C	-3.052838684	2.896037448	-1.708780087
C	-3.592455817	4.165662132	-1.492032187
C	-5.222788965	3.334484702	-0.125509032
H	-5.271260230	1.205168085	0.227236162
H	-2.179886748	2.778325039	-2.354235739
H	-3.142639603	5.043121187	-1.966354806
H	-6.094567175	3.538183689	0.503554973
C	-4.311101461	-1.756951320	-0.375620119
N	-6.303969227	-3.763777316	-0.658177274
C	-4.447897193	-2.499635565	-1.560280368
C	-5.205242474	-2.061186841	0.661697525
C	-6.169470220	-3.055434288	0.474678686
C	-5.443067393	-3.474656072	-1.649562370
H	-3.784794300	-2.330230450	-2.411707971
H	-5.150601806	-1.526493316	1.612943855
H	-6.873062660	-3.298210798	1.276670663
H	-5.558954670	-4.059311904	-2.566984769
C	4.311101461	1.756951320	0.375620119
N	6.303969227	3.763777316	0.658177274
C	4.447897193	2.499635565	1.560280368
C	5.205242474	2.061186841	-0.661697525
C	6.169470220	3.055434288	-0.474678686
C	5.443067393	3.474656072	1.649562370
H	3.784794300	2.330230450	2.411707971
H	5.150601806	1.526493316	-1.612943855
H	6.873062660	3.298210798	-1.276670663
H	5.558954670	4.059311904	2.566984769
C	3.641816539	-1.781832594	1.090787925
N	4.661366898	-4.404083613	0.712790816
C	3.052838684	-2.896037448	1.708780087
C	4.758201048	-2.025220224	0.278388636
C	5.222788965	-3.334484702	0.125509032
C	3.592455817	-4.165662132	1.492032187
H	2.179886748	-2.778325039	2.354235739
H	5.271260230	-1.205168085	-0.227236162
H	6.094567175	-3.538183689	-0.503554973
H	3.142639603	-5.043121187	1.966354806

Table A2. Continued

lad-1e (C_s)

C	-1.054542660	0.609511991	0.799394536
H	-1.142276406	-0.271718521	1.446952228
C	2.896776820	1.017323359	0.805732153
C	0.320141398	1.310025207	0.797268037
H	0.421013028	2.205537520	1.429368039
C	-3.688133635	1.102016722	0.802381848
C	-3.688133635	1.102016722	-0.802381848
C	-1.054542660	0.609511991	-0.799394536
H	-1.142276406	-0.271718521	-1.446952228
C	-2.213287924	1.625609109	-0.791796964
H	-2.053785704	2.527277959	-1.400086571
C	-2.213287924	1.625609109	0.791796964
H	-2.053785704	2.527277959	1.400086571
C	0.320141398	1.310025207	-0.797268037
H	0.421013028	2.205537520	-1.429368039
C	1.506386639	0.322218906	-0.788551726
H	1.401685602	-0.580055609	-1.406036063
C	2.896776820	1.017323359	-0.805732153
C	1.506386639	0.322218906	0.788551726
H	1.401685602	-0.580055609	1.406036063
H	-4.323214979	1.950963548	-1.093210504
H	-4.323214979	1.950963548	1.093210504
C	-4.148570654	-0.050134152	1.657171155
N	-5.137438009	-2.118454868	3.356685191
C	-5.238540333	0.147064385	2.523985916
C	-3.577881725	-1.334321603	1.677008217
C	-4.098066528	-2.312178912	2.529068690
C	-5.689093374	-0.893830561	3.337578987
H	-5.736448615	1.118784264	2.565163928
H	-2.734271937	-1.590389823	1.040467471
H	-3.654036523	-3.312016789	2.547427224
H	-6.536976892	-0.739364701	4.011513805
C	-4.148570654	-0.050134152	-1.657171155
N	-5.137438009	-2.118454868	-3.356685191
C	-3.577881725	-1.334321603	-1.677008217
C	-5.238540333	0.147064385	-2.523985916
C	-5.689093374	-0.893830561	-3.337578987
C	-4.098066528	-2.312178912	-2.529068690
H	-2.734271937	-1.590389823	-1.040467471
H	-5.736448615	1.118784264	-2.565163928
H	-6.536976892	-0.739364701	-4.011513805
H	-3.654036523	-3.312016789	-2.547427224
H	2.838506573	2.050979281	-1.179801619
H	2.838506573	2.050979281	1.179801619
C	4.038047048	0.336728824	1.509945895
N	6.247232451	-0.869841633	2.831976663
C	4.094987224	-1.046138510	1.738095544
C	5.130750960	1.091850561	1.966400707
C	6.193141175	0.454488802	2.608962902

Table A2. Continued

C	5.203075170	-1.590610627	2.393506470
H	3.285884307	-1.705100496	1.420454011
H	5.148494607	2.175707269	1.830391142
H	7.045939438	1.035534121	2.972482595
H	5.254503462	-2.667465024	2.580295942
C	4.038047048	0.336728824	-1.509945895
N	6.247232451	-0.869841633	-2.831976663
C	4.094987224	-1.046138510	-1.738095544
C	5.130750960	1.091850561	-1.966400707
C	6.193141175	0.454488802	-2.608962902
C	5.203075170	-1.590610627	-2.393506470
H	3.285884307	-1.705100496	-1.420454011
H	5.148494607	2.175707269	-1.830391142
H	7.045939438	1.035534121	-2.972482595
H	5.254503462	-2.667465024	-2.580295942

APPENDIX B. SUPPORTING NMR SPECTROSCOPY DATA FOR CHAPTER 4

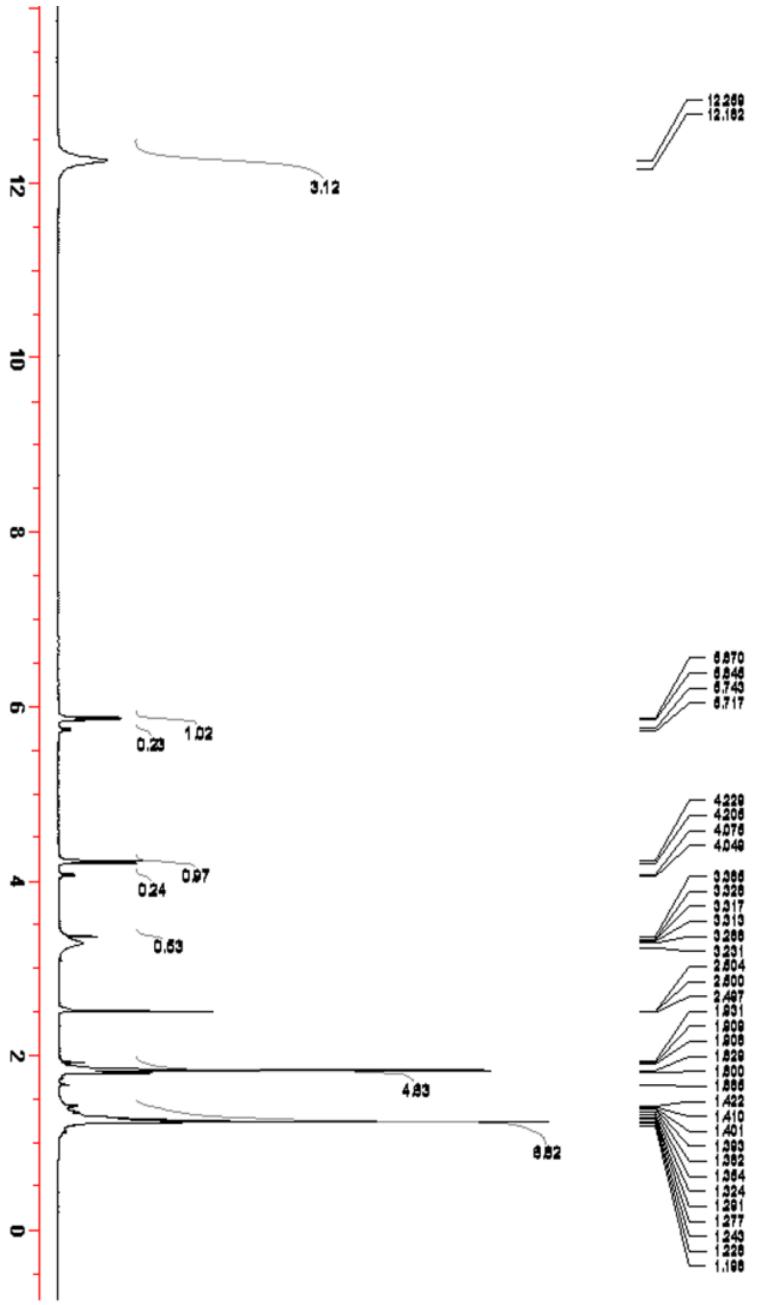

Figure B1. ^{1}H NMR spectrum of dmma before photoreaction

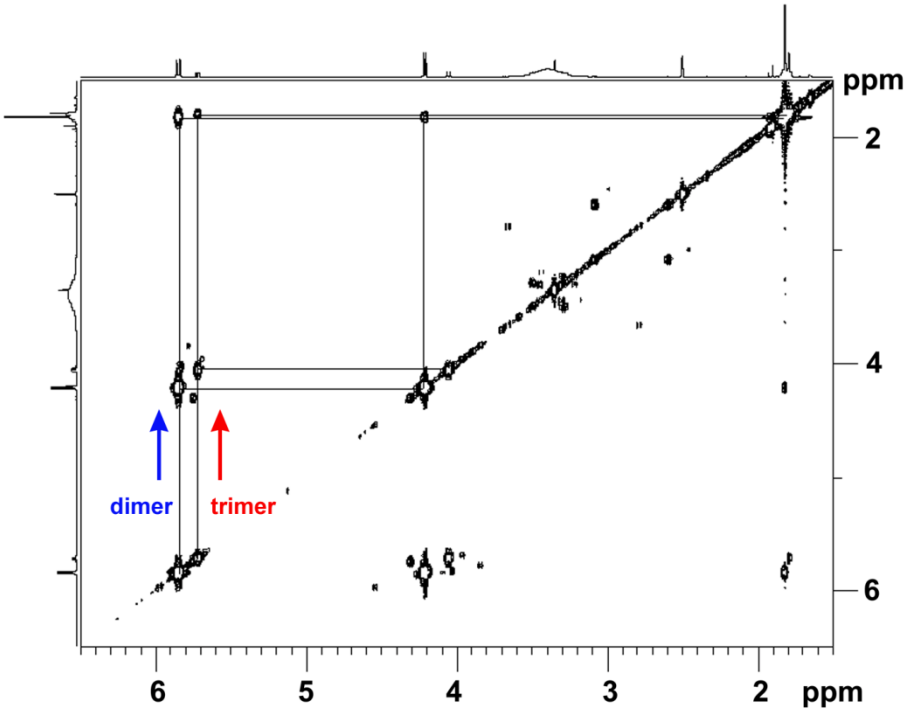

Figure B2. ^{1}H-^{1}H COSY cross section of the mixture containing a dimer and a trimer in DMSO-*d*6.

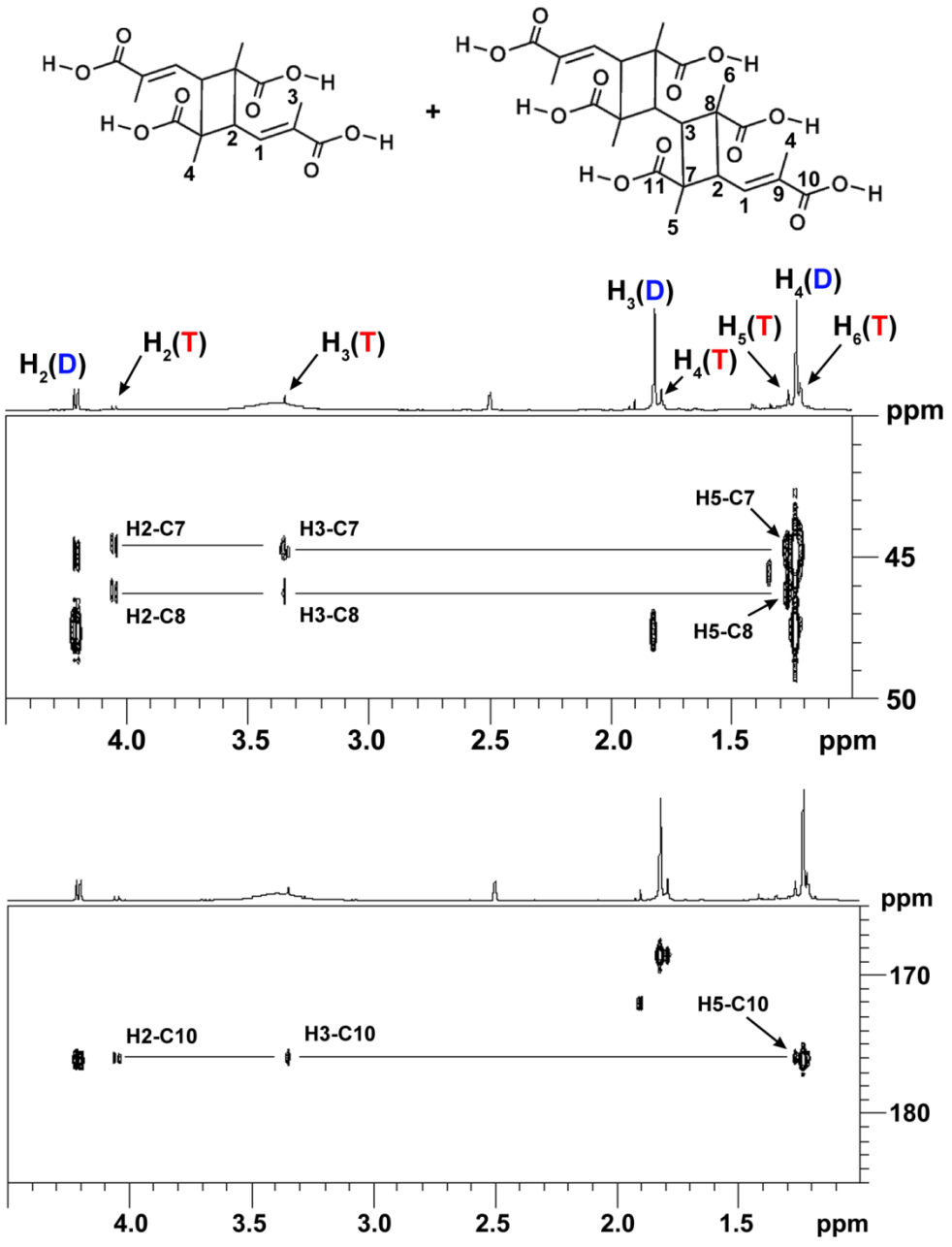

Figure B3. ^{1}H-^{13}C HMBC spectral cross sections of cbta-1a and bha photoreacted mixture. The singlet proton at 3.35 ppm displays correlations with C5, C7, and C8 of bha.

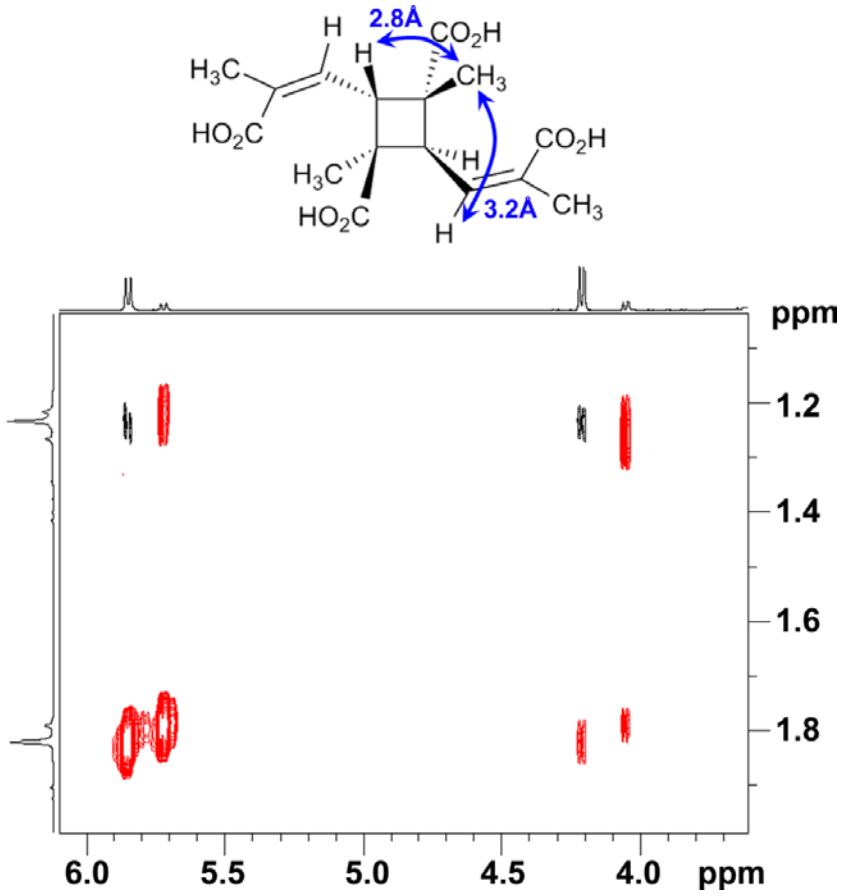

Figure B4. 2D NOESY spectrum cross section of cbta-1a showing magnetization transfer between the cyclobutyl methyl group with the cyclobutyl proton (*r* = 2.8Å) and the olefinic proton (*r* =3.2Å). The cross peaks in "red" are of the same sign as the diagonal peaks and arise due to the incomplete cancelation of residual J-cross peaks.

Table B1. ^{1}H and ^{13}C Chemical shifts of bha.

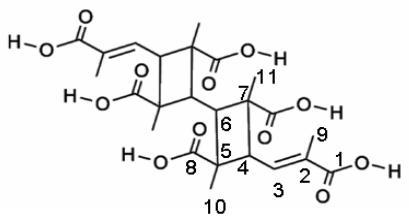

Atom Position	^{1}H	^{13}C
1		168.6
2		131.1
3	5.72	134.5
4	4.04	44.6
5		44.7
6	3.35	44.5
7		46.3
8		176.1
9	1.79	20.79
10	1.26	19.9
11	1.21	19.9

Table B2. ^{1}H and ^{13}C chemical shifts of cbta-1b.

	1H	13C
1		170.0
2		132.0*
3	6.03	131.8
4	3.39	43.8
5		*
6		*
7	1.78	20.2
8	1.26	28.3

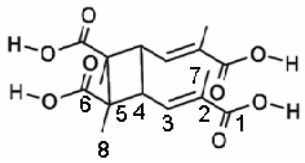

*Either tentative or cannot be assigned due to resonance overlap or lack of HMBC correlations.

APPENDIX C. SUPPORTING NMR SPECTROSCOPY DATA FOR CHAPTER 5

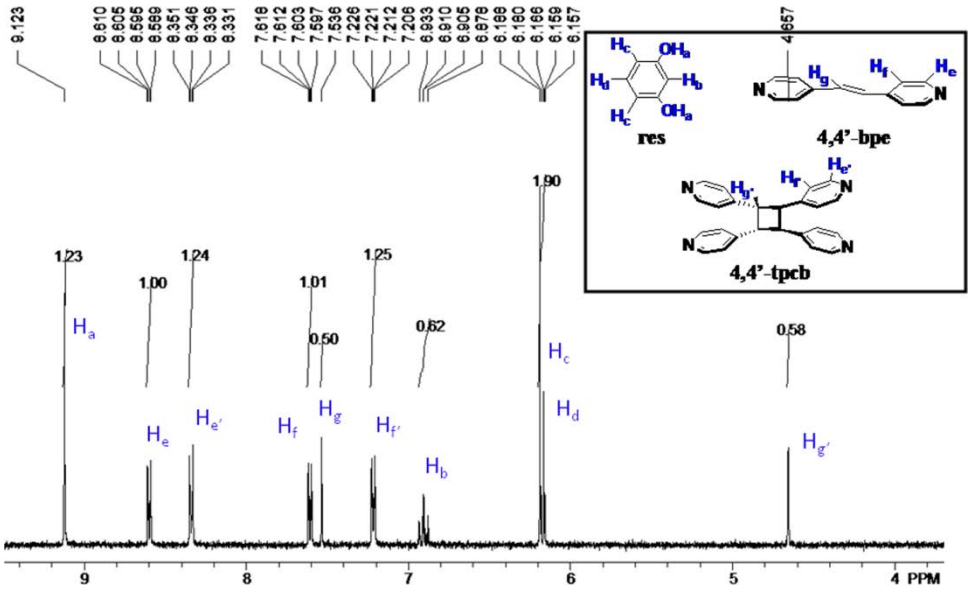

Figure C1. ^{1}H-NMR spectrum of ground dry mixture of res and 4,4-bpe after UV-irradiation.